

# **FINAL REPORT**

**to the**

**UNITED STATES DEPARTMENT OF TRANSPORTATION  
OFFICE OF THE ASSISTANT SECRETARY FOR  
RESEARCH AND TECHNOLOGY**

**For Cooperative Agreement No. OASRTRS-14-H-RPI**

**Remote Sensing Decision Support System for Optimal Access  
Restoration in Post Disaster Environments**

**Principal Investigator:**

Rensselaer Polytechnic Institute  
Dr. Jose Holguin-Veras, Professor  
Dept. of Civil and Environmental Engineering  
Center for Infrastructure, Transportation and the Environment  
110 8th Street, Room JEC 4030  
Troy, NY 12180-3590  
Tel: 518-276-6221  
Email: [jhv@rpi.edu](mailto:jhv@rpi.edu)

**Program Administrator:**

U.S. Department of Transportation  
Caesar Singh, P.E.  
Director, University Grants Programs  
Office of the Assistant Secretary for Research and Technology (OST-R)  
1200 New Jersey Avenue, E33-306  
Washington, DC 20590  
Tel: 202-366-3252  
Email: [Caesar.singh@dot.gov](mailto:Caesar.singh@dot.gov)



---

# Remote Sensing Decision Support System for Optimal Access Restoration in Post Disaster Environments

FINAL REPORT

Submitted by:

RENSSELAER POLYTECHNIC INSTITUTE, ROCHESTER

INSTITUTE OF TECHNOLOGY and

NEW YORK CITY DEPARTMENT OF TRANSPORTATION

2017



#### **DISCLAIMER STATEMENT**

The views, opinions, findings and conclusions reflected in this publication are solely those of the authors and do not represent the official policy or position of the USDOT/OST-R, or any State or other entity. USDOT/OST-R does not endorse any third party products or services that may be included in this publication or associated materials.”



# TABLE OF CONTENTS

EXECUTIVE SUMMARY .....	ix
1. Introduction .....	1
2. Development of CRS Techniques.....	3
2.1 Introduction .....	3
2.2 Development of CRS Technologies .....	3
2.2.1 Debris Detection.....	3
2.2.2 Flood Detection .....	8
2.2.3 Results .....	14
2.3 Quantification of Debris and Floods .....	18
2.3.1 Debris Volume Estimation .....	18
2.3.2 Flood Depth Estimation .....	19
2.3.3 Results .....	22
2.4 Integration of Multi-Modal/Temporal Data to Assess Disaster Impacts.....	28
2.4.1 Crowdsourcing vs. Data Mining .....	28
2.4.2 Data Sources.....	30
2.4.3 The Use of Flickr and Panoramio for Validation .....	30
2.4.4 Other Means of Validation .....	32
2.5 Estimation of Network Conditions and Disaster Impacts .....	33
2.5.1 Methods.....	34
2.6 Conclusions .....	37
3. ARP mathematical models .....	38
3.1 Introduction .....	38
3.1.1 Agencies Involved in AR .....	38
3.1.2 AR in Practice: Initial Assessment and Classification of Roads .....	39
3.2 Problem Definition.....	39

3.2.1	Characterization of the Disaster Site.....	39
3.2.2	Time Dependent Capacity Constraints.....	40
3.3	Review of Priority Metrics.....	41
3.4	Mathematical Model of Access Restoration .....	41
3.5	Solution Algorithm.....	43
3.6	Heuristic Solution.....	43
3.7	Numerical Experiments.....	45
3.7.1	Sioux Falls Network.....	45
3.7.2	Manhattan, New York.....	48
3.7.3	Analysis of the Number of Entry Points Available.....	48
3.7.4	Effect of Capacity Constraints .....	49
3.8	Conclusions.....	50
4.	Transition to Practice.....	51
4.1	Introduction.....	51
4.2	Technical Advisory Council (TAC).....	51
4.3	Outreach and Validation.....	53
4.4	Transition to Implementation.....	53
4.4.1	System Integration .....	54
4.4.2	Pilot Testing and Improvement.....	56
5.	Procedures For Integration of Outside Help.....	58
5.1	Introduction.....	58
5.2	Emergency Management.....	59
5.3	ERM Coordination.....	60
5.4	Review of Current Practices.....	62
5.4.1	National Disaster Recovery Framework (FEMA).....	62
5.4.2	National Voluntary Organizations Active in Disaster (National VOAD).....	63
5.4.3	Hyogo Framework .....	64

5.4.4	Montana Emergency Response Framework.....	65
5.4.5	Nepal National Disaster Response Framework.....	66
5.4.6	Sudan Emergency Response Framework.....	66
6.	Concluding Remarks .....	67
7.	References .....	68
	Appendices.....	71

**LIST OF APPENDICIES**

- Appendix A: Algorithms for Debris Volume and Water Depth Computation
- Appendix B: Algorithms for Detection of Roadway Debris and Flooding
- Appendix C: Generating GIS Products from Detection and Characterization Algorithm Outputs
- Appendix D: Technical Advisory Committee Meeting Slides
- Appendix E: CRS Playbook
- Appendix F: Access Restoration Planning User Manual
- Appendix G: Debris Utility User Manual
- Appendix H: Flood Utility User Manual

# LIST OF FIGURES

Figure 1: Airborne lidar point cloud and roadbed in Manhattan.....	4
Figure 2: A point cloud before and after preprocessing .....	5
Figure 3: Point filtering .....	6
Figure 4: Region growing .....	7
Figure 5: Object filtering.....	8
Figure 6: Image of a house surrounded by severe flooding from the Mississippi River.....	9
Figure 7: Hue channel .....	10
Figure 8: The set of homogeneous regions produced from Otsu’s method .....	11
Figure 9: Seed Pixel .....	12
Figure 10: The flood pixels detected by the QMF are shown in cyan .....	13
Figure 11: Roadway detection.....	14
Figure 12: Debris results validation .....	15
Figure 13: Roadway flood detection scene .....	17
Figure 14: Roadway flood detection scene 2 .....	18
Figure 15: Volume estimation.....	19
Figure 16: A classified flood image and the corresponding digital elevation model .....	20
Figure 17: Flood pixels .....	20
Figure 18: Water elevation.....	21
Figure 19: A depth map for regions of the image that were classified as flooded .....	21
Figure 20: The depth map produced by the algorithm .....	22
Figure 21: Debris estimation results.....	23
Figure 22: Volume estimation results .....	23
Figure 23: Volume error estimates.....	25
Figure 24: Water depth estimation illustration.....	26
Figure 25: Overlay of roadway water depths near the water-land edge.....	27
Figure 26: Depth profile.....	27
Figure 27: 3-D view of the DEM .....	27
Figure 28: Example of the Tomnod application.....	29
Figure 29: A map of flood alerts in Boulder, CO from multi modal data sources .....	29
Figure 30: Workflow for roadway obstruction validation from data mining of geo-tagged images.....	30
Figure 31: Automatically generated shapefile.....	31

Figure 32: A Flickr image confirms that validity of debris pile.....	31
Figure 33: A screenshot from FEMA’s Disaster Reporter application .....	32
Figure 34: Geolocation of Tweets .....	33
Figure 35: Close up view of debris polygons.....	34
Figure 36: Passable width illustration .....	35
Figure 37: ArcGIS Screenshot of road polygons and debris piles .....	36
Figure 38: ArcGIS screenshot of flood polygons.....	36
Figure 39: Flood depth estimates .....	37
Figure 40: Schematic of Manhattan .....	40
Figure 41: Super node representation in Manhattan .....	44
Figure 42: Sioux Falls Network .....	46
Figure 43: Capacity equal to 1 .....	46
Figure 44: Capacity equal to 2 .....	47
Figure 45: Capacity equal or larger than to 3.....	47
Figure 46: Access restoration results for Manhattan.....	49
Figure 47: Social costs results for different levels of capacity.....	50
Figure 48: System integration .....	54
Figure 49: Lidar tiles and road network in Rockaway Beach .....	56
Figure 50: Debris piles in Rockaway Beach .....	57
Figure 51: Optimal restoration .....	57

## LIST OF TABLES

Table 1: Debris detection results for the seven test sites.....	15
Table 2: Roadway flood pixel detection results .....	16
Table 3: Comparison of volume estimates using terrestrial lidar and airborne lidar .....	24
Table 4: Comparison of volume estimates using terrestrial lidar and airborne lidar .....	25
Table 5: Parameters used in the experiments .....	45
Table 6: Results for different levels of capacity in Sioux Falls .....	45
Table 7: Summary results for different values of capacity .....	49
Table 8: Roadway pixel classification results .....	58
Table 8: Emergency Functions (EF) .....	60



## EXECUTIVE SUMMARY

Access restoration is an extremely important part of disaster response. Without access to the site, critically important emergency functions like search and rescue, emergency evacuation, and relief distribution, cannot commence. Frequently, roads are opened in descending order of functional class. While this may work in simple cases, it does not take into account the urgency of the needs at the demand nodes, which represent population and economic centers or critical infrastructure that need access restored quickly. The key to optimal allocation of resources is proper prioritization. Such prioritization is possible only with state-of-the-art computing power that supports a Decision Support System (DSS) based on Commercial Remote Sensing (CRS), given the large area coverage, the complexity of the decision process, the need for rapid action, and the spatial nature of the impacts. This project has developed a DSS based on the following principles: (1) that CRS is key to estimating both network conditions and disaster impacts; (2) that Access Restoration Plans (ARPs) are more effective when they explicitly take into account priority rules/metrics and the resource constraints faced by responders; (3) that such priority rules/metrics must consider the impacts on population, economic centers, and critical facilities; (4) that cutting-edge optimization algorithms—using CRS inputs and priority rules/metrics—are the best way to reach sound decisions; and (5) that the proposed DST, with modifications, could play a key role during various phases of the disaster cycle, including response and effective recovery.

The DST is comprised of 4 modules. The first module assesses the impacts on the transport network, using a CRS multi-modal data collection/processing at its core. The second module identifies the resource constraints (e.g., number of trucks available at time  $t$ ). The third module specifies the rules/metrics that define the level of importance of the competing needs. Finally, an optimization procedure uses the other modules' outputs to estimate the optimal Access Restoration Path.

The CRS technologies developed as part of this project implemented algorithms that use road network shapefiles and CRS data (lidar for debris, imagery for flooding) to automatically detect obstructions to the roadway. The methodology implemented in the project to quantify debris and floods allows debris volumes and water depths to be automatically estimated from the output of the detection algorithms. The outputs from these algorithms (debris volumes and water depths) are converted into GIS shapefiles for easy viewing and integration with the Access Restoration module.

This project has also developed a mathematical model that solves the problem of access restoration (AR). The mathematical model incorporates the impact of the allocation decisions using social costs (SC) as the objective function, although other priority metrics can be considered, such as population, time, cost and deprivation cost. The mathematical model integrates scheduling and capacity constraints into the process of AR. The model recognizes the temporal evolution of needs and availability of resources in the inclusion of varying parameters of capacity in different time periods along the planning horizon. This allows for integration of arriving resources into disaster response operations throughout the response. From the computational perspective, the complexity of the model makes it unfeasible to use commercial software to find optimal solutions to large instances. In response to this limitation, the team developed a heuristic procedure able to solve large instances in short execution times.

Throughout the course of this project, the team wanted to ensure that the research and associated DSS tools could be smoothly transitioned into practice, fully validated, and useful to responders. It was important to ensure that the DSS met the expectations of the end users, in terms of ease of use, quality of results, and usefulness. To accomplish this, the research team created a Technical Advisory Council, and conducted outreach, validation and training to assist with transitioning the research into practice. All of the components of the solution developed are

integrated in a web-based software application. The team has created a project website that provides an overview of the solution components, and provided access to the web application to stakeholders that have been trained in the use of the software.

The project was a collaboration of the Rensselaer Polytechnic Institute (RPI), the Rochester Institute of Technology (RIT) the New York City Department of Transportation (NYCDOT), Ohio University and Emprata LLC. The RPI team worked on: the DST's core mathematical models; research to produce priority rules/metrics; coordination and outreach with public-sector practitioners; project management and system integration. RIT was in charge of the development of the CRS algorithms. NYCDOT provided guidance on implementation, contributed datasets and expertise, and pilot-tested the DST.

# 1. INTRODUCTION

Post-disaster logistics encompasses a series of actions that are intended to address the different needs of the impacted population and the response itself (Holguín-Veras and Jaller 2012, Holguín-Veras et al. 2012). Multi-focused, the effort is also multi-staged. In a very simplified way, one could identify several key stages: (1) preliminary needs assessment, (2) access restoration, (3) deployment of the assets required to conduct the various emergency response functions, (4) local distribution of supplies, (5) debris removal, and (6) infrastructure restoration. This project focused on the first two elements, which are the key determinants of the effort as a whole.

Access restoration is, without a doubt, an extremely important part of disaster response. Without access to the site, critically important emergency functions like search and rescue, emergency evacuation, and relief distribution, cannot commence. After the 2010 Haiti earthquake, and the 2011 Japan earthquake and tsunami, 3-6ft and 5-10ft of debris, respectively, had to be removed to access impacted areas; during the Super Storm Sandy response, many of the impacted towns had to remove 1-2ft of debris to allow first responders access to the disaster areas. In catastrophic events, access restoration is even more important, given that the bulk of the aid must come from the outside (Holguín-Veras et al. 2012).

The team's fieldwork shows that access restoration efforts are guided by the intuition of equipment operators, working with limited information to prioritize and optimize their decisions. Frequently, roads are opened in descending order of functional class. While this may work in simple cases, it does not take into account the urgency of the needs at the *demand nodes*, which represent population and economic centers or critical infrastructure that need access restored. Moreover, after large disasters key facilities such as the port in Port-au-Prince (Holguín-Veras et al. 2012), and the Port of Sendai in Japan (Holguín-Veras et al. 2012) need major repairs. Thus, prioritizing port repairs could significantly hasten the overall response. The key to optimal allocation of resources is proper prioritization. Such prioritization is possible only with state-of-the-art computing power that supports a Decision Support System (DSS) based on CRS, given the large area coverage, the complexity of the decision process, the need for rapid action, and the spatial nature of the impacts.

Resources and demands are also very dynamic. For example, restoring access to a population that is otherwise fine, but isolated by rubble, may not be a high priority. However, if that isolation leads to water shortages, the priority rapidly increases. While construction equipment will likely be in short supply at the beginning, once responders arrive with equipment, that constraint disappears as a new one emerges: coordinating convergent groups of responders and equipment (Fritz and Mathewson 1957, Holguín-Veras et al. 2013). Since many volunteers come in response to media accounts, they tend to bring equipment and supplies to those localities mentioned in the news. This leads to an onslaught of resources at some locations, with few to none in others. Coordinating the timeliness and location of disaster response is a complex and dynamic process; one that is best accomplished with the CRS-based DSS developed by the team (Messinger et al. 2010, van Aardt et al. 2011). This DSS uses high spatial resolution air- and space-borne imagery and LiDAR data. The former provides context and spectral ("color") information, (e.g., object classification), while the latter adds a structural dimension (3D) (e.g., debris height and texture, flood extent/depth). Jointly, the two CRS modalities enable type and condition characterization of a scene, i.e., "*What is located where, and is it intact?*" The approach is sensor agnostic: any high-resolution spectral sensor and LiDAR sensor works. This will provide maximum flexibility to the end users of the DSS, enabling them to use CRS inputs from multiple vendors.

More specifically, the project's main goal was to develop a state-of-the-art DSS that uses CRS assessments of network conditions and disaster impacts to produce an optimal access restoration plan (ARP). This Optimal ARP

will help responders use their scarce resources to orchestrate the opening of roads, prioritize work, and facilitate the cooperation of multiple groups to maximize effectiveness. The DST processes CRS data to update estimates of disaster impacts, and optimization techniques to refresh the ARP as new data become available.

The project was based on the following principles: (1) that CRS is key to estimating both network conditions and disaster impacts; (2) that ARPs are more effective when they explicitly take into account priority rules/metrics and the resource constraints faced by responders; (3) that such priority rules/metrics must consider the impacts on population, economic centers, and critical facilities; (4) that cutting-edge optimization algorithms—using CRS inputs and priority rules/metrics—are the best way to reach sound decisions; and (5) that the proposed DST, with modifications, could play a key role during various phases of the disaster cycle, including response and effective recovery. To achieve this overall goal, the team’s objectives were to: (1) develop CRS techniques that produce quick assessments of network conditions and disaster impacts; (2) integrate multi-modal temporal data to assess disaster impacts (e.g., CRS data, social media feeds, ground surveys); (3) develop proper priority rules/metrics (that account for impacts on population, economic centers, and critical facilities) so that optimization algorithms are guided by sound objective functions; (4) develop mathematical procedures that, given estimates of network conditions and disaster impacts, produce an ARP that would be updated as data become available; (5) develop appropriate procedures to integrate private-sector partners into the response; (6) validate the DST with case studies and disaster-response experts; and (7) conduct a vigorous outreach and training process to properly integrate the DST into standard response procedures and protocols.

The DST will help disaster response agencies: (1) maximize their response effectiveness by producing ARPs that both reflect the needs on the ground, and are consistent with the resource constraints; (2) minimize restoration time by defining optimal ways to subdivide the work among multiple groups for efficient collaboration; (3) make sound decisions by integrating multiple data streams to produce a more accurate view of the needs on the ground; and, (4) plan ahead by providing estimates of the number and type of equipment needed to optimally restore access after a disaster.

The DST is comprised of 4 modules. The first module assesses the impacts on the transport network, using a CRS multi-modal data collection/processing at its core. The second module identifies the resource constraints (e.g., number of trucks available at time  $t$ ). The third module specifies the rules/metrics that define the level of importance of the competing needs. Finally, an optimization procedure uses the other modules’ outputs to estimate the optimal ARP for time  $t$ . Due to the dynamic nature of resources and demands, the process could be refreshed for the next time  $t+1$ , or when new/improved data become available. This will ensure that the restoration plan responds to the dynamic needs on the ground.

The project was a collaboration of the Rensselaer Polytechnic Institute (RPI), the Rochester Institute of Technology (RIT), the New York City Department of Transportation (NYCDOT), Ohio University and Emprata LLC. The RPI team worked on: the DST’s core mathematical models; research to produce priority rules/metrics; coordination and outreach with public-sector practitioners; project management and system integration. RIT was in charge of the development of the CRS algorithms. NYCDOT provided guidance on implementation, contributed datasets and expertise, and pilot-tested the DST. Emprata created the software for the project.

This report provides a succinct description of the process followed during the research, the main results obtained, and a description of the DST. The report has 5 sections in addition to this introduction; the second section describes the CRS techniques developed, including debris and flood detection and quantification algorithms. The third section details the mathematical models that produce the optimal access restoration plan. The fourth section details the process followed to transition the research findings into practice. The fifth section summarizes the procedures for integration of outside help, and the sixth section provides concluding remarks.

## **2. DEVELOPMENT OF CRS TECHNIQUES**

### **2.1 Introduction**

In the hours and days following a natural disaster, response efforts are typically focused on performing search and rescue missions, delivering relief to those who urgently need it, transporting the injured to medical facilities, and in some cases evacuating people, if there is still an immediate threat. All of these operations are dependent on unimpeded use of the road network. Obstructions to navigability of these roads, such as large debris piles and floodwater, slow down response and recovery and therefore must be addressed immediately.

Remote sensing platforms provide a fast and safe way to gather overhead data of the entire region affected by the disaster. However, the data alone are not enough. Information needs to be extracted from the data: in this case, the location of the blocked roadways. Typically, this requires a lot of time and manpower to meticulously look through the data, compare it to baseline data, and eventually identify obstructions. Such manual interpretation requires a lot of resources and is subjective; one observer might not agree with the findings of another.

Computer programs that can automatically turn raw CRS data into useful information products (blockage maps, optimal routes and restoration plans) help to alleviate the uncertainty and resource cost of manual methods. Although these programs are designed to be simple “black boxes” for the user, understanding how and why they work can help the user obtain the best results.

### **2.2 Development of CRS Technologies**

The debris and flood detection algorithms are very different – they use different data and mathematics to accomplish essentially the same task: detect roadway obstructions in the input data. Therefore, the methods will be split into a separate debris and flood section.

#### **2.2.1 Debris Detection**

The ultimate goal of the debris detection algorithm is to not only find occurrences of roadway debris piles, but also to characterize them in terms of volume, additional information related to this can be found in Appendix A: Algorithms for Debris Volume and Water Depth Computation. Volume estimation requires 3-D data, so the decision was made to use airborne light detection and ranging (lidar) point clouds as the data input. The algorithm needs two input files to run: an airborne lidar point cloud LAS file (\*.las) and a shapefile containing the road network as a series of polygons (\*.shp). Figure 1 shows an example point cloud and road network from Manhattan.

**Figure 1: Airborne lidar point cloud and roadbed in Manhattan**



### 2.2.1.1 Preprocessing

The point cloud and road network polygons need to be processed before detection is performed. The road network is truncated to the bounds of the point cloud, and all points outside of the roadbed are discarded using the boundaries of the truncated road polygons. Point clouds often contain unwanted points (noise, points from birds, power lines, etc.) that can affect operations and must be removed. Statistical outlier removal is used to remove these points. The statistical outlier removal stage operates by first calculating the mean Euclidean distance,  $\bar{d}$ , between each point,  $p$ , and its  $k$  closest neighbors. The mean ( $\mu_k$ ) and standard deviation ( $\sigma_k$ ) of the distribution of mean distance are calculated, and points that have a mean Euclidean distance higher than multiple standard deviations above the distribution mean are classified as outliers and removed:

$$P^* = \{p \in P \mid \bar{d} \leq (\mu_k + \gamma \cdot \sigma_k)\}$$

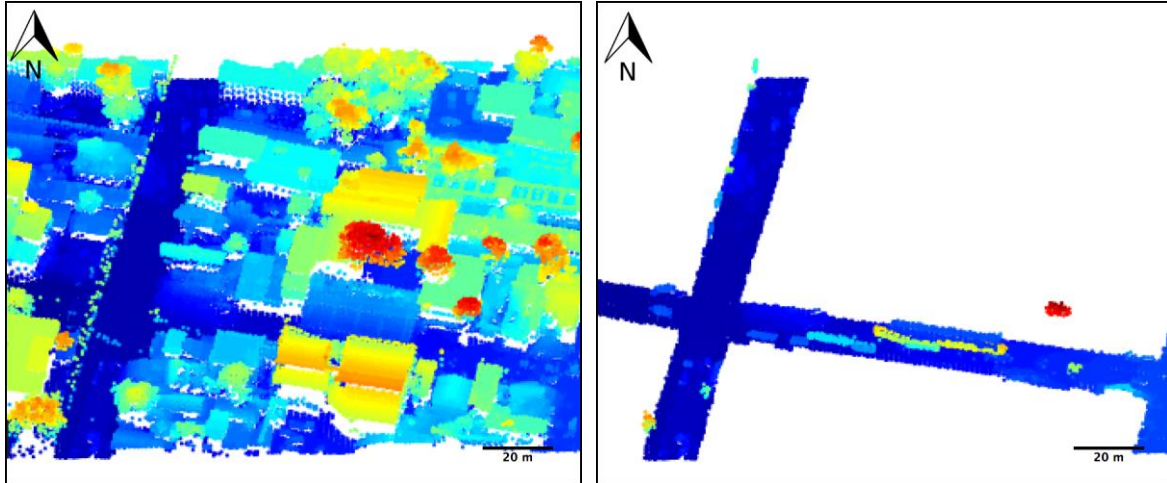
where  $P^*$  is the entire point cloud after statistical outlier removal, and  $\gamma$  is a scalar multiplier to control the severity of the point removal (lower  $\gamma$  = more points removed).

Following statistical outlier removal, a digital elevation model (DEM) is generated. A DEM is a point cloud that contains only the points that represent the bare earth. In a case where ground points have been classified by the vendor, the DEM is computed by performing a Delaunay Triangulation on the known ground points using natural neighbor interpolation. If the point cloud does not have classified ground points, the DEM is produced using the Simple Morphological Filter (SMRF). The SMRF uses a linearly increasing window size, along with slope thresholding, to progressively remove objects from the bare earth until the DEM is achieved. Regardless of which method is used, the DEM grid spacing is set to  $\mu_k$ . A normalized digital surface model (nDSM) is created by subtracting the point cloud from the DEM. The nDSM represents the height of all objects above the ground and is used later in the workflow for height thresholding. At this point the cloud is properly prepared for debris detection. Figure 2 shows a portion of a point cloud before and after preprocessing.

### 2.2.1.2 Point Filtering

It is challenging to define a single set of features to identify debris, because it varies remarkably in size, shape, and composition. Instead, individual points that are highly unlikely to be debris are first systematically removed using local surface properties and elevation cues. One of the main benefits of working with 3-D data is the ability to estimate the normal vectors of individual points, as well as the local distribution of normal vectors.

**Figure 2: A point cloud before and after preprocessing**



These properties give insight to the underlying geometry of the surface that each point,  $p$ , belongs to. The normal vector of  $p$  can be calculated using all points in a local neighborhood,  $N_p$ , defined by the radius,  $r$ . For each query point,  $p$ , the neighborhood points are obtained using:

$$N_p = \{ q \in P | d(p, q) < r \}$$

where  $q$  are all of the points in the entire point cloud  $P$ , and  $d$  is the Euclidean distance between two 3-D points. Eigen-analysis of the covariance matrix of  $N_p$  produces the eigenvalues  $\lambda_1 < \lambda_2 < \lambda_3$ . The eigenvector corresponding to  $\lambda_1$  is the estimate of the point normal,  $\vec{n}$ . Airborne lidar data are collected from above, so the absolute value of the z-component of  $\vec{n}$  is used to ensure the normal vector points outward from the surface.

The angle,  $\theta$ , between each normal vector and horizontal is another useful property for point filtering:

$$\theta = 90^\circ - \arccos(\vec{n}_z)$$

where  $\vec{n}_z$  is the z-component of the normal vector. Points sampled from a horizontal surface have a  $\theta$  of  $90^\circ$ . The neighborhood analysis is taken one step further by computing the distribution of normals in  $N_p$ . Eigenanalysis is again used, but this time on the covariance matrix of  $N_p$  resulting in  $\lambda_1^n < \lambda_2^n < \lambda_3^n$ . The eigenvalue corresponding to  $\lambda_2^n$  represents the maximum variation of normals on the Gaussian sphere, and is useful for discerning points on a smooth surface (e.g., road, roof, etc.) from points on a rough surface (e.g., a debris pile).

A majority of the non-debris points can be identified and discarded using a combination of  $\theta$ ,  $\lambda_2^n$ , and height above ground,  $h$ . There are two sets of points that need to be removed in this stage: very low points (e.g., road, sidewalk, etc.) and points that are above the ground, but on very smooth surfaces (e.g., trucks, road barriers, etc.). Low points are removed by finding those points that fall below a normal variation threshold ( $T_\lambda$ ) and minimum height threshold ( $T_h$ ).  $T_h$  is typically set to the vertical positioning accuracy of the system used to collect the data

(0.15 m for this research). Smooth points are identified by using a normal variation threshold that is 5x smaller without any height threshold. In both cases, a normal angle threshold ( $T_\theta$ ) is included to make sure that points on high-angle surfaces are not removed (these are much more likely to be debris).

$$I_1 = \{ p \in P \mid (\lambda_2^n < T_\lambda) \wedge (h < T_h) \wedge (\theta > T_\theta) \}$$

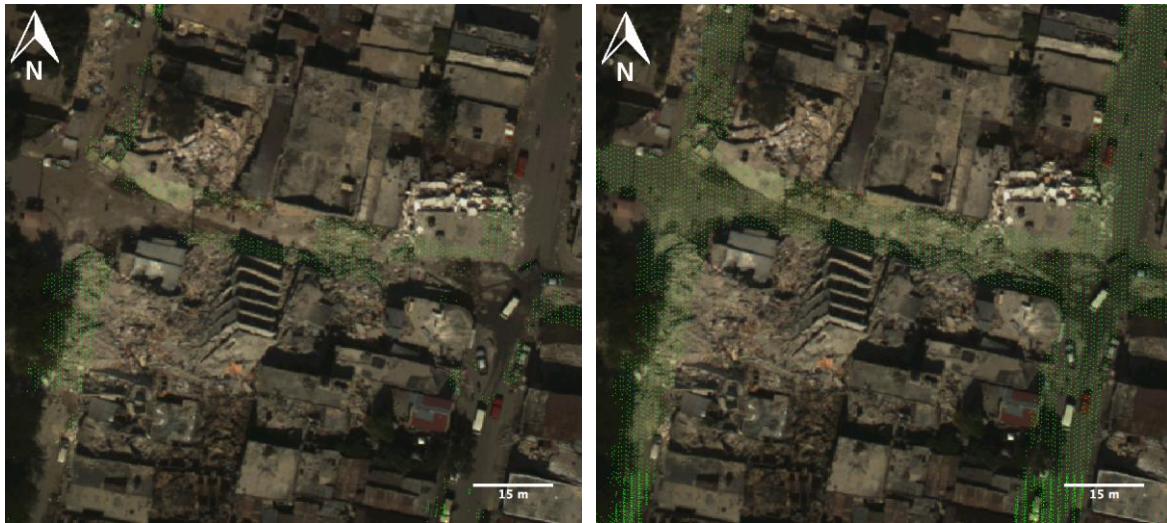
$$I_2 = \left\{ p \in P \mid \left( \lambda_2^n < \frac{T_\lambda}{5} \right) \wedge (h < T_h) \wedge (\theta > T_\theta) \right\}$$

where  $I_1$  and  $I_2$  are the indices of points classified as non-debris by the two equations above. The values of  $T_\lambda$  and  $T_\theta$  are automatically derived from critical points in the histograms of  $\lambda_2^n$  and  $\theta$ , respectively.  $T_h$  is set to the vertical point accuracy of the laser scanner. Figure 3 shows an image of a debris littered street, along with the corresponding point cloud, before and after point filtering. A majority of the points remaining after filtering belong to debris, although some points on cars and small objects near the side of the road are still sometimes present.

### 2.2.1.3 Region Growing

In order to process and analyze debris piles at the object level, individual points belonging to the same pile must be clustered together. This is accomplished through a process called “region growing.” A seed point is randomly chosen from the point cloud. The angle between the normal of the seed point, and the normals of each of its neighbors,  $\beta$ , is computed.

**Figure 3: Point filtering**

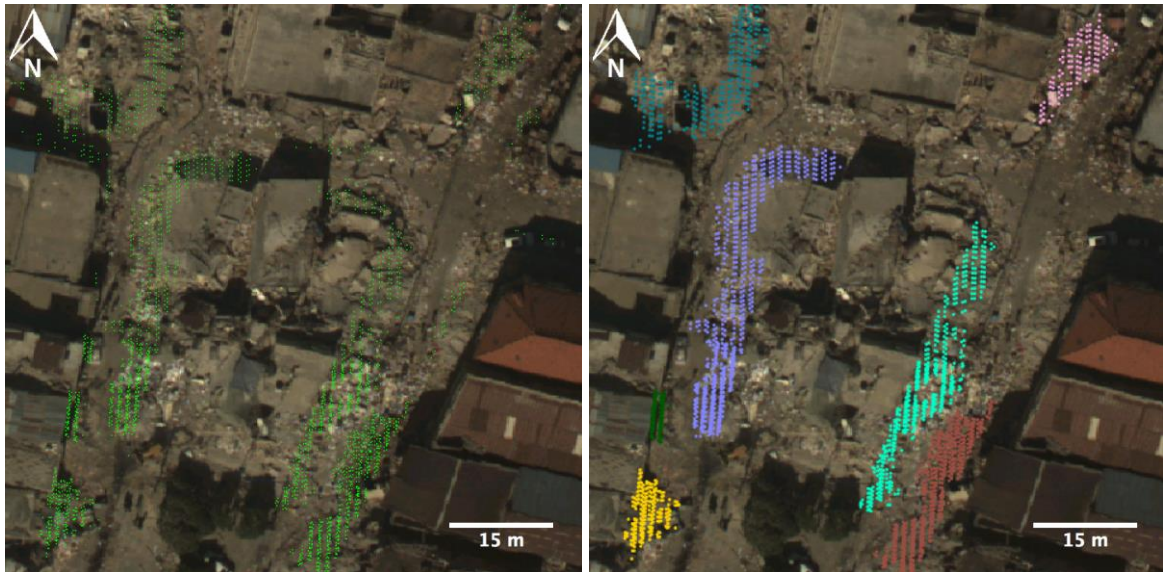


*Non-debris points in a region affected by the earthquake are removed through point filtering, the points are overlaid on an aerial image for clarity*

Any neighbor with a  $\beta$  below a certain threshold,  $T_\beta$ , is added to the region of the seed point. Through experimentation, a  $T_\beta$ , of  $10^\circ$  proved to be sufficient for preventing separate objects from merging. Points are iteratively added to the region until no points can be added, and then a new seed point is chosen. This process is repeated until all points have either been added to a region or discarded, because they couldn't be added to any region. A minimum region size of 15 points is used to discard regions that are too small to be significant. It should be noted that the minimum region size is only for the process of region growing. Debris piles are also discarded later on in the workflow after volume has been estimated by using a minimum volume threshold. Figure

4 shows the results when region growing is applied to a set of filtered points in an area with several collapsed buildings, each region is assigned a unique color.

**Figure 4: Region growing**



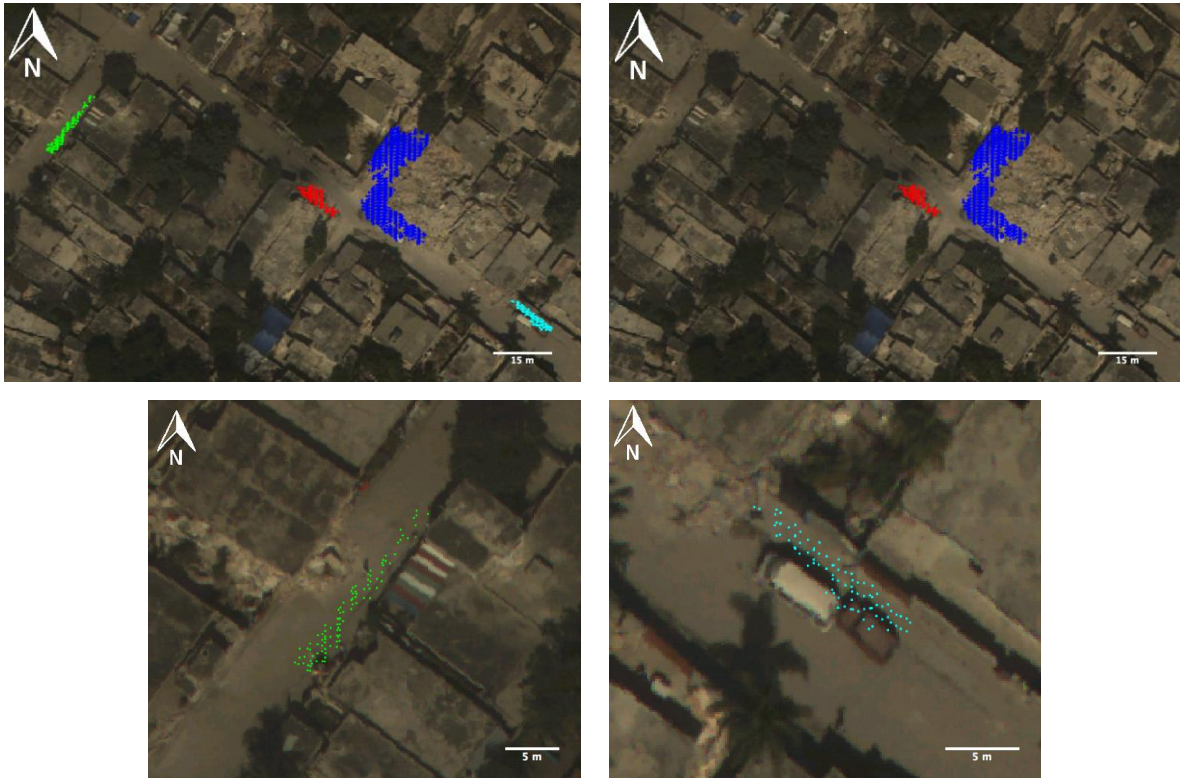
#### 2.2.1.4 Object Filtering

At this point, the initial set of objects (i.e., debris piles) has been detected. However, the results are likely to contain false alarms from small, non-debris objects such as small cars, road barriers, and medians. To filter out these objects, a metric called the height ratio (HR) is computed for each object. The height ratio is a measure of the portion of the object that is very low to the ground. Objects that have a HR greater than a threshold,  $T_{HR}$ , are discarded as non-debris objects.

$$HR = \frac{\#P_o < 2 \cdot T_H}{\#P_o}$$

where  $P_o$  are all of the points that make up an object (produced from region growing). Figure 5 shows a set of objects before and after object filtering. Object filtering is performed and removes two non-debris objects that were obtained from region growing; the two objects that are removed are a section of terrain and two vehicles parked very closely together that were mistaken for debris.

**Figure 5: Object filtering**



At this point, all of the debris piles have been detected and clustered as objects, and the debris detection stage is therefore complete.

### **2.2.2 Flood Detection**

The algorithm for detecting flooding in the roadways takes a GeoTIFF flood image (\*.tif) and a road network shapefile (\*.shp) and detects all of the pixels in the image that are believed to contain floodwater. It is highly recommended to use imagery that contains at least four spectral bands (red, green, blue, and near infrared), but the algorithm will run on three band imagery (red, green, and blue) or imagery with more than four bands (multispectral imagery). An example input flood image from the January 2016 flooding of the Mississippi River is displayed in Figure 6.

**Figure 6: Image of a house surrounded by severe flooding from the Mississippi River**



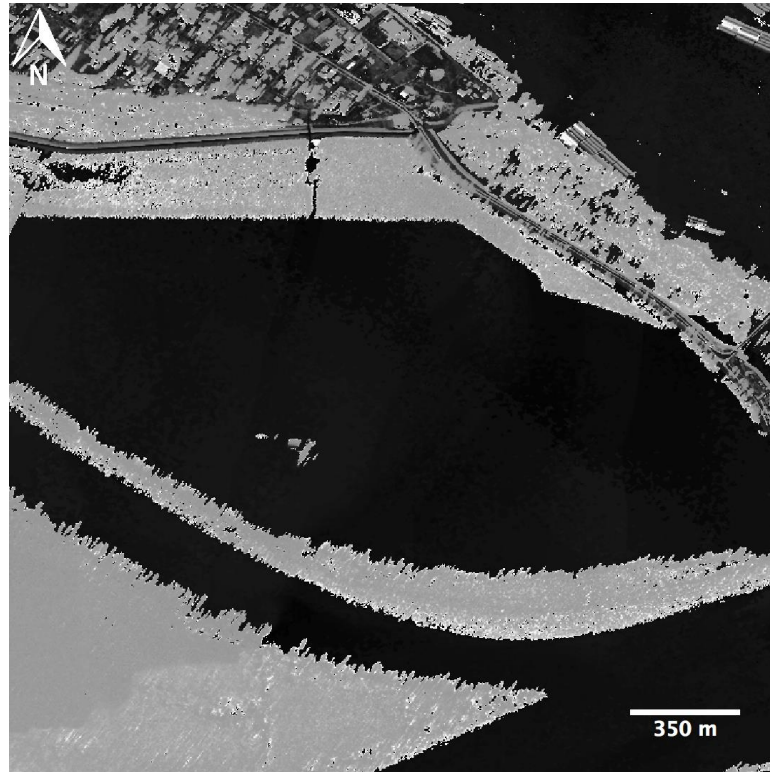
*The road from the house to the nearest street is completely flooded.*

#### 2.2.2.1 Finding a Seed Pixel

The premise behind the whole algorithm is that if one flood pixel can be obtained, then spectral information about that pixel can be used to find the rest of the flood pixels in the image. The initial flood pixel is referred to as a “seed pixel.” The algorithm was constructed such that the user has the option to pick the seed pixel(s) (a foolproof method of guaranteeing a true flood pixel is selected), or let the algorithm attempt to automatically find the seed pixel (advantageous if you need to run the algorithm on several images). Additionally, the user can select the seed pixel for one image and then use that pixel to process several images. The rest of the section will describe the automatic method of finding the seed pixel.

Apart from very shallow water, floodwaters tend to look very homogeneous from overhead imagery (as can be seen in Figure 6). To find a seed pixel, the algorithm tries to find a pixel at the center of the most homogeneous region of the image. First, the image is converted from the RGB color space to the HSV, or hue-saturation-value, color space. The hue channel is a good single band representation of the uniformity of the water. Figure 7 shows an image in RGB and the corresponding hue band.

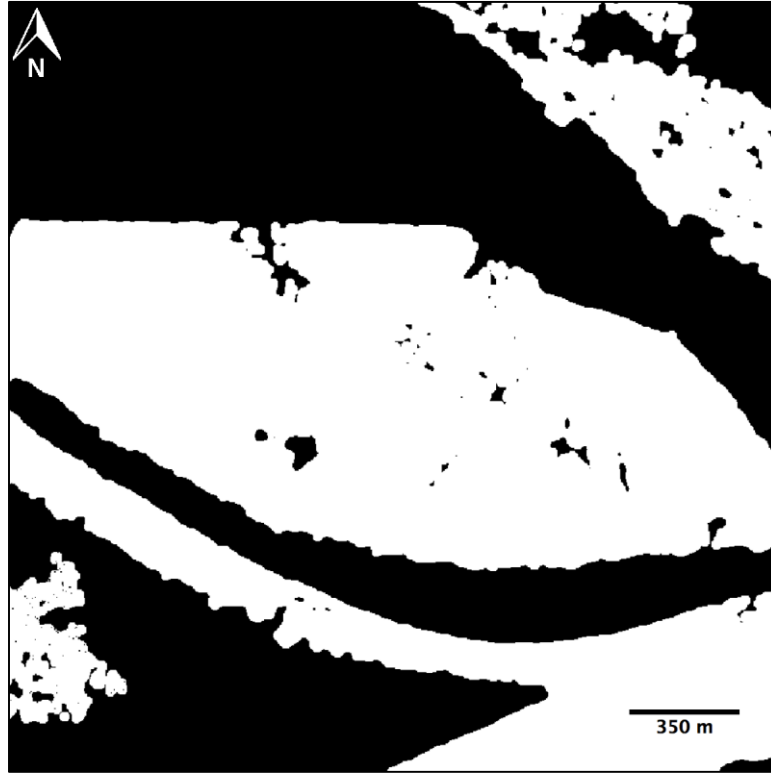
**Figure 7: Hue channel**



*Hue channel from the HSV color space of the flood image from Figure 6.  
The water appears very uniform in hue.*

An entropy image of the hue band is then calculated. Entropy is a statistical measure of randomness, and is good for analyzing texture. The entropy of each pixel is calculated using a 9x9 window of pixels around it. The lower the entropy of a pixel is, the more homogeneous the region it sits in is. This makes it a good metric for detecting water regions. The entropy image is then converted into a binary image using Otsu's method. Otsu's method creates a binary image from a grayscale image by finding a threshold that maximizes the variance between two classes, while simultaneously minimizing the variance within the classes. In this case, the two classes are high entropy regions and low entropy regions. Small areas in the resulting binary image are removed by performing a morphological opening with a disk-shaped structuring element with radius  $r_{se}$ , which is typically set to 5 pixels. Finally, connected components with less than 500 pixels are removed in an operation known as area opening. At this point, the remaining binary image contains a set of homogeneous regions. However, not all of these homogeneous regions belong to water. Figure 8 shows the set of homogeneous regions for the flood image in Figure 6.

**Figure 8: The set of homogeneous regions produced from Otsu's method**



*Morphological opening, and area opening.*

The next step is to remove regions that are unlikely to be water. These regions can be grass fields, shadows, asphalt, or any other large homogeneous area. Two masks are created to remove the erroneous regions: a dark mask and a vegetation mask. The dark mask is created by finding very dark pixels (i.e., shadows, asphalt, etc.), and the vegetation mask is created using either the Normalized Difference Vegetation Index (NDVI) if the image is 4 bands, or by finding green pixels if the image is 3 bands:

$$M_{dark} = (R < .05) \wedge (G < .05) \wedge (B < .05),$$

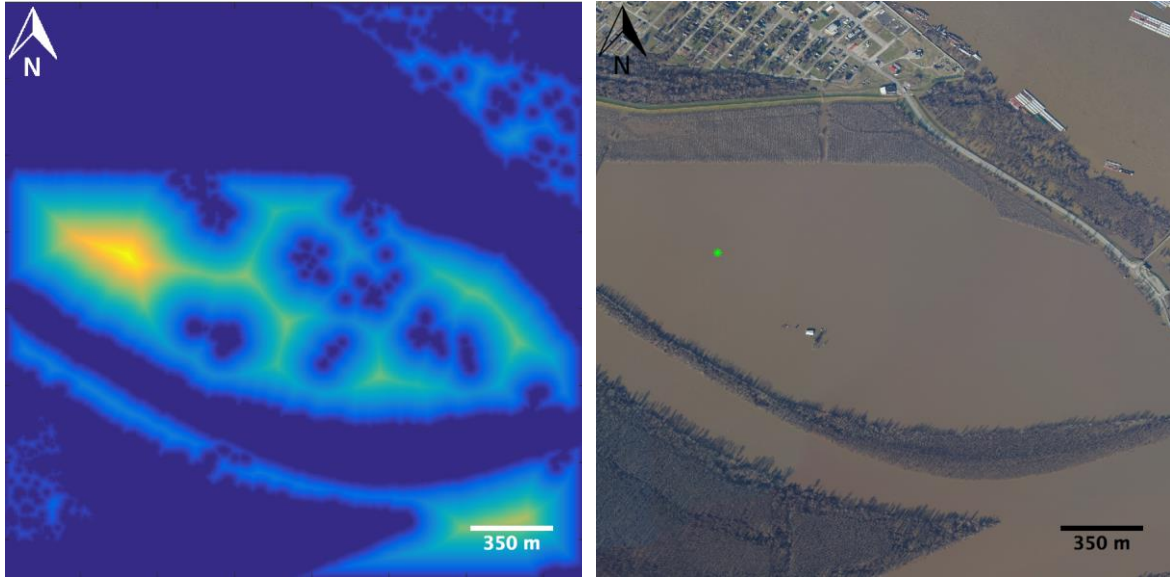
$$M_{veg4} = NDVI < -.25,$$

$$M_{veg3} = (G > R) \wedge (G > B),$$

$$NDVI = \frac{NIR - RED}{NIR + RED}$$

At this point, the remaining regions are assumed to belong to floodwater. An assumption is made that the most “flood-like” pixel will be in the middle of a homogeneous region. Therefore, the Euclidean distance transform image is calculated, and the pixel with the highest value is selected as the seed pixel. Figure 9 shows the distance transform image and the resulting seed pixel. As mentioned before, the seed pixel(s) can also be chosen manually. If there is no flooding present in the image, the automatic process will still choose a seed pixel from the most homogeneous region.

**Figure 9: Seed Pixel**



(Left) The Euclidean Distance transform is used to find the pixel the farthest from the edge (yellow = larger distance).  
 (Right) The chosen seed pixel is marked with a green star.

### 2.2.2.2 Detecting all Flood Pixels

Once a seed pixel is automatically detected or selected, it is used to detect similar pixels (i.e., flood pixels) in the image. First, spectral angle mapper (SAM) is used to find pixels that are very similar to the seed pixel. SAM is a target detection method that works by calculating the angle between the spectral vector of the seed pixel and the spectral vector of all other pixels in the image. Pixels with spectral angles below a certain threshold,  $T_{SAM}$ , are stored for use in the next step.  $T_{SAM}$  is set to 0.075 in practice. The equation for calculating the SAM statistic is:

$$r_{SAM}(\mathbf{x}) = -\cos^{-1}\left(\frac{\mathbf{s}^T \mathbf{x}}{\sqrt{(\mathbf{s}^T \mathbf{s})(\mathbf{x}^T \mathbf{x})}}\right)$$

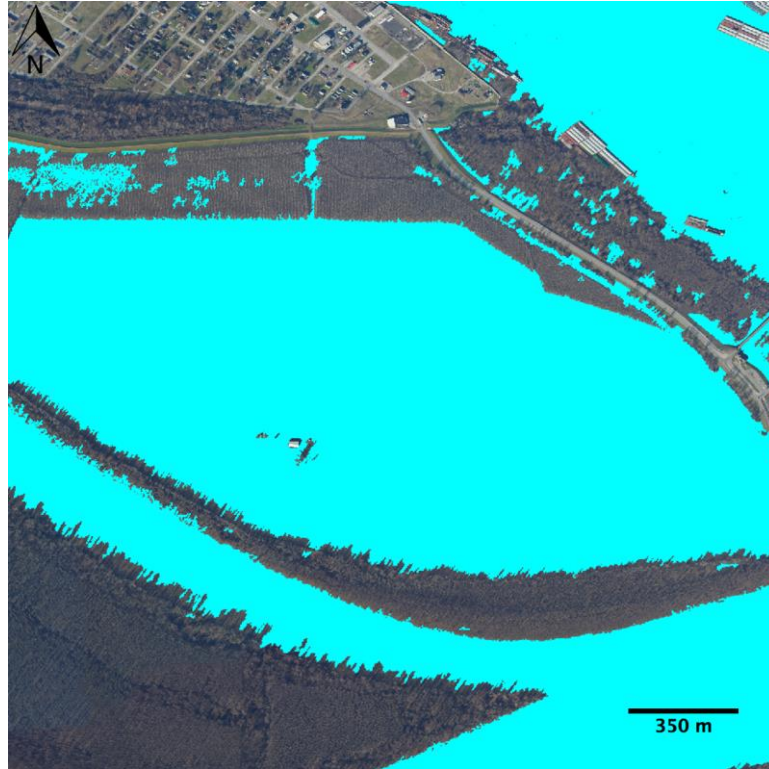
where  $\mathbf{s}$  is the spectral vector of the seed pixel (or the mean of all seed pixels if there are multiple), and  $\mathbf{x}$  is the spectral vector of a test pixel.

There is some variation in the spectra of flood pixels due to things like water flow and water depth. To try to detect all of the flood pixels despite these variations, another target detection method, the Quadratic Matched Filter (QMF) is used. The QMF takes into account the variation of both the background and the target, and is good at mitigating false alarms. Typically the QMF would also take into account noise, but it was decided to ignore this term for simplicity in the implemented algorithm. Pixels with a QMF detection statistic,  $r_{QMF}$ , greater than a certain threshold,  $T_{QMF}$ , are the detected flood pixels.  $T_{QMF}$  was set to 80 during testing. The QMF equation is:

$$r_{QMF}(\mathbf{x}) = (\mathbf{x} - \boldsymbol{\mu}_b)^T \boldsymbol{\Sigma}_b^{-1} (\mathbf{x} - \boldsymbol{\mu}_b) - (\mathbf{x} - \boldsymbol{\mu}_s)^T \boldsymbol{\Sigma}_s^{-1} (\mathbf{x} - \boldsymbol{\mu}_s) + \log \frac{|\boldsymbol{\Sigma}_b|}{|\boldsymbol{\Sigma}_s|}$$

where  $\mu_b$  is the mean spectrum of the background (in this case, the entire image),  $\mu_s$  is the mean spectrum of the target pixels (the pixels detected from SAM),  $\Sigma_b$  is the covariance matrix of the background, and  $\Sigma_s$  is the covariance matrix of the target pixels. Figure 10 shows the results of QMF on the flood image from Figure 6.

**Figure 10: The flood pixels detected by the QMF are shown in cyan**



At this point, all the flood pixels in the entire image have been detected. The goal is to find flood pixels in the roadways, so the detection can then be segmented to the roadways by simply multiplying by a road mask. The road mask is calculated by converting the road network shapefile into a road mask the same size as the flood image. Figure 11 shows the roadway flood pixels, as well as a pre-flood image of the same scene for comparison.

**Figure 11: Roadway detection**



(Left) A pre-flood image of the scene from Google Maps.  
(Right) The detected roadway flooding pixels

### 2.2.3 Results

To understand the performance capabilities of the algorithms, it is vital to test them on datasets for which some reference of what the expected results should be has been created.

#### 2.2.3.1 Debris Results

Reference data to validate the debris detection results for seven scenes in Haiti were created by manually tracing every pile visible in the high-resolution (0.15m) imagery that was simultaneously captured with the lidar data. The bounding polygons of the 2-D projections of the detected debris piles are intersected with the set of validation polygons for each scene. If a debris pile polygon detected by the algorithm overlaps with a validation polygon, then it is classified as a true positive (TP). If there is no overlap between the detected debris polygon and any of the validation polygons, then it is labeled as a false positive (FP). If a validation polygon does not overlap any of the detected debris polygons, then it is classified as a false negative (FN). The validation polygons are sometimes larger than the detected polygons because debris that was present in the nadir aerial imagery is very low to the ground and discarded during the point filtering stage of debris detection. The low points are intentionally discarded as insignificant contributions to the overall debris pile. Therefore, no threshold is placed on the amount of overlap between the two sets of polygons to achieve a correct detection. During validation, if a digitized pile was found to be completely below the minimum height threshold, it was deleted and the results were recalculated. The TP, FP and FN counts are used to characterize the performance in terms of completeness, correctness, and quality

$$\text{Completeness} = \frac{TP}{TP + FN} \times 100$$

$$\text{Correctness} = \frac{TP}{TP + FP} \times 100$$

$$\text{Quality} = \frac{TP}{TP + FP + FN} \times 100$$

. Completeness reflects the percentage of validation debris piles that are detected by the algorithm. Correctness reflects the percentage of detections that are true debris piles. Quality is a measure of overall performance that takes into account both the completeness and the correctness of the results. The results for all seven of the scenes are displayed in Table 1.

**Table 1: Debris detection results for the seven test sites**

Site	Number of Validation Piles	TP	FP	FN	Completeness [%]
1	21	24	3	0	100
2	5	5	0	0	100
3	14	13	0	0	100
4	9	8	1	1	88.89
5	11	11	3	0	100
6	7	7	1	0	100
7	21	24	3	1	96
<b>All</b>	<b>88</b>	<b>92</b>	<b>11</b>	<b>2</b>	<b>97.87</b>

The proposed algorithm achieved an overall quality score of approximately 88% when tested on seven scenes (containing a total of 88 validation debris piles), indicating that it is capable of satisfactory performance in automated roadway debris pile detection. Even more importantly, the algorithm achieved a completeness score of approximately 98%. The completeness metric penalizes false negatives, which in the case of debris detection for emergency response, are arguably more costly than false positives. A false negative could result in an ambulance that is transporting critically injured survivors to take a route to the hospital that is blocked by debris. The ambulance would have to turn around and attempt to find a new route, preventing the injured from getting timely treatment and possibly even resulting in death. Of the 88 validation debris piles, only two were missed, and no more than one pile was missed in a single scene. Figure 12 shows debris pile polygons (red), and polygons of the debris piles detected by the algorithm (teal), are overlaid on aerial imagery.

**Figure 12: Debris results validation**



The eleven false positives that were detected were the result of large vehicles or clusters of small vehicles being mistaken for debris. These false positives are much smaller than the actual debris piles produced from collapsed

buildings, and could be alleviated using a higher minimum volume threshold (20m<sup>3</sup> was used during testing) or using lidar data with a higher point density.

### 2.2.3.2 Flooding Results

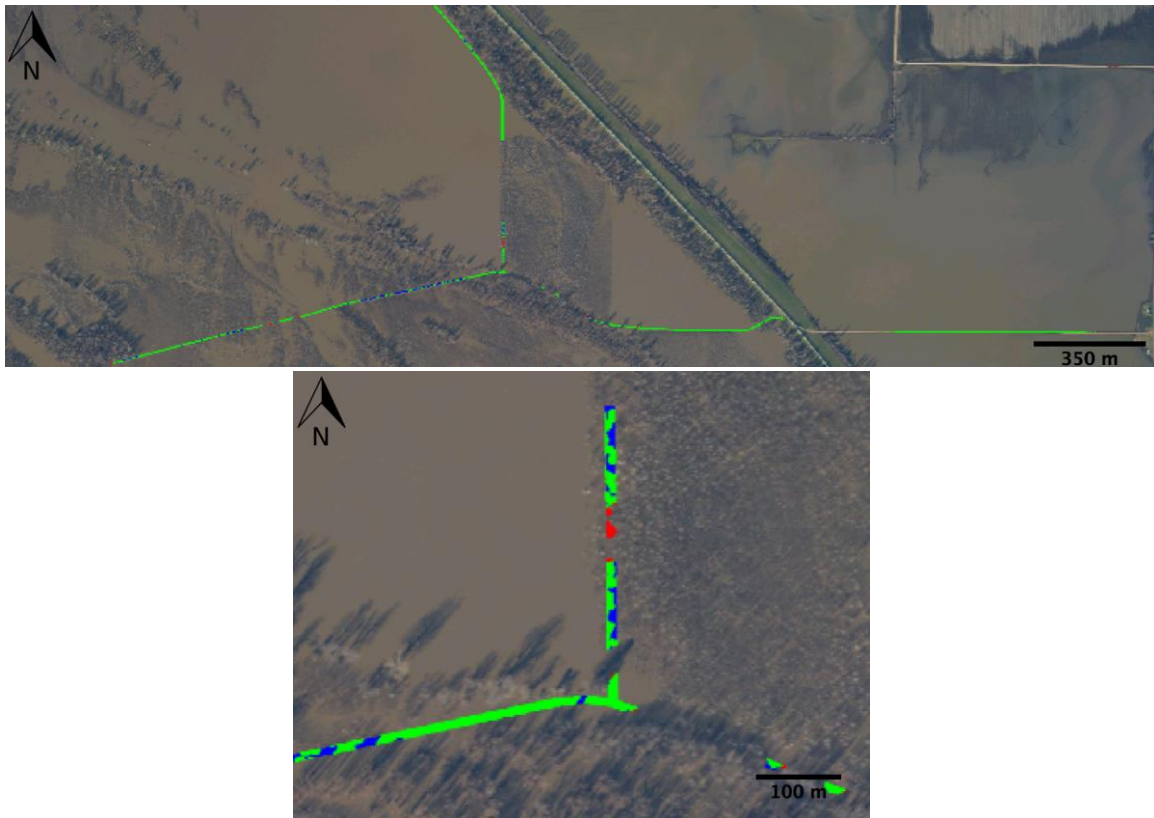
The goal of the flood detection algorithm is to detect flooded roadways. To assess the results of the algorithm, bounding polygons of flood pixels within road boundaries were manually digitized using GIS software. The flood algorithm was tested on five flood images and a pixel-to-pixel comparison was performed using the output and the validation polygons. The same metrics that were used for the debris detection validation (TP, FP, FN, completeness, correctness, and quality) were used for flooding. Overall, the flood detection algorithm was successful in detecting roadway flood pixels, achieving a quality score of 92% across the five scenes. Completeness and correctness scores of approximately 95% and 97%, respectively, suggest that false negatives and false positives are minimal. Figures 13 and 14 show the detection results for the first two scenes, along with some examples of false positives and false negatives.

**Table 2: Roadway flood pixel detection results**

<b>Image ID</b>	<b>Number of Flood Pixels</b>	<b>TP</b>	<b>FP</b>	<b>FN</b>	<b>Completeness [%]</b>	<b>Correctness [%]</b>	<b>Quality [%]</b>
flood1	91,297	83,156	6,002	8,141	91.08	93.27	85.46
flood2	125,444	122,698	926	2,746	97.81	99.25	97.09
flood3	33,171	30,687	1,415	2,484	92.51	95.59	88.73
flood4	37,862	36,067	115	1,795	95.26	99.68	94.97
flood5	16,836	16,307	976	529	96.86	94.35	91.55
<b>All</b>	<b>304,610</b>	<b>288,915</b>	<b>9,434</b>	<b>15,695</b>	<b>94.85</b>	<b>96.84</b>	<b>92</b>

Figure 13 displays a detection result image for the first flooding scene. The image is color coded such that a green pixel indicates a true positive, a red pixel indicates a false positive, and a blue pixel indicates a false negative. The false positives for this image mostly appear in pixels within areas with a lot of trees. It is likely that these false positives are actually true flooding pixels that were neglected when the validation set was created. It is extremely meticulous to label every pixel, especially when they are individual or small groups of pixels in between trees. A majority of the false negatives are caused by shadows cast by trees across the roadways. The shadows affect the spectra of the pixels in regions that are actually flooded, preventing them from being detected. Additional spectral bands in the shortwave infrared (SWIR) could help to prevent shadowed flood pixels from being neglected. Despite the small amount of false positives and false negatives, a vast majority of the roadway flood pixels are detected and can be passed on to the depth estimation stage of the algorithm.

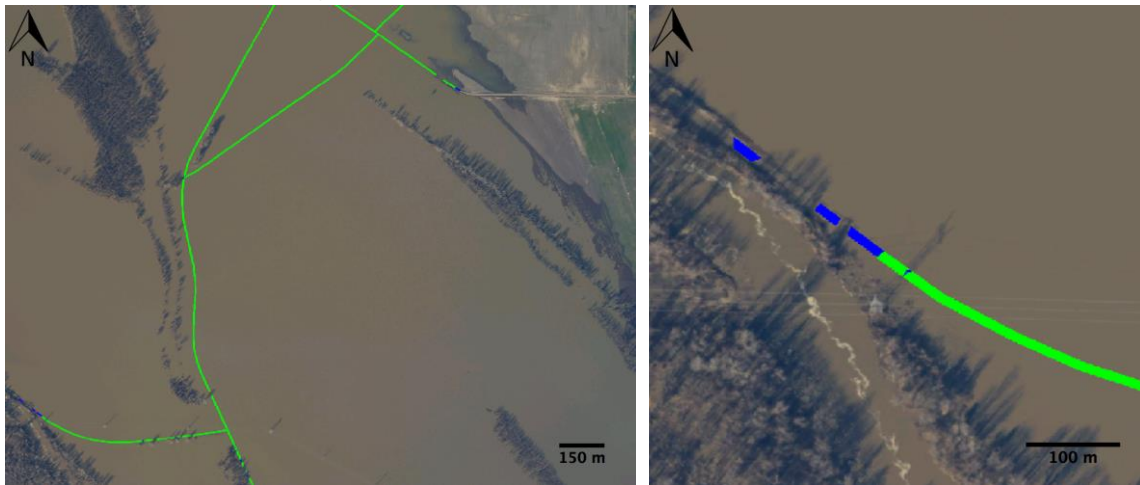
**Figure 13: Roadway flood detection scene**



*(Top) Roadway flood detection results for scene 1. Green = TP, red = FP, blue = FN.  
(Bottom) A zoom view reveals that most FPs and FNs are caused by shadows, trees, etc.*

Scene two (Figure 14) contained almost no false positives. Similar to scene one, the majority of the false negatives are the result of shadow regions. In some cases, the shadow regions are detected by the QMF, but are so small because they are isolated from the rest of the pixels that they are accidentally removed during the area opening stage. Given the 97% completeness and 98% correctness for this image, it is safe to say that accurate information products can be derived from the detected roadway flood pixels.

**Figure 14: Roadway flood detection scene 2**



*(Left) Roadway flood detection results for scene 2. Green = TP, red = FP, blue = FN.*

*(Right) A zoom view reveals that most FNs are caused by small flood regions that were removed during the morphological and area openings*

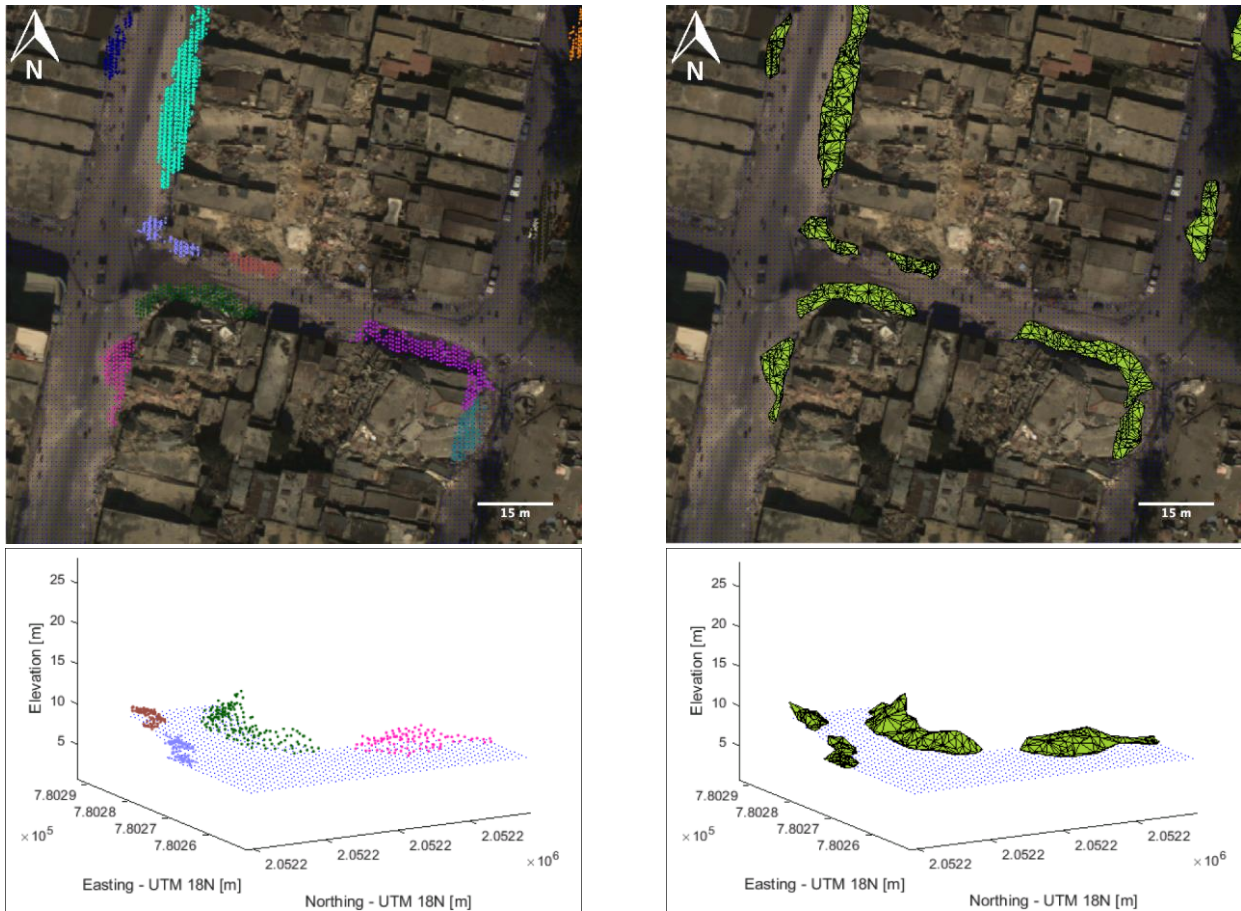
## 2.3 Quantification of Debris and Floods

In the previous section, the algorithms for detecting roadway debris piles and flooded areas were described in detail. Those algorithms take CRS data as input and automatically detect the roadway obstructions. Although the location of obstructions are a valuable information product, it is beneficial to take the processing a step further and characterize the obstructions in terms of size. For debris piles in the roadway, this means calculating the volume. For flooded portions of the roadway, this means calculating the depth of the water. Not only does this additional information allow someone to look at a map of the obstructions and determine their severity, but it also feeds into the Access Restoration module to determine restoration times and optimal routes.

### 2.3.1 Debris Volume Estimation

Debris detection results in a set of debris pile point clusters, or the lidar points that sample the true surface of the debris pile. The volumes of these debris piles are then estimated one by one. First, the DEM points that fall within the boundaries of the 2-D projection of a debris pile are appended to the pile for improved volume estimation. This is because it is assumed that each debris pile sits flush on the terrain below it. Each pile is then modeled as a 3-D surface using alpha shapes. Alpha shapes are parameterized by an alpha radius,  $\alpha$ , which controls how tightly the surface wraps around the set of points. For volume estimation, it is important that the alpha radius is large enough to form a closed surface around the points. Setting  $\alpha$  to  $3 \cdot \mu_k$  (where  $\mu_k$  is the mean distance between a point and its  $k$  neighbors) is sufficient for generating closed surfaces around the debris piles. Once a debris pile has been modeled using alpha shapes, it can be treated as a set of tetrahedrons whose individual volumes are computed and summed to find the total volume for the pile. This process is carried out for each debris pile. Figure 15 shows a set of roadway debris piles in Haiti before and after alpha shape reconstruction. Additional information about this can be found in Appendix B: Algorithms for Detection of Roadway Debris and Flooding. Moreover, a user manual was developed to illustrate the usage of these algorithms, the manual can be found in Appendix G: Debris Utility User Manual.

**Figure 15: Volume estimation**

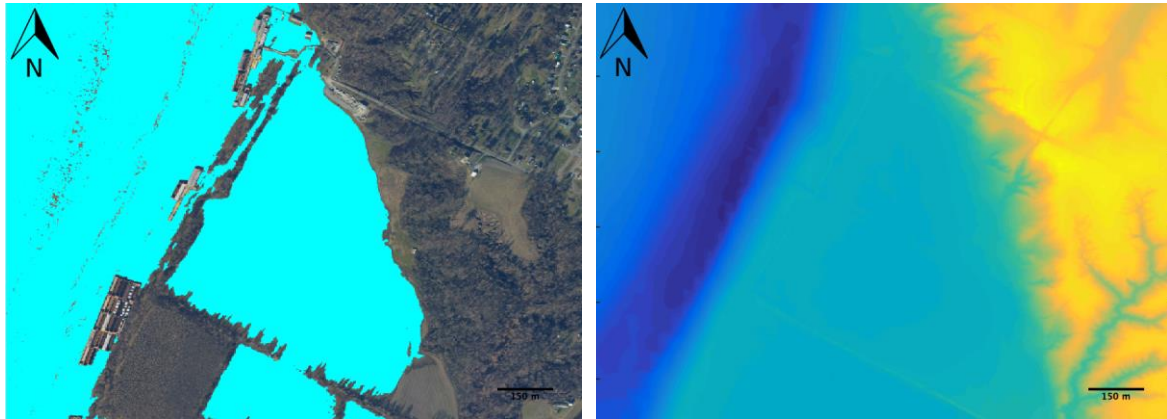


*A set of detected roadway debris piles from Haiti is reconstructed as alpha shapes for volume estimation. The images above show an overhead view overlaid on imagery, and 3-D views are shown below. The colors in the top left image correspond to those in the bottom left view.*

### 2.3.2 Flood Depth Estimation

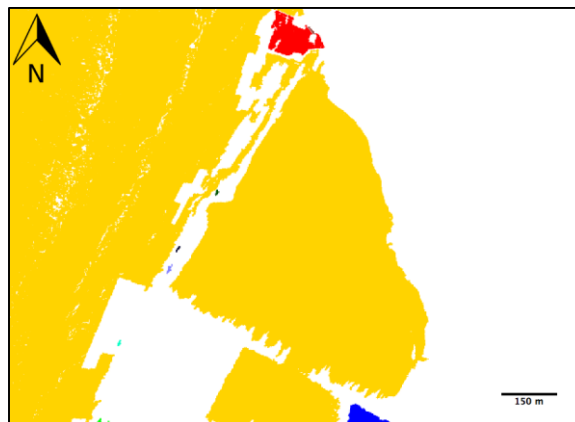
Inputs to the depth estimation stage include the road mask (produced from the road network shapefile in the detection stage), the flood classification image (produced in the detection stage), and a digital elevation model (DEM) raster that covers the same region as the flood image that was the input in the detection stage (it can cover a larger region as long as it fully covers the flood image). The DEM image is converted to the same coordinate system as the flood image, and then resampled to match its resolution. Figure 16 displays a classified flood image and a corresponding resampled DEM.

**Figure 16: A classified flood image and the corresponding digital elevation model**



Rather than estimate the depth for all flood pixels at once, the depth is estimated for each connected component separately. This follows the assumption that continuous regions of water sit at the same level. The flood image is converted into a label image in which each connected component is assigned a unique integer. Figure 17 shows the label image for the flood map in Figure 16.

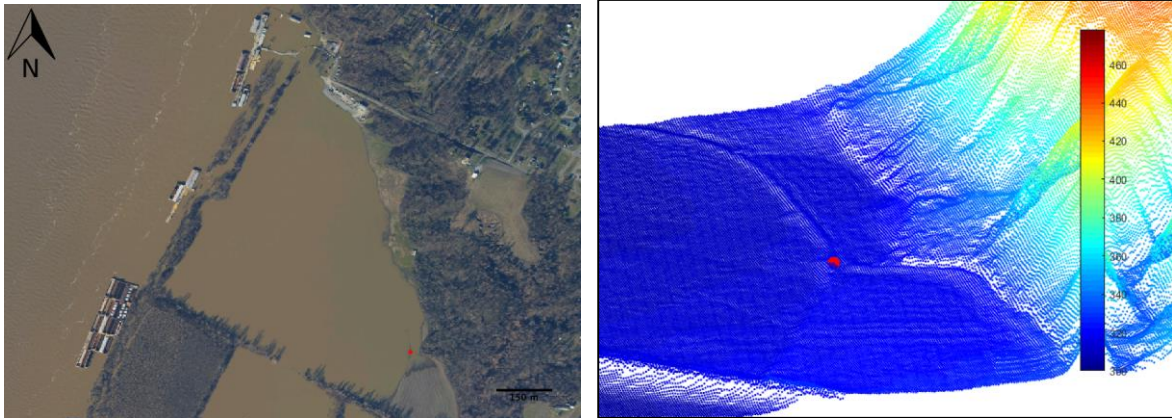
**Figure 17: Flood pixels**



*Each connected component of the flood pixels is assigned a unique integer (shown as different colors).*

The next step is to find the water depth for each flood pixel in the roadways. This is accomplished by finding the elevation at the boundary between water and land for each connected component. We are only interested in connected components that touch the roads, so the other components are discarded. There are several hundred or thousand pixels at the border of each connected component, but we only want to take the elevation from one. The pixel with the max elevation is chosen because it is typically the most accurate measure of the water level. The difference in elevation between each DEM pixel and the pixel at the water border is equivalent to the water depth, so all of the DEM pixels in the connected component are subtracted from the max elevation pixel. Figure 18 shows the max elevation pixel selected for an image, as well as the max elevation point on a 3-D view of the DEM. The 3-D view illustrates that the calculated max elevation point is indeed on a raised ridge, confirming that it is a high point at which the water meets the land.

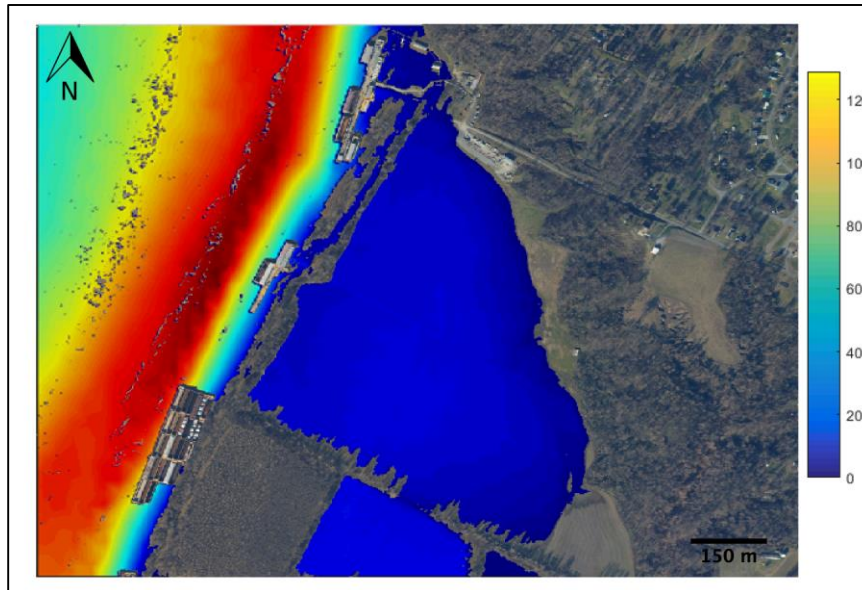
**Figure 18: Water elevation**



*The maximum elevation at which the water meets the land is calculated and represented as a red circle in both an overhead image and the DEM point cloud. From the 3-D view it can be seen that the point lies on a raised ridge. The scalebar on the DEM corresponds to elevation in feet.*

Figure 19 shows the calculated water depths (in feet) overlaid on top of the regular image. It should be noted that the water depths are only valid for regions that are land flooded by water. Regions that are already water (in this case, the Mississippi River) have an elevation value of zero in the DEM, and therefore blow up to really large values when subtracted from the max elevation.

**Figure 19: A depth map for regions of the image that were classified as flooded**

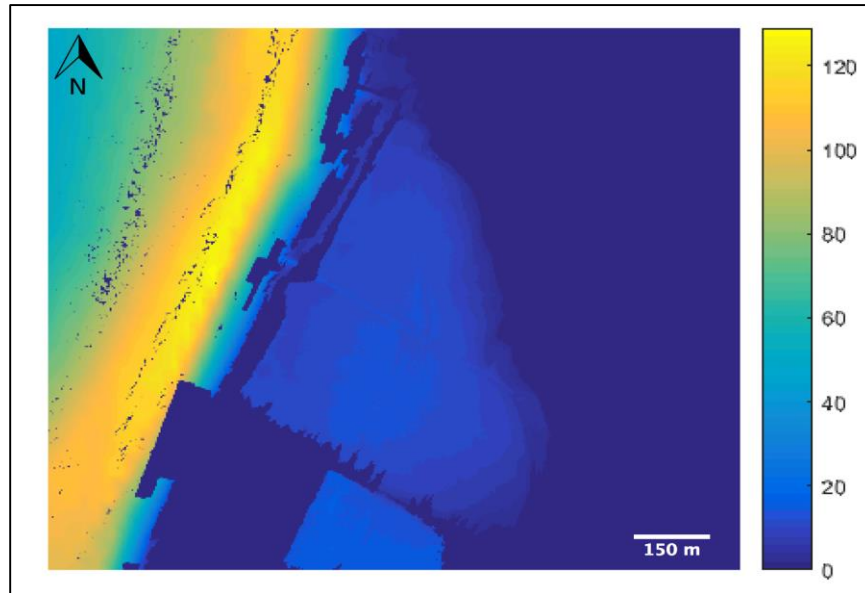


*The colorbar shows the water depths in feet. The depths are only valid for actual land regions (the extremely large depths on the left of the image are caused by DEM values of zero in the Mississippi River).*

This could be avoided by limiting the depth image to only the roadways, but that would also throw out a lot of valid flood depth information, so it is retained instead. When the depths are exported to shapefiles, only the roadway water depths are included. Figure 20 shows the actual depth image that the algorithm produces (the overlay is just for visualization here). Additional information can be found in Appendix C: Generating GIS

Products from Detection and Characterization Algorithm Outputs. Moreover, a user manual was developed to illustrate the usage of these algorithms, the manual can be found in Appendix H: Flood Utility User Manual.

**Figure 20: The depth map produced by the algorithm**



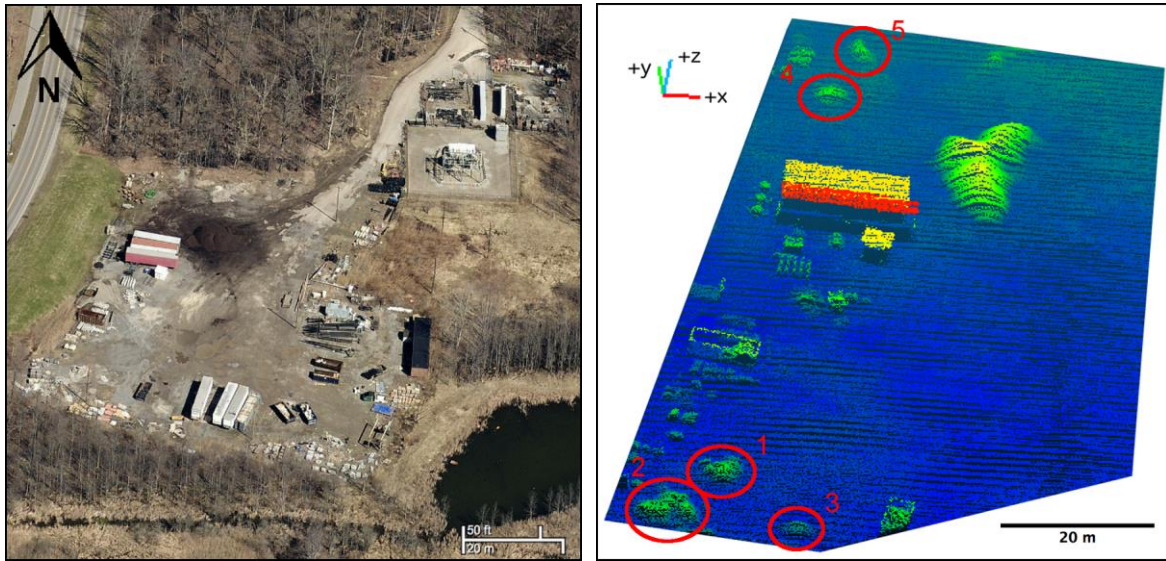
*Pixels that were classified as non-flood have values of zero. The colorbar shows the water depths in feet.*

### 2.3.3 Results

#### 2.3.3.1 Debris Volume Estimation

There is no direct way to validate the volumes estimated for the debris piles in Haiti because no field data were ever published for the volume of individual piles. Even if individual pile volume data were published, it would have to have been measured within a few days of when the lidar data were collected to be consistent. Rather than validating the volumes directly, an experiment was conducted to measure the agreement between volumes obtained from high resolution, ground-based scans and airborne scans of debris piles from construction sites. This method characterizes the volume estimates from airborne lidar data in comparison to what can be obtained on the ground. Terrestrial and airborne laser scans were collected of debris piles at two locations in Rochester, NY. Figure 21 shows an image and lidar scan of one of the construction sites. Figure 22 shows both airborne and terrestrial point clouds of the same debris pile to highlight the difference in point densities of the two modalities.

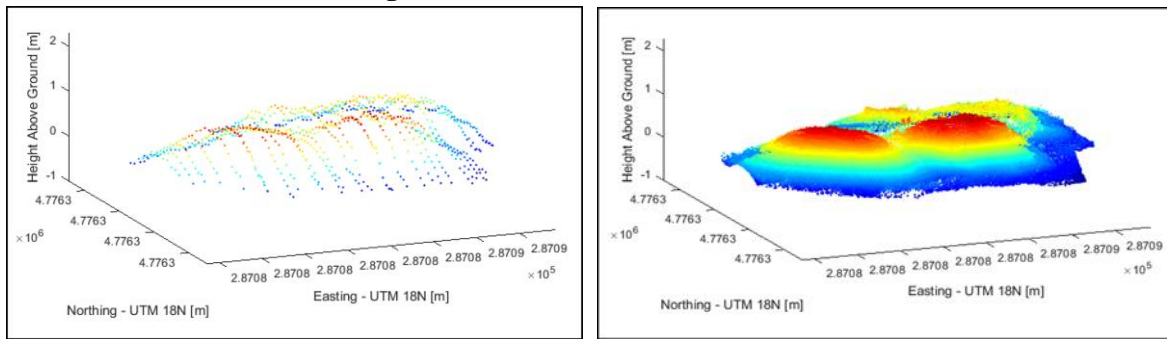
**Figure 21: Debris estimation results**



*One of the two construction sites in Rochester, NY. The image was taken two months before the lidar data were collected, so the contents of the site differ in many spots. The five debris piles used in this study are circled in red and numbered.*

Each of the two airborne point clouds (one for each construction site) was input to the debris detection and volume estimation algorithm. The debris piles are in parking lots, rather than roads, so no road vector input was used in this case. The algorithm produces a set of debris pile point clouds, as well as a set of alpha shape reconstructions of the piles. The algorithm detected many more debris piles than were actually scanned (only a portion of the debris piles at each site were scanned due to time constraints), and in some cases, piles that were in close proximity to one another were segmented as one large pile. To be able to accurately compare the volume estimates, only the piles matching the ground-based piles could be considered. To ensure that this was the case, the piles were segmented using the bounding polygons of the ground-based piles and then reconstructed again as alpha shapes. Once the piles are reconstructed as alpha shapes, the volume is computed by simply summing the volumes of the individual tetrahedrons that make up the alpha shape.

**Figure 22: Volume estimation results**



*Point clouds of a debris pile from a construction site in Rochester, NY. The terrestrial cloud is much denser with 59,348 points compared to the 899 points of the airborne cloud.*

The debris piles from the terrestrial lidar scans are already segmented into individual piles so they cannot be used as inputs to the algorithm. Instead, they are simply reconstructed as alpha shapes and the volumes are obtained. A comparison of the volumes computed for the airborne and terrestrial scans is presented in Table 3.

At full density (52.3 pts/m<sup>2</sup> and 20.6pts/m<sup>2</sup> for lots 1 and 2, respectively) the algorithm calculated volumes with a mean error of  $1.25 \pm 0.9$  m<sup>3</sup>, with a maximum error of 3.33 m<sup>3</sup>. The absolute value of the volume differences was used to obtain the mean error. This translates to a mean error of  $9.83 \pm 8.58\%$ . If the analysis is limited to debris piles with a ground-measured volume of 20 m<sup>3</sup> or higher (this is the minimum volume threshold used for the detection testing) the mean volume error becomes  $1.71 \pm 1.06$  m<sup>3</sup>, translating to a mean error of  $4.26 \pm 3.47\%$  (see Table 3). Debris-clearing rates of typical machinery can be in excess of 200 m<sup>3</sup>/hr so an estimation error of around 3 m<sup>3</sup> would likely be insignificant to a mathematical model used for prioritization of response activities. These results suggest that at these resolutions, airborne lidar scans can be used as inputs to the proposed algorithm, and will generate reasonably accurate estimates.

**Table 3: Comparison of volume estimates using terrestrial lidar and airborne lidar**

Pile ID	# Points (Ground)	# Points (Air)	Volume (Ground) [m <sup>3</sup> ]	Volume (Air) [m <sup>3</sup> ]	Volume Difference [m <sup>3</sup> ]	Volume Difference [%]
LOT1 PILE1	37367	529	10.26	10.78	-0.52	5.03
LOT1 PILE2	129688	1132	22.62	22.82	-0.2	0.88
LOT1 PILE3	74199	313	4.13	3.41	0.71	17.33
LOT1 PILE4	87192	398	5.09	4.74	0.35	6.84
LOT1 PILE5	43891	303	3.04	2.79	0.25	8.21
LOT2 PILE1	107566	1210	75.81	77.78	-1.97	2.6
LOT2 PILE2	96333	1813	100.19	100.58	-0.39	0.39
LOT2 PILE3	110248	1088	47.23	50	-2.77	5.86
LOT2 PILE5	37382	188	5.82	3.95	1.87	32.07
LOT2 PILE6	59348	899	25.44	24	1.44	5.68
LOT2 PILE7	53419	346	12	11.36	0.65	5.38
LOT2 PILE8	47209	787	32.45	29.12	3.33	10.27
LOT2 PILE9	56451	202	5.22	4.46	0.76	14.59
LOT2 PILE10	60483	814	25.25	26.99	-1.75	6.92
LOT2 PILE11	35678	224	6.27	5.44	0.83	13.22
LOT2 PILE12	182391	2168	123.11	121.24	1.86	1.51
LOT2 PILE13	33535	168	7.06	5.23	1.83	25.89
LOT2 PILE14	17205	210	6.71	5.74	0.96	14.34
				<b>Mean</b>	<b>1.25</b>	<b>9.83</b>
				<b>St. Dev.</b>	<b>0.9</b>	<b>8.58</b>

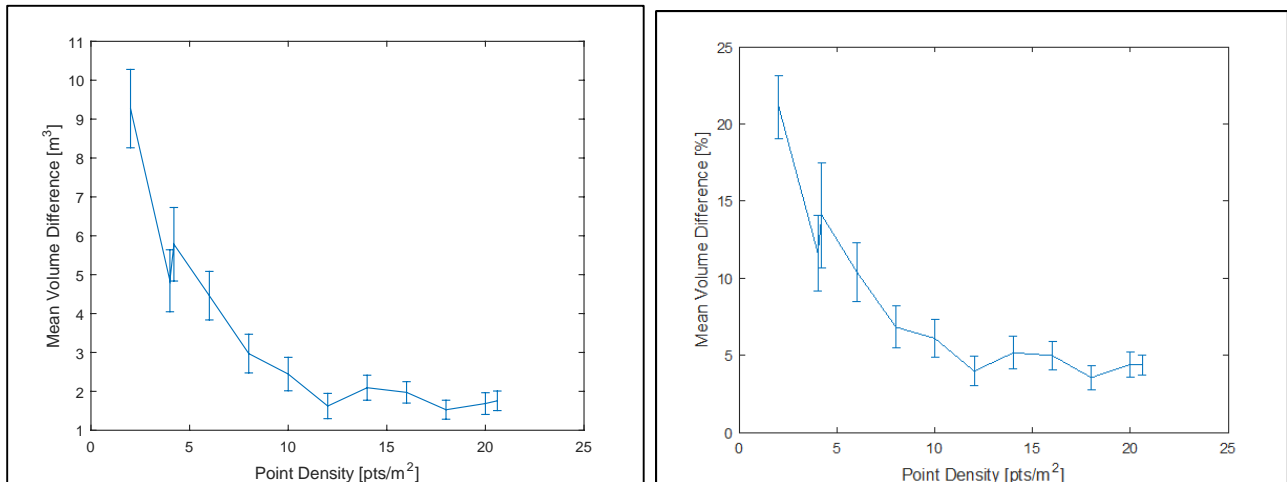
**Table 4: Comparison of volume estimates using terrestrial lidar and airborne lidar**

File ID	# Points (Ground)	# Points (Air)	Volume (Ground) [m <sup>3</sup> ]	Volume (Air) [m <sup>3</sup> ]	Volume Difference [m <sup>3</sup> ]	Volume Difference [%]	
LOT1 PILE2	129688	1132	22.62	22.82	-0.2	0.88	
LOT2 PILE1	107566	1210	75.81	77.78	-1.97	2.6	
LOT2 PILE2	96333	1813	100.19	100.58	-0.39	0.39	
LOT2 PILE3	110248	1088	47.23	50	-2.77	5.86	
LOT2 PILE6	59348	899	25.44	24	1.44	5.68	
LOT2 PILE8	47209	787	32.45	29.12	3.33	10.27	
LOT2 PILE10	60483	814	25.25	26.99	-1.75	6.92	
LOT2 PILE12	182391	2168	123.11	121.24	1.86	1.51	
					<b>Mean</b>	<b>1.71</b>	<b>4.26</b>
					<b>St. Dev.</b>	<b>1.06</b>	<b>3.47</b>

*Only debris piles with a ground-measured volume of 20 m<sup>3</sup> are included in this table.*

Although the results presented in Table 4 suggest that the proposed algorithm is able to produce accurate estimates of debris pile volumes at full resolution (52.3 pts/m<sup>2</sup> and 20.6pts/m<sup>2</sup>), it is necessary to investigate the accuracy of estimates at the resolution of the Haiti point clouds (4.2 pts/m<sup>2</sup> on average). To accomplish this, the point clouds were randomly subsampled from 20.6 pts/m<sup>2</sup> to 2 pts/m<sup>2</sup> in increments of 2 pts/m<sup>2</sup>, and the same volume comparisons were performed. Only debris piles with a ground-measured volume of 20 m<sup>3</sup> or greater were considered for this analysis. Figure 23 contains plots of the results for mean volume error in terms of both m<sup>3</sup> and percent. At the highest point density (20.6 pts/m<sup>2</sup>) errors of around 1.75 m<sup>3</sup> or 5% are obtained, and at the lowest point density (2 pts/m<sup>2</sup>) the errors are about 9.25 m<sup>3</sup> or 22%. At the mean point density of the Haiti data (4.2 pts/m<sup>2</sup>) the error is about 5.75 m<sup>3</sup> or 14%. These results suggest that while higher density data is certainly beneficial, reasonable results can still be obtained at low point densities. A mean error on the order of  $\approx 6$  m<sup>3</sup> will not have a significant effect on the computation of restoration times.

**Figure 23: Volume error estimates**



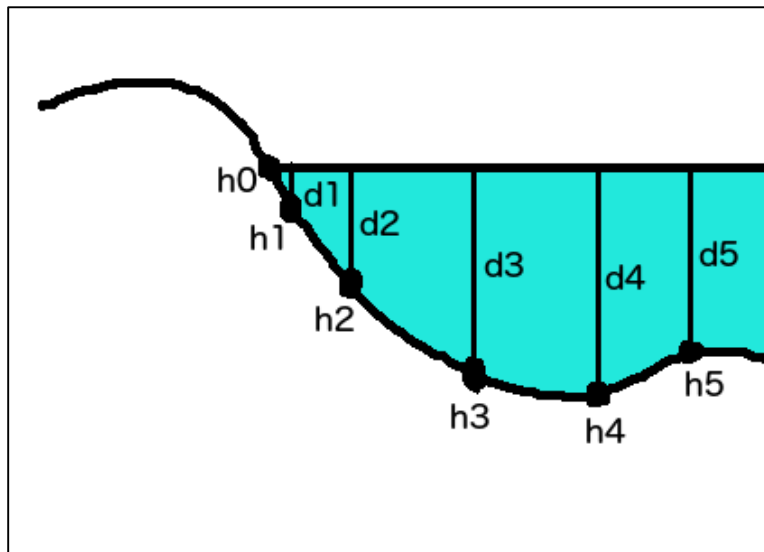
*(Left) Mean volume error in m<sup>3</sup> as a function of point density.*

*(Right) Mean volume error in % as a function of point density. Only debris piles with a ground-measured volume of 20 m<sup>3</sup> were considered for this analysis.*

### 2.3.3.2 Water Depth Estimation

Unfortunately, there is no way to validate the water depths estimated in the roadways of the Mississippi River flood imagery. To our knowledge, no roadway water depth maps were ever published. Even if they were, they would have to match up with the day the imagery was collected. Despite the lack of validation data, there are some logical checks that can be used to verify that the estimates are approximately correct. For example, the water depth should be approximately zero right at the land-water border. If the algorithm is producing very small depths at the border region (i.e., the first few pixels away from land) then it is matching what one would expect. The depths for the rest of the pixels in the same connected component can then be considered as accurate as the elevations from the DEM raster, because that is what they are based off of. Figure 24 illustrates this concept. The depth  $d_1$  is calculated by simply subtracting the pixel elevation  $h_1$  from the elevation at the land and water border,  $h_0$ . As long as the algorithm correctly finds  $h_0$ , then it is safe to assume the rest of the depths are correct. We can check that  $h_0$  is nearly correct by examining the smallest depths ( $d_1$ ,  $d_2$ , etc.).

**Figure 24: Water depth estimation illustration**



*The point  $h_0$  is the point where water meets land,  $d_1$  is the depth of the water equal to  $h_0-h_1$ ,  $d_2$  is the depth of the water equal to  $h_0-h_2$ , etc.*

Figures 25, 26 and 27 show an area of a flooded roadway at the very edge of the flood region. A depth profile is plotted for the pixels along the green line. The water depth stays flat at zero until it hits the border and then slowly increases. Figure 25 shows the overlay of roadway water depths near the water-land edge, while Figure 26 shows the depth profile of the green line from the top image, and Figure 27 shows the 2-D view of the DEM with the same depth.

**Figure 25: Overlay of roadway water depths near the water-land edge**

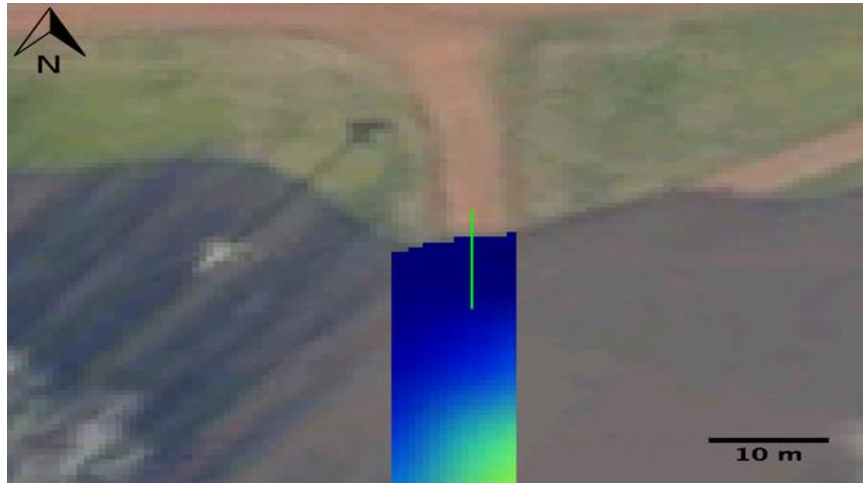


**Figure 26: Depth profile**

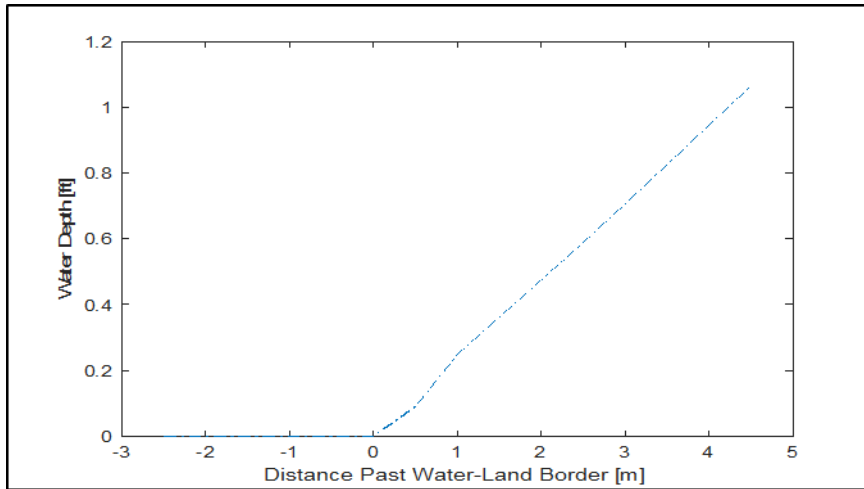
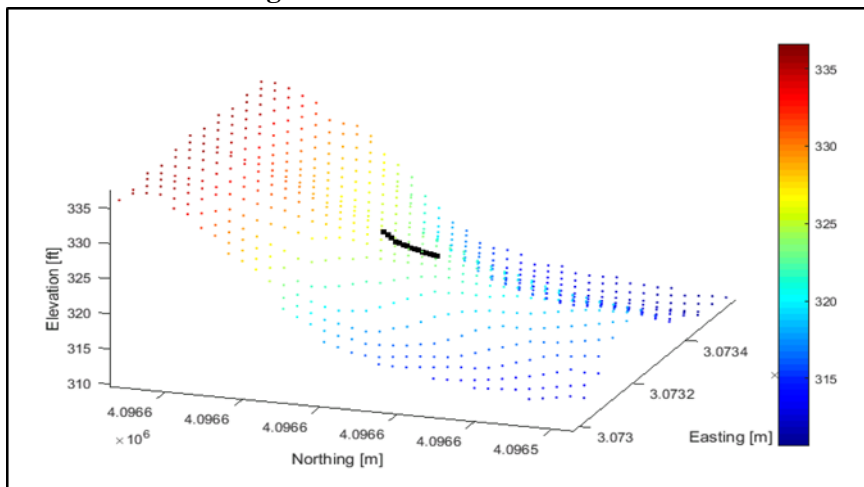


**Figure 27: 3-D view of the DEM**



The three views in Figures 25-27 show what we were expecting to find at the borders between water and land. The water depth is zero before the border, is very shallow right past the border, and then follows the shape of the DEM. The pixels in the flood imagery are 0.5 m, so every one-meter tick mark in the plot represents two pixels. The water depths are about .2 ft (2.4 in) and .4 ft (4.8 in) at distances of two and four pixels from the border, respectively. Analysis of the five test scenes revealed similar results. Although this isn't a definitive method of validation, it shows that the algorithm is estimating water depths as expected.

## **2.4 Integration of Multi-Modal/Temporal Data to Assess Disaster Impacts**

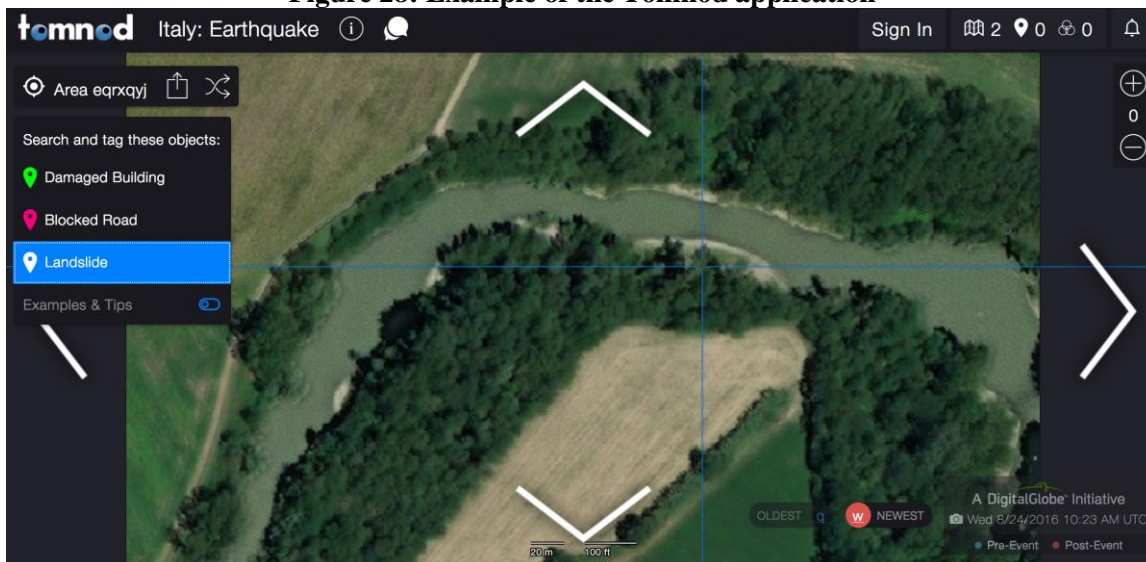
Remote sensing is the most effective way to rapidly assess the state of the transportation network and other infrastructure of a region immediately after a disaster. Overhead collection not only provides a broad view of the situation at hand, but it also allows areas that are still unsafe on the ground to be probed from above. CRS products such as lidar point clouds and high-resolution imagery can be fed into computer programs in which algorithms convert them from a raw data product into a useful information product such as a map of road obstructions. Although it was demonstrated that these programs provide a high level of accuracy, they are not without failure. No system is perfect; inevitably some amount of false positives and false negatives will exist in the outputs of these algorithms. Fortunately, a wealth of non-CRS data exists that is constantly growing and freely available to the public: volunteered geographical information (VGI).

We live in a world with a strong social media and image-sharing presence. People are constantly uploading images to their Facebook, Instagram and various other web outlets. Despite the majority of these posts being useless in the context of disaster response and transportation network analysis, the sheer volume of imagery that is constantly produced means that even the minority of useful data is still large enough to augment the information produced from CRS data. VGI can be used in many aspects of disaster response, from dictating CRS data collection schemes to crowdsourcing mapping efforts. In this report we focus on how geo-tagged image feeds can be used for validation. This section details types of non-CRS (commercial remote sensing) data that are useful for validating the information products produced from CRS data, as well as how they are best utilized.

### **2.4.1 Crowdsourcing vs. Data Mining**

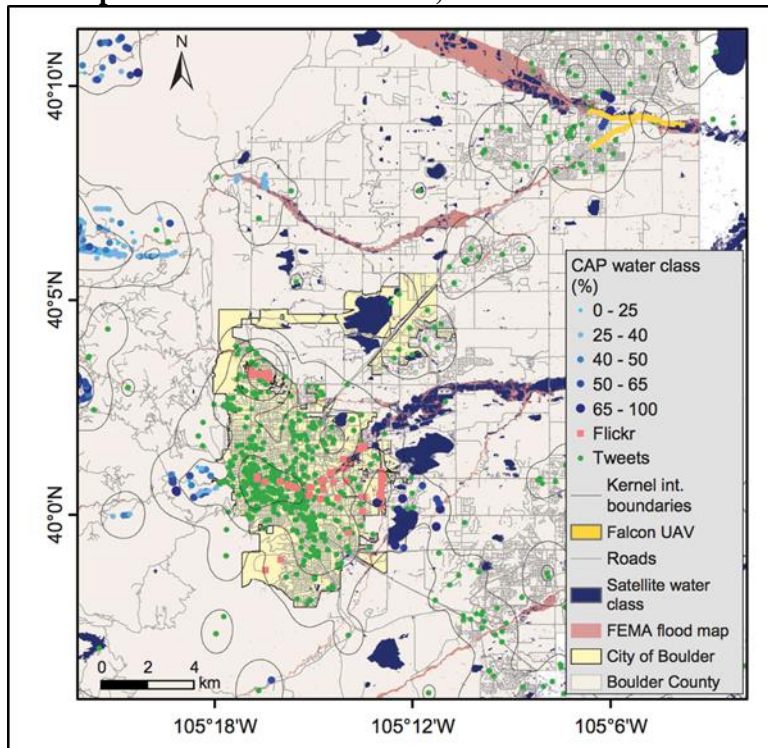
Two main methods of using non-CRS data in the disaster response process have gained popularity in recent years: crowdsourcing and data mining. Crowdsourcing typically involves a sophisticated web platform that allows users (sometimes anyone can volunteer, sometimes credentials are required) to voluntarily perform tasks that aid in the response effort. For example, tomnod is a project by Digital Globe that presents volunteers with satellite imagery and asks them to identify and label certain features (e.g., damaged buildings and blocked roadways). OpenStreetMap is a crowdsourced, worldwide mapping effort that has called on volunteers to map roads and buildings in certain disaster situations, such as the 2010 Haiti earthquake and the 2013 Typhoon Haiyan in the Philippines. Figure 28 shows a screen shot from the tomnod program. The user is presented with Digital Globe satellite imagery and asked to mark damaged buildings, blocked roads, and landslides.

**Figure 28: Example of the Tomnod application**



Data mining leverages publicly posted, geo-tagged entries (such as images or Twitter posts) to gather information about a situation. For example Cervone et. al. (2016) mined Flickr images and tweets (Twitter posts) to guide CRS image collection and infrastructure damage assessment during the 2013 floods in Boulder, Colorado. In this report we focus on data mining of imagery to validate results produced from CRS data. Figure 29 shows a map of several flood alerts obtained through data mining by Cervone et. al. (2016).

**Figure 29: A map of flood alerts in Boulder, CO from multi modal data sources**



Sources such as Twitter, Flickr, UAV imagery, and Civil Air Patrol imagery.  
Credit: Cervone et. al. (2016)

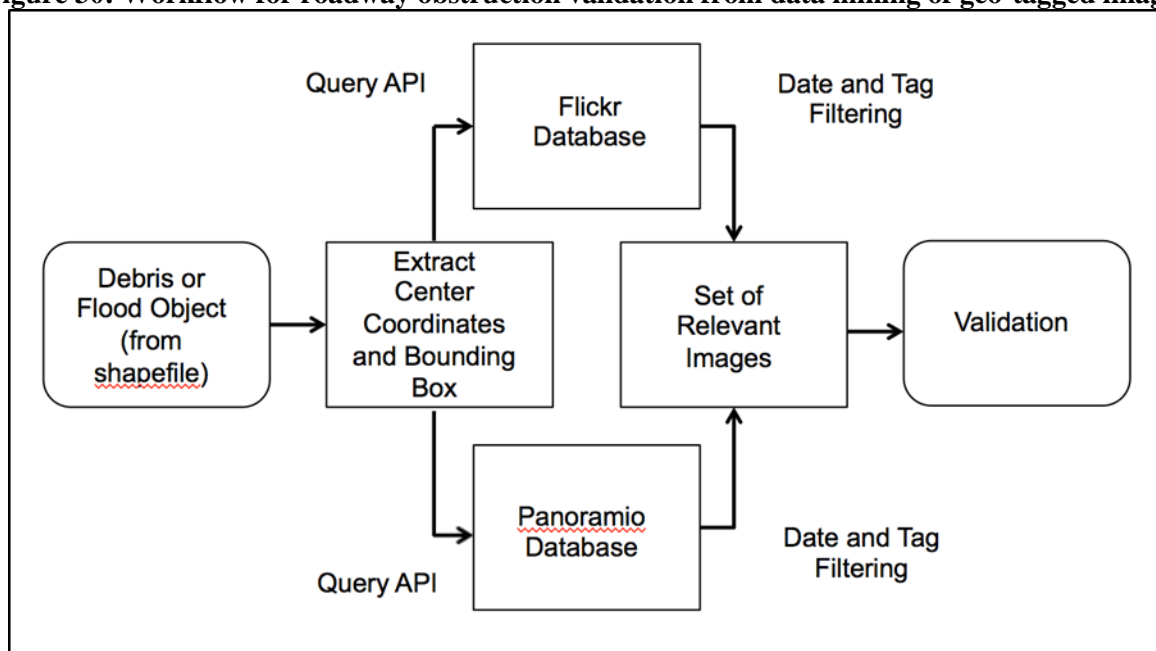
## 2.4.2 Data Sources

Photo-sharing applications such as Flickr and Panoramio allow users to upload imagery to store as well as share with their friends or the public. Along with an image, the user is able to include tags (descriptive words) about the scene, and more importantly, the geographic location at which the image was taken (in terms of latitude and longitude). The user can manually geo-tag the image by choosing the location in a map or automatically geo-tag the image if coordinates are embedded in the exchangeable image file format (EXIF) metadata. It used to be that one had to purchase an expensive camera with a built-in GPS to embed coordinate data into imagery, but the smartphone revolution changed that. Now, anyone with a standard smartphone (iPhone, Android, etc.) can choose to have their phone automatically store GPS coordinates when capturing imagery. The result of this has been a huge increase in geo-tagged images being uploaded to the Internet, with recent estimates suggesting as high as 100 million per day. Luckily, both Flickr (a Yahoo company) and Panoramio (a Google company) have application program interfaces (APIs) that facilitate the mining of imagery. There are several other outlets similar to Flickr and Panoramio, but they are smaller and less accessible so they will be excluded from this discussion.

## 2.4.3 The Use of Flickr and Panoramio for Validation

This section discusses an example of how Flickr and Panoramio could be used to validate the outputs of the debris and flood detection algorithms, and to some extent the volume and depth estimation algorithms. For each debris or flood location, a query is placed to both Flickr and Panoramio through their respective APIs for all of the geo-tagged photos in the nearby area within an appropriate range of dates. The photos could optionally be filtered by tag as well. Figure 30 shows a flow chart of the validation process.

**Figure 30: Workflow for roadway obstruction validation from data mining of geo-tagged images**



For each debris or flood object, the centroid coordinates (in terms of latitude and longitude) are used to construct a bounding box that will be used to query the Flickr and Panoramio APIs. Figure 31 shows an example of a debris pile, along with its centroid and bounding box coordinates. These would be programmatically entered into the APIs, along with a range of dates to retrieve images from the databases.

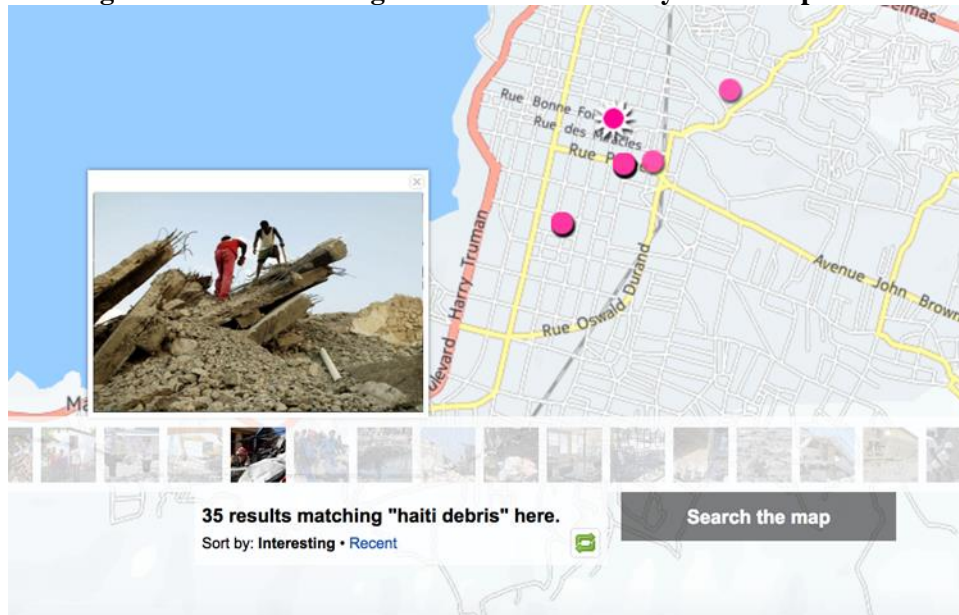
**Figure 31: Automatically generated shapefile**



*Centroid and bounding box coordinates for one of the debris piles.*

A set of images (if existing) is then returned by the Flickr and Panoramio APIs. These images can be filtered by tags to reduce the number, and only those relevant to the disaster can be kept. For example, Figure 32 shows the results when searching the Flickr database for images near the debris pile in Figure 31. The resulting images suggest that there is indeed debris there and the results are valid.

**Figure 32: A Flickr image confirms that validity of debris pile**



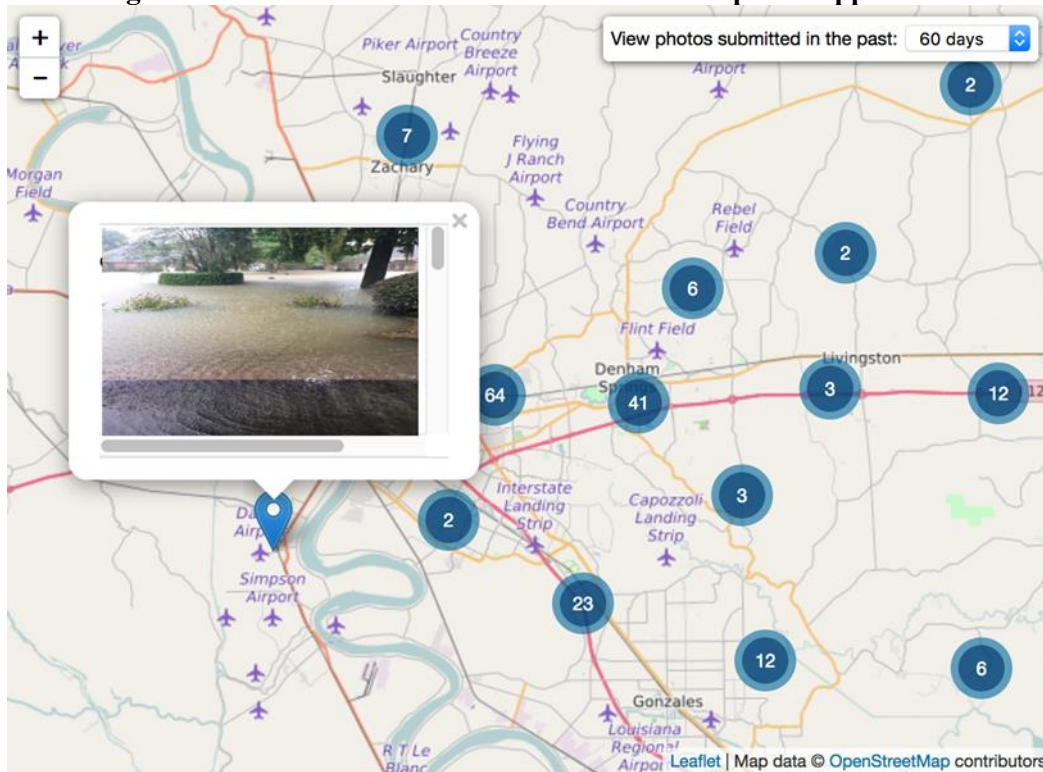
The example shown here was created by a simple search using the centroid coordinates of the debris pile. In practice, scripts would be created to programmatically loop through each debris pile or flood occurrence and query both the Flickr and Panoramio APIs (or any other desired outlets). Although it is extremely beneficial to be

able to access databases via computer programs, there are other outlets that provide means of validation if you are willing to manually search them.

#### 2.4.4 Other Means of Validation

Some websites contain geo-tagged photos, but don't provide APIs to access them. For example, the Federal Emergency Management Agency (FEMA) has an application specifically for the purpose of uploading disaster photos. The app is called the Disaster Reporter, which allows users to upload geo-tagged, disaster-related photos to help paint a picture of what is happening on the ground. The app can be downloaded for iOS or Android, and also features a convenient online map view. Figure 33 shows a screenshot of the online web portal for the Disaster Reporter, which currently (as of 9/25/16) has a lot of recent entries due to the flooding in Louisiana. Upon clicking on one of the entries, the geo-tagged image pops up (in this case it is a flooded residential street).

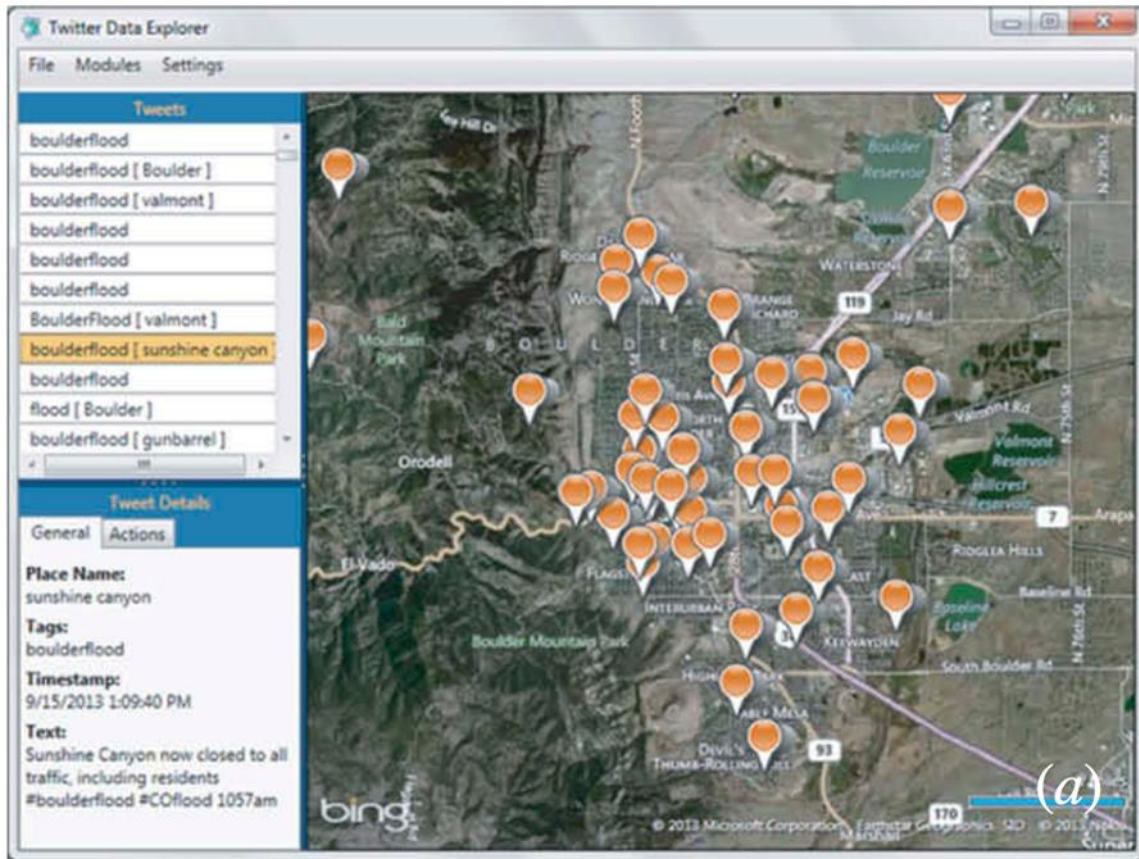
**Figure 33: A screenshot from FEMA's Disaster Reporter application**



*The image shows that over 100 geo-tagged images relating to flooding in Louisiana have been submitted.*

Twitter is another massive source of geo-tagged information. Rather than sharing images, users submit “tweets” of 140 characters or less. While the lack of images prevents a “true” validation, a great deal of information can still be gathered from Twitter. Going back to the example of the Boulder flooding, Cervone et al. (2016) performed data mining on tweets by searching for specific hash-tags (users can add tweets to searchable categories by putting a “#” in front of the word or group of words), such as #boulderflood and #flood, while also restricting the location of the tweets to a bounding box in Boulder. In doing this, the team was able to identify “hotspots” of flooding activity to further direct them in image mining. Figure 34 shows an example of the geolocated tweet map.

**Figure 34: Geolocation of Tweets**



*Tweets pertaining to Boulder flooding are used to get an idea of where flooding is present Cervone et. al. (2016)*

## 2.5 Estimation of Network Conditions and Disaster Impacts

This section details the methodology used to take the outputs from the detection (debris and flood) and estimation (volume and depth) algorithms and package them into map-ready GIS products that can be viewed as standalone information products, and also passed into RPI's ARP module. Therefore, the previous three sections have strong bearing on the actual assessment of network condition and disaster impacts, whereas here we detail the translation of algorithms into spatial products.

The detection and estimation algorithms are able to ingest raw CRS data and automatically detect debris piles, flooded roadways, and estimate their volumes and depths, respectively. Although some functionality is included in the standalone applications to save output images such as the flood detection image and the water depth image, the true utility of the algorithms is its ability to automatically convert the results into a GIS-ready shapefile.

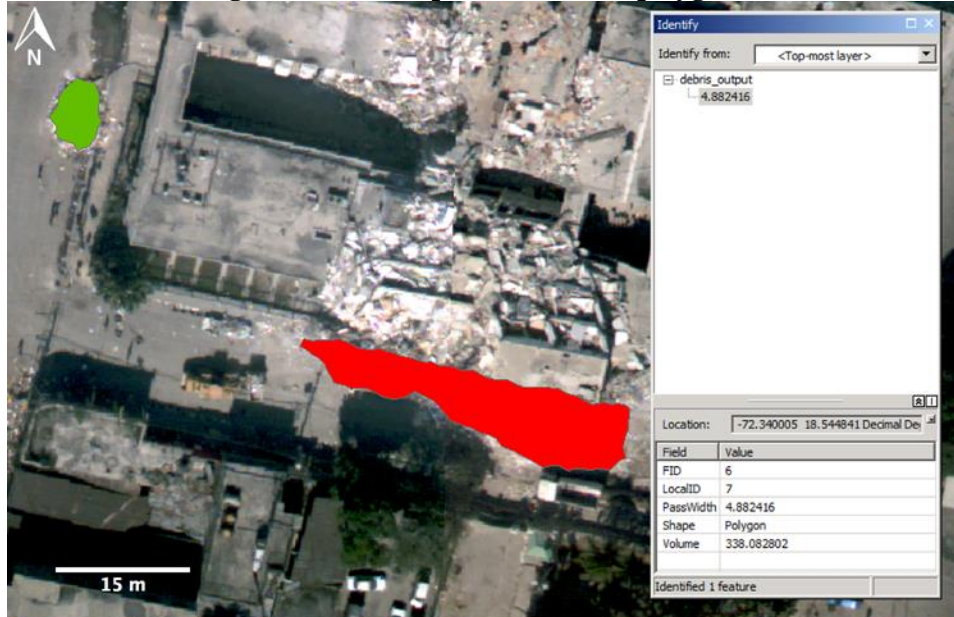
The shapefiles provide a convenient and comprehensive way of viewing the spatial location and extent of debris piles and flooding, while also embedding attributes within the polygon of each obstruction (volume, passable width, depth, etc.). Additionally, the shapefiles provide the data necessary to seamlessly integrate with the Access Restoration module, which provides further visualization and allows for restoration times to be computed.

## 2.5.1 Methods

### 2.5.1.1 Debris Shapefiles

Two shapefiles are produced when running the debris application. The first shapefile is the debris shapefile. The debris shapefile contains a set of polygons. Each polygon represents a debris pile and contains the following attributes: LocalID, Volume, and PassWidth. Figure 35 shows a screenshot from ArcGIS zoomed into one of the debris polygons for a scene in Haiti. The information on the box shows the attributes for the red debris polygon in the center of the image.

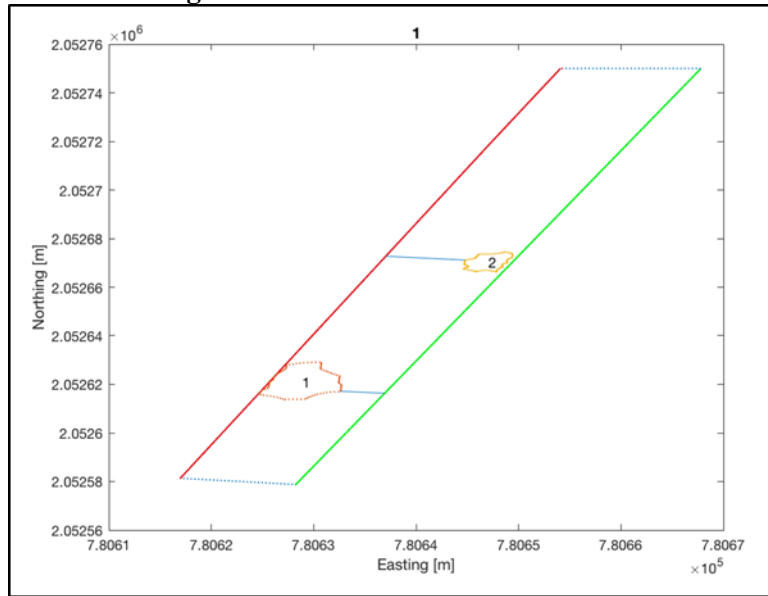
**Figure 35: Close up view of debris polygons**



*A screenshot from ArcGIS shows a close-up view of what the debris polygons look like in a GIS viewer. The polygons are colored by volume (green = less volume, red = more volume). Clicking the red polygon reveals its attributes, such as passable width (in meters) and volume (in m<sup>3</sup>).*

- The **LocalID** attribute is used for internal debugging, and will likely be removed in future releases once integration with RPI has been completed.
- The **Volume** attribute represents the estimated volume of the debris pile in m<sup>3</sup>, and is computed by the algorithm presented in Section 2.2.1 and in Appendix A. In Figure 35, the volume attribute is used to color the debris pile (the lowest volumes are in green, and the largest are in red).
- The **PassWidth** attribute stands for “passable width” and represents the amount of room that a vehicle has to pass through the road because of the debris pile. The passable width is calculated based on the distances between the side of the road and other adjacent debris piles. Figure 36 shows an example of the passable width for two debris piles in a roadway. Two debris piles are shown on a roadway (opposing road edges are marked in red and green). The blue line illustrates the passable width between the debris pile and road edge.

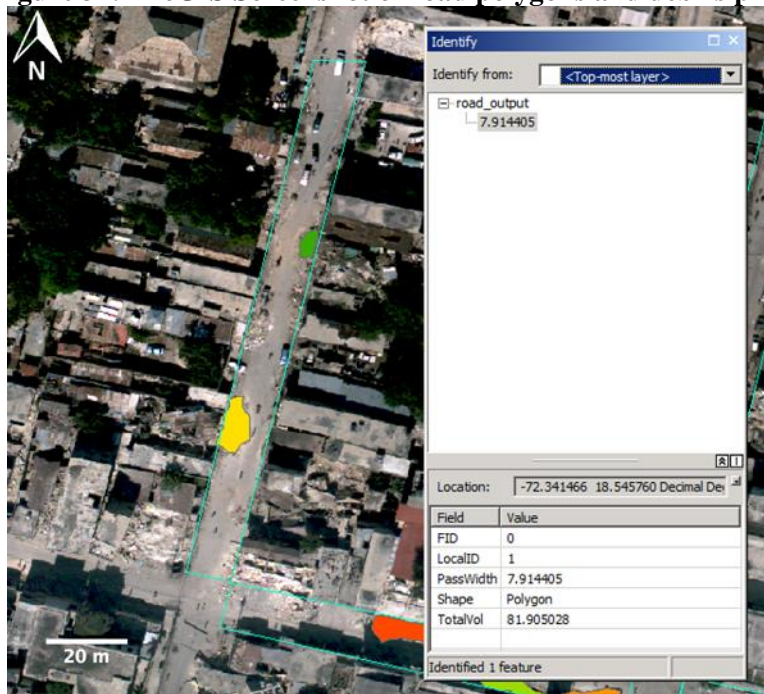
**Figure 36: Passable width illustration**



The road shapefile is a set of polygons of roads that contain debris. The polygons come directly from the input road network shapefile (only for roads that contain debris, the others are excluded). Each road polygon contains a LocalID, PassWidth, and TotalVol attribute. Figure 37 shows a screenshot from ArcGIS of road polygons (outlined in teal) as well as the debris piles. The information box shows the attributes for the given road, such as passable width and total volume of debris on the road.

- The **LocalID** attribute is used for internal debugging, and will likely be removed in future releases once integration with RPI has been completed.
- The **TotalVol** attribute is the sum of the individual volumes of all debris piles located within the boundaries of the road polygon. The total volume is expressed in terms of m<sup>3</sup>.
- The **PassWidth** attribute represents the passable width of the entire road. This value is calculated by taking the minimum passable width for all debris piles within the road. The minimum passable width of all debris piles is the limiting factor for a vehicle to travel from one end of the road to the other.

**Figure 37: ArcGIS Screenshot of road polygons and debris piles**



### 2.5.1.2 Flooding Shapefiles

The flooding application produces a single shapefile. This shapefile contains polygons that represent areas of approximately equivalent water depth in the roadway. Figure 38 shows an ArcGIS screenshot of roadway flood polygons overlaid on a flooding image from the Mississippi River. The polygons are colored by depth (green = shallow, red = deep). The information box shows attributes such as depth and area for a single polygon.

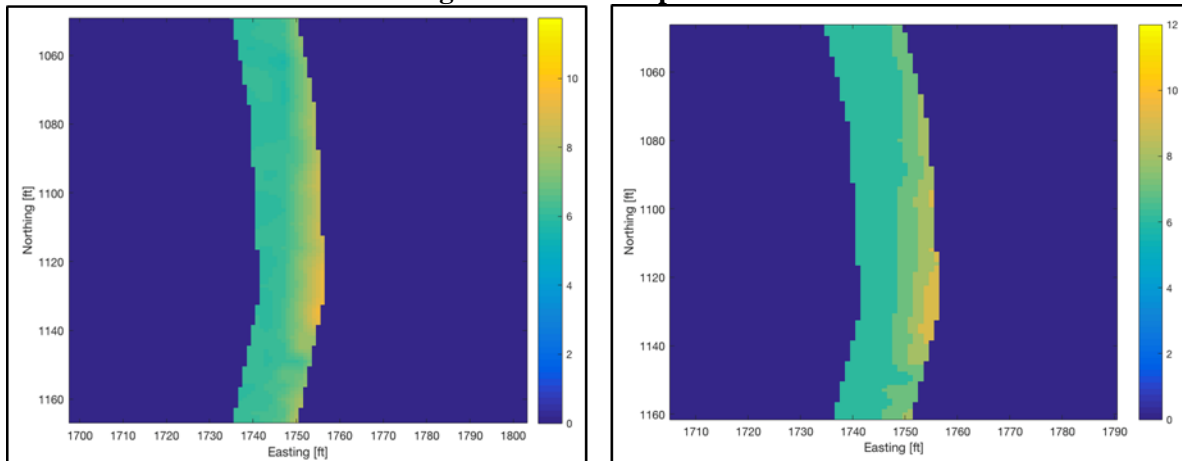
**Figure 38: ArcGIS screenshot of flood polygons**



The flooding shapefile contains two attributes for each polygon: depth and area. The depth attribute is the approximate depth of water throughout the polygon (rounded to the nearest foot), and the area of the polygon (in ft<sup>2</sup>). As part of the depth estimation algorithm (outlined in Section 2.2.1 and Appendix A), a depth raster is produced for roadway flood pixels. The raster represents the water depth at each of the pixels. Clearly it would be extremely inefficient and memory intensive to produce a separate shapefile for each pixel. Instead, pixels are

rounded to the nearest foot, and then pixels with the same depth are combined to form polygons. These are the polygons you see in Figure 38. The areas of the polygons are computed using the known pixel sizes. Figure 39 shows a depth image for a section of flooded roadway before and after rounding. The image on the right shows how the rounding creates regions of equal depth, which then become the polygons in the shapefile.

**Figure 39: Flood depth estimates**



*(Left) Depths for a flooded section of roadway before rounding; each pixel represents a decimal depth.*

*(Right) Depths for a flooded section of roadway after rounding. Regions of equal depth form after rounding, which then become polygons in the shapefile.*

Shapefiles provide an easy, universal way to visualize the results of the depth and flood detection and estimation algorithms. The shapefiles can be loaded into any GIS program and are automatically placed in the right location regardless of projection. The shapefiles can be placed on top of imagery or base maps (such as OpenStreetMap, USGS, etc.) to view the debris piles or flooded roadways in context. Each debris, road, or flood polygon contains characteristics such as debris volume, passable width, water depth, and area. Along with being convenient for visualization and analysis, the shapefiles can feed directly into RPI's algorithms for calculation of restoration times.

## 2.6 Conclusions

The CRS technologies developed as part of this project implemented algorithms which use road network shapefiles and CRS data (lidar for debris, imagery for flooding) to automatically detect obstructions to the roadway. By testing the debris detection algorithm on seven point clouds from the 2010 earthquake in Haiti, we have shown that nearly 98% of all debris can be detected, with an overall quality of performance of over 86%. Using 4-band flooding imagery from the January 2016 Mississippi River flooding we have shown that the flood detection algorithm was able to detect 95% of roadway flood pixels, while achieving an overall quality of 92%. Similar results can be expected when these algorithms are applied to other post-disaster lidar data or flood imagery. Although there are many different types of algorithms that could be applied to these types of CRS data, the proposed algorithms were chosen because they provide accurate and reliable results.

The methodology implemented in the project to quantify debris and floods allows debris volumes and water depths to be automatically estimated from the output of the detection algorithms. Alpha shapes are used to derive volume estimates from individual debris pile point clouds. A mean error of 6 m<sup>3</sup> was obtained through a validation experiment using real debris pile lidar data. Collecting data at a higher point density can significantly reduce the error, but even at low density the error is essentially insignificant (several debris piles in Haiti had volumes that

were hundreds of cubic meters). Digital elevation model rasters are used to determine floodwater depth by finding the elevation where the water meets land. Although no validation data were available, results produced from testing the algorithm on real data were reasonable and exactly what one would expect. The outputs from these algorithms (debris volumes and water depths) are converted into shapefiles for easy viewing and integration with the Access Restoration module.

Moreover, regardless of the demonstrated accuracy of a particular algorithm, it is always good practice to further validate results when there are multiple modalities of data available. People routinely post images or information following disasters, whether to let their friends know that they are okay, to warn others of danger, or to seek aid. These geo-tagged updates are a rich resource for painting a clearer picture of what is happening on the ground, and when appropriately queried, can directly validate results obtained from CRS data.

In terms of estimation of network conditions and disaster impacts, shapefiles provide an easy, universal way to visualize the results of the depth and flood detection and estimation algorithms. The shapefiles can be loaded into any GIS program and are automatically placed in the right location regardless of projection. The shapefiles can be placed on top of imagery or base maps (such as OpenStreetMap, USGS, etc.) to view the debris piles or flooded roadways in context. Each debris, road, or flood polygon contains characteristics such as debris volume, passable width, water depth, and area. Along with being convenient for visualization and analysis, the shapefiles can feed directly into RPI's algorithms for calculation of restoration times. As part of this project, two standalone programs were generated. One application was created to handle all of debris detection, volume estimation, and debris shapefile output. The other application covers flood detection, depth estimation, and flood shapefile output.

### **3. ARP MATHEMATICAL MODELS**

#### **3.1 Introduction**

This project delivers a mathematical model and solution procedure that determines the order in which streets need to be restored to open access to specific points inside the disaster site. Different priority metrics are analyzed, including the time to restore access to population centers according to size and restoration time. The model allocates resources to minimize the costs to the user, and takes into account capacity and scheduling constraints. The model explicitly considers the effect on the impacted population during disaster response operations by using the summation of private costs and the externalities imposed on the population as the objective function. As pointed out in section 4.3, externalities are incorporated using deprivation cost functions that are the economic valuation of the lack of access to a good or service by the impacted population. The nonlinear mathematical model cannot be solved in short execution times by current commercial software. As a consequence, a heuristic procedure has been developed to solve large instances in short execution times.

To capture the complexities of the process, the team conducted interviews with experts working for the New York State Department of Transportation (NYSDOT) and the New York State Office of Emergency Management (NYSOEM) with experience and/or management positions in disaster response. The results of these interviews allowed us to validate the model developed. During the interviews, a set of questions was asked about the interviewee's own experience, decision-making process, tasks to perform, and lessons learned during disaster response operations. The following sections summarize the main findings.

##### **3.1.1 Agencies Involved in AR**

The first priority during disaster response is to open access to address life safety concerns. One of the critical issues in disaster response is coordination between agencies. Agencies require quick and reliable information to

coordinate their activities; situation awareness is key for a better operation. The process of AR involves the coordination of several institutions according to the type, magnitude, and extension of the disaster. In the case of the state of New York, the NYSOEM represents the coordinating institution that has direct communication with the NYSDOT. NYSDOT has the assets (e.g. plow trucks and personnel) to evaluate and respond to emergencies. Other agencies such as the New York State Parks Recreation & Historic Preservation Department, the Department of Sanitation, and the Department of Citywide Administrative Services can be involved in the response depending on the type of disaster, impacted zones, and type of debris that needs to be removed. The US Army Corps of Engineers supports the assessment, response and recovery of disaster operations. This illustrates the complexity of disaster response operations where, in the same disaster, more than seven agencies can be involved in the response.

The NYSDOT, which has the largest fleet of plow trucks in the state of New York, has assets prepositioned throughout the state. They are able to deploy assets in relatively short periods of time, including mobilizing trucks and personnel from throughout the state. In addition, the NYSOEM has four stockpiles of equipment strategically prepositioned in the state. The use of technologies plays an important role in the coordination of the response. NYSDOT has an internal tool that tracks where all assets are located in the state.

### **3.1.2 AR in Practice: Initial Assessment and Classification of Roads**

In most cases, the information for the initial assessment comes from citizens and personnel on the ground, including police and fire departments. As soon as practically possible, technical teams are deployed to specific places in the disaster zone to evaluate the impact on the transportation network and critical infrastructure. Social media is also used by the agencies to determine needs in different places across the state. With regards to bridges, USDOT deploys damage assessment teams that conduct a quick assessment, and upload this information to a GIS-based system. Every team has two engineers and a technician using a laptop prepopulated with the information related to the location and characteristics of the infrastructure. One priority is to restore the traffic signals at intersections. In critical intersections, signals can be powered by generators, but these must be deployed after access is restored.

Once the needs assessment has been completed, agencies begin the coordination of disaster response operations. The NYSDOT works with utility companies to restore access and services to the impacted population. In terms of restoration of roads, NYSDOT has a hierarchy of facilities by functional class. Roads are classified as primary, secondary and tertiary roads, and this is the order in which these roads are restored. Critical infrastructure such as bridges and main avenues are considered primary roads. Then, according to volume they are classified as secondary and tertiary. Performance measures include the time between closures and opening of roads, and the time to fully restore the infrastructure according to type of damage.

## **3.2 Problem Definition**

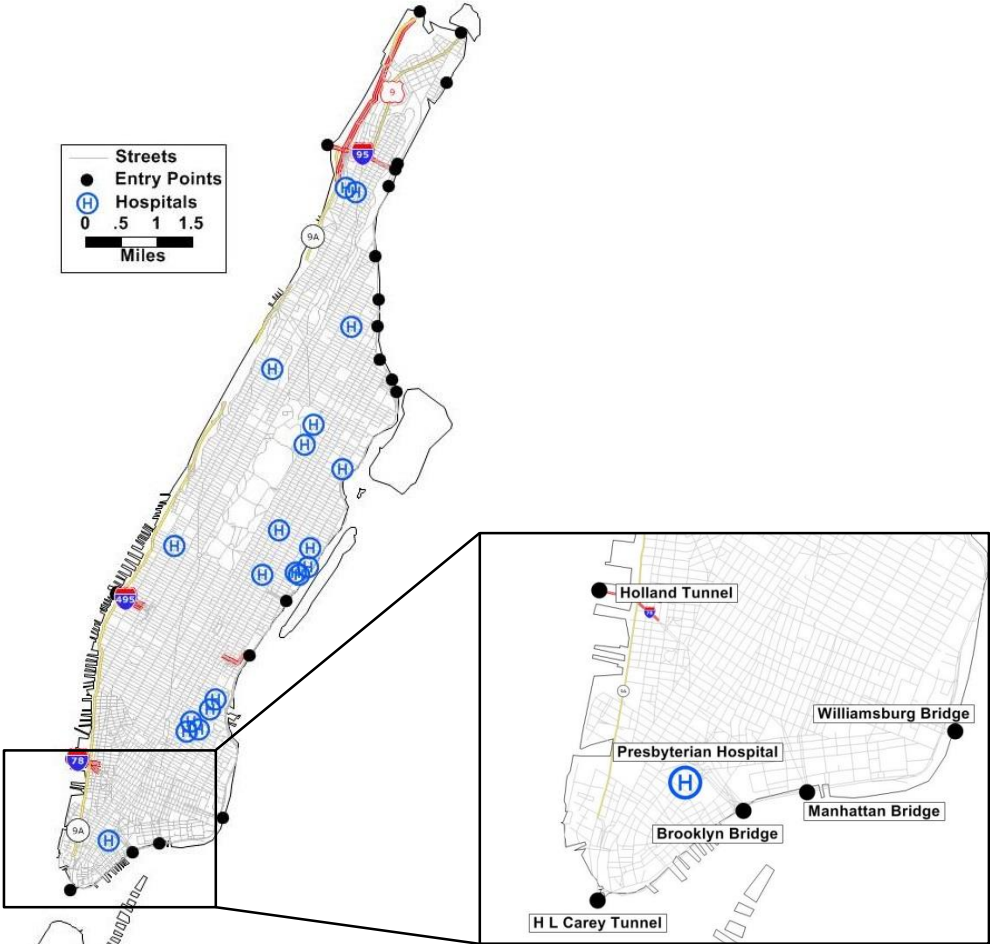
This section focuses on the problem of AR after disasters and reviews its most important challenges, such as the characterization of the impacted area and the introduction of capacity constraints.

### **3.2.1 Characterization of the Disaster Site**

The impacted area corresponds to the geographic extension of the disaster. Once the extension of the damage has been determined, the next step is to determine the locations inside the impacted area that need to be reached from the outside. Demand nodes include population and economic centers, critical infrastructure, and any asset that can play a role in the response (e.g., warehouses, stores, and government buildings). It is also necessary to determine the entry points to the impacted area. These include streets, highways, bridges, tunnels, ports, or airports that connect the outside with the impacted area. The restoration of access will start from the entry points, and use

the transportation network to reach the demand nodes. Figure 40 shows a schematic of Manhattan, NY as the impacted area. In the case of Manhattan, there are twenty-one bridges and tunnels connecting the island with its surrounding boroughs; these are the entry points. Every intersection represents a node inside the disaster area, and the streets connecting the intersections are the links. As an example, the figure shows twenty hospitals that are considered demand nodes to which AR is required.

**Figure 40: Schematic of Manhattan**



**3.2.2 Time Dependent Capacity Constraints**

The order in which each street needs to be restored is an Access Restoration Plan (ARP). The time at which a street can be restored depends on whether there is: (1) access to the streets, and (2) capacity available to work on the street. Therefore capacity constraints play a key role in the design of ARPs. In the context of AR, capacity is understood as the ability of the system to work on one or more links at the same time. If unlimited resources are available, the optimal ARP will be the one that reaches all points of interest in the shortest time possible. This implies opening access using the shortest path between each location of importance and its closest entry point. Unfortunately, in most disasters this is not possible, and ARPs need to consider the limited capacity available.

In addition to the consideration of capacity, ARPs need to be adjusted to take into account incoming resources and updated information about the conditions of the transportation network. To illustrate this, consider a large

disaster such as the earthquake in Haiti: during the first hours the response will be led by national responders. Once the state of emergency has been declared and international help is requested, search-and-rescue teams and supplies will come from all over the world. This will increase the resources for the response in the days following a disaster. What is a benefit can easily become a nightmare, however, given a deluge of materials and the complexity of the communication and coordination between local agencies, governments and non-governmental organizations. This is why ARPs must consider the evolution of the response as resources become available. Inclusion of capacity constraints will modify the response to the disaster and lead to, for example, the prioritization of opening access to the largest population centers in the earliest stages of the response.

### 3.3 Review of Priority Metrics

This section reviews and evaluates priority metrics for access restoration.

**Population:** the use of population in the process of access restoration responds to the need to open access as soon as possible to population centers where people have sought refuge. This can include hospitals, schools and any facility that is either a meeting point for the community, or has become a meeting point since the disaster. For example, after the earthquake in Haiti, the Silvio Cator Stadium and the front of the Presidential Palace became refugee centers. Both places are open and relatively hazard-free environments, in addition to being highly visible for authorities and responding agencies.

**Private cost:** the cost of the access restoration process mainly consists of equipment and personnel working on the ground. In terms of equipment, it is important to account for all operating expenses such as fuel. Equipment utilized can be highly specialized, particularly when considering restoration of access to collapsed infrastructures in population centers.

**Time:** time is the total time to open access to an isolated population center. Time as a metric can be used interchangeably with cost, since most cost components can be interpreted on a unit time measure.

**Deprivation time and cost:** it is widely accepted that the effect of a marginal time waited for supplies is highly dependent on how long survivors have already been waiting: one extra hour waiting is completely different when an individual has been waiting for twenty minutes versus five or six hours. The time that an individual or community has been deprived of supplies is denominated deprivation time. Deprivation time is particularly critical in infants, when waiting for water or milk for one extra hour is harmless right after feeding, but waiting one extra hour after five hours of deprivation can be fatal. The negative effects of deprivation time can be monetized and incorporated into mathematical models using deprivation cost functions.

**Social costs:** both private and deprivation costs can be merged into a single metric, denominated as social costs. This metric will measure not only the cost of the restoration in terms of equipment and personnel, but also the impact on survivors produced by the deprivation time in which they have been waiting for supplies.

### 3.4 Mathematical Model of Access Restoration

The mathematical model developed follows the traditional network design type approach commonly used in the literature of transportation engineering and operations research (Ahuja et al. 1993). The mathematical formulation considers a complete graph  $G = (N, A)$ , where  $N$  and  $A$  represent the set of nodes and links, respectively. There is a set of points of interest normally referred to in the literature as demand nodes ( $D$ ), representing population centers and other locations of importance inside the disaster area. Entry points ( $S$ ) represent the nodes from which the restoration must start. The population ( $\pi_d$ ) is noted at each demand node  $d$ . The deprivation time ( $\delta_d$ ) function is used when social costs are used as objective function. The impact on people due to the deprivation time is represented by the non-linear, convex, non-decreasing deprivation cost function  $\gamma(\delta_d)$ . Each link has an associated restoration time  $\tau_{ij}$ , and the capacity of working in different arcs in parallel is

determined using the integer parameter  $q_t$ . The model determines which links  $(i, j)$  should be solved to reach destination  $d$  at time  $t$  using the binary variable  $x_{ij}^{dt}$ . Finally, the scheduling binary variable  $\alpha_{ij}^t$  captures the capacity constraint of the model.

Objective Function:

$$\text{MIN } \sum_{d \in D} \pi_d \gamma(\delta_d) + \Omega(X, T) \quad (1)$$

Constraints:

$$\sum_{(i,j) \in A} x_{ij}^{d\tau_{ij}} \geq 1 \text{ for } i \in S, d \in D \quad (2)$$

$$\sum_{(i,d) \in A} \sum_{t \in T} x_{id}^{dt} \geq 1 \quad \text{for } d \in D \quad (3)$$

$$\sum_{(i,k) \in A} x_{ik}^{dt} - \sum_{(k,j) \in A} \sum_{i=t}^T x_{kj}^{dt} \leq 0 \quad \text{for } d \in D, k \in N \setminus (S \cup d), t = 1 \dots T \quad (4)$$

$$\alpha_{ij}^t - x_{ij}^{dt} \geq 0 \text{ for } (i, j) \in A, d \in D, t = 1 \dots T \quad (5)$$

$$\sum_{(i,j) \in A} \sum_{s=t}^{t+\tau_{ij}-1} \alpha_{ij}^s \leq q_t \quad \text{for } t = 1 \dots T \quad (6)$$

$$\delta_d \geq \sum_{t \in T} \sum_{(i,d) \in A} t x_{id}^{dt} \quad \text{for } d \in D \quad (7)$$

$$x_{ij}^{dt}, \alpha_{ij}^t \in \{0, 1\}, \delta_d \geq 0$$

The objective function in equation (1) minimizes total social costs (or any other metric): in this case, this is the addition of deprivation costs—imposed on the population—to the logistics costs  $\Omega(X, T)$  of the restoration. Equation (2) ensures that the AR begins at an entry point, and equation (3) ensures that all points of interest are reached. Equation (4) is a flow conservation constraint that captures the deprivation time. The way this constraint works is by requiring that the flows leaving a node must be larger than the entering flow; this reflects the fact that restoring an arc will benefit the destinations that can be reached from that point on. Then, the key is to consider all the flows leaving the node from time  $t$  to the end of the planning horizon. This represents a temporal flow conservation that will capture the time required to wait for resources to become available for use. In essence, this means that once the node has been reached by the restoration, it can be used in the future to restore access to any other destination; a necessary condition of a mathematical model addressing the problem of access restoration. Equation (5) states that a node cannot be used if it has not yet been restored. This is the traditional scheduling constraint used in the literature (Nurre et al. 2012). Equation (6) introduces a capacity constraint into the model to ensure that resources in use are always less than or equal to available resources. The time dependency of this constraint is an important consideration since availability of resources varies along the planning horizon. Therefore, the model can be responsive to changes, incorporating information regarding future increases/decreases of capacity throughout the response. (For example, international aid will take at least a couple of days to arrive since it has to be requested by the country affected, and deployed by a different country or institution.) Finally, equation (7) determines the deprivation time of each of the population nodes.

The model captures the main characteristics of access restoration and incorporates social costs to the objective function producing a social cost mathematical model. This approach combines recent developments in the field

of disaster research (Holguín-Veras et al. 2013) with traditionally used methodologies in operations research and transportation engineering.

### 3.5 Solution Algorithm

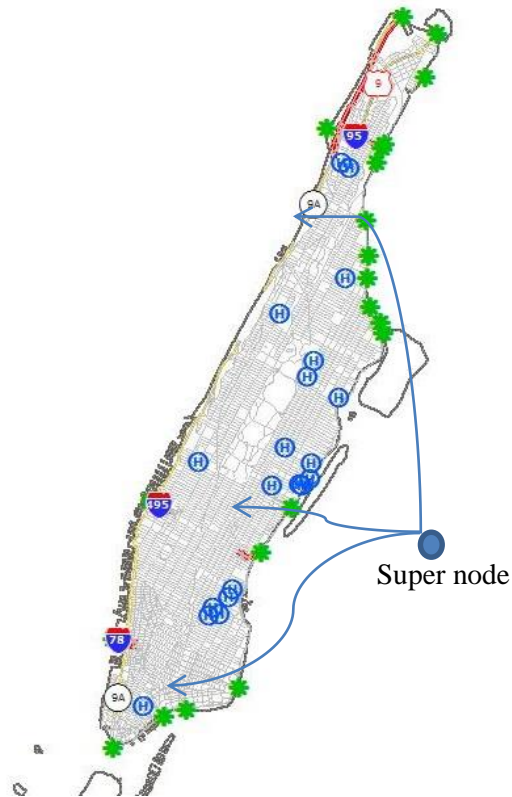
This section focuses on the development of a heuristic solution algorithm for the problem of access restoration. The solution of the model cannot be addressed using commercial software for real-world scenarios. To provide an idea of the magnitude of the problem, the solution by complete enumeration of the paths from one entry point in a city like New York would generate more than  $5.15 \times 10^{47}$  different solutions; this is more options than the legal number of plays in a game of chess. The number of solutions increases with the number of entry points available for the response. On top of that, the inclusion of capacity constraints would make it impossible to solve, as NP-Hard problems are the most difficult to solve known to humankind. In essence, what is needed is the development of heuristic procedures that produce close-to-optimal solutions of the problem. In the following description of the algorithm, the term “terminal node” is used, which corresponds to any point of interest inside the disaster zone. Consequently, “non-terminal” nodes are streets intersections and other nodes in the network that are restored in the progress towards opening access to terminal nodes.

### 3.6 Heuristic Solution

The heuristic developed in this report is based on the shortest path heuristic proposed by Takahashi and Matsuyama (1980), which is a modification of Prim’s algorithm (Prim 1957). Prim’s algorithm determines the minimum spanning tree (MST) in a network with only terminal nodes. The algorithm starts from an arbitrary node, and sequentially incorporates the closest node (in terms of distance) to the tree, until all nodes have been reached. The application of Prim’s algorithm to the network Steiner Tree Problem has the distinctive challenge of dealing with non-terminal nodes. Using a similar idea, Takahashi and Matsuyama (1980) build the tree using the shortest path to decide which terminal to connect to the tree. At each step, the heuristic adds to the tree the terminal node plus the non-terminal nodes belonging to the shortest path between the tree and the terminal node. Both Prim (1957) and Takahashi and Matsuyama (1980) use as decision criteria the shortest distance between the tree and the terminal node to be incorporated. This is the critical step in the heuristic that determines its performance when solving the access restoration problem. Since the access restoration mathematical model deals with a non-linear cost function of deprivation time, several variants of the algorithm can be made according to population, deprivation time, marginal cost, and combinations of the above.

A number of modifications have been made to the shortest path-based heuristic by Takahashi and Matsuyama (1980) to make it suitable to solve the access restoration mathematical model. The first modification is the incorporation of a super node connected to the available entry points of the network at cost zero (see **Figure 41**). By simply imposing this super node to be the first one added to the tree, this modification anchors the heuristic to start the restoration of access from an entry point (equation 2 in the mathematical formulation). In addition, it allows the use of a subset of the entry points by simply deleting the links connecting the super node to the unavailable entry points of the disaster area. A similar result can be reached by using a large value of the restoration time for the entry points heavily impacted by the disaster. As pointed out before, the decision rule used by Prim’s algorithm is the distance that can be easily adapted to time assuming a restoration rate. This would lead to a heuristic that selects the terminal that can be restored first.

**Figure 41: Super node representation in Manhattan**



The termination condition of the heuristic is the same as Prim's algorithm: all  $n$  terminal nodes must be reached.

**Input:** A complete graph  $G=(N,A)$ , entry points and demand nodes

**Output:** An ARP and social cost for each demand node

Let  $E$  be the set of demand nodes without access

Let  $T$  be the set of demand nodes with access  $T=\{super\ node\}$

**While:**  $E$  is nonempty **do**

**For each:** node  $j \in T$

        Calculate the SC to all  $i \in E$  using Dijkstra's algorithm for the restoration times per link

        Let  $k \in E$  denote the node with the smallest social cost per individual

        Let  $sp \in G$  denote the set of nodes in the shortest path from  $T$  to  $k$

$T=\{T+k+sp\}$

**End**

**End**

**Return** T

The execution time of this heuristic is conditioned by the computation of the shortest path between all the components of the tree and the terminal nodes that have not been reached. The shortest path is calculated using Dijkstra's algorithm (Dijkstra 1959). As the heuristic progresses, the number of executions of Dijkstra's algorithm increases in a combinatorial fashion. Therefore, the main drivers of the execution time of this heuristic are the number of entry points and terminals inside the disaster zone, in addition to the size of the network.

### 3.7 Numerical Experiments

The first set of experiments use the Sioux Falls Network. The benefit of using this network is the possibility of validating the solutions via visual inspection. The second set of experiments analyzes the capability of the AR algorithm to solve large-scale problems. With Manhattan considered as the impacted zone, where every corner is a node and the streets are the links, the objective is to open access to twenty hospitals that represent the demand nodes, and twenty-one bridges and tunnels connecting Manhattan to the surrounding boroughs that represent the entry points. Solving the Sioux Falls Network takes less than one second, while solving the Manhattan experiments takes around three minutes for all instances using the AR algorithm. Results using the Sioux Falls network were validated using CPLEX, with execution times ranging from half hour to more than two hours depending on capacity constraints.

**Table 5: Parameters used in the experiments**

Private cost	\$55 per hour of restoration
Deprivation cost function	$\gamma(\delta_d) = \exp(1.503 + 0.0967 * \delta_d) - \exp(1.503)$
Valuation of human life	\$500,000 when $\delta_d = 120$ hours

#### 3.7.1 Sioux Falls Network

The Sioux Falls Network, shown in Figure 42, is composed of 24 nodes and 38 links. Each link has an associated restoration time. The demand nodes are 5, 11, 7, 15 and 20, and the population ( $\pi$ ) at each demand node is shown in the figure as well. Node 1 is the only entry point to the network.

Table 6 shows the results of the model for different levels of capacity. As expected, the more capacity the lower the social cost imposed by the restoration. However, there is no extra benefit to having more than three units of capacity. In this case, there are 5 demand nodes and the SC does not decrease by adding capacity beyond 3 units. This is the first relevant empirical finding of the numerical experiments: the diminishing marginal benefits of capacity in AR.

**Table 6: Results for different levels of capacity in Sioux Falls**

	Deprivation Time			Social Cost		
	Cap=1	Cap=2	Cap=3	Cap=1	Cap=2	Cap=3
Node 5	51	51	51	51,061	48,806	48,806
Node 7	86	86	75	847,450	847,450	295,845
Node 11	134	56	56	49,576,500	29,239	29,239
Node 15	145	75	75	38,668,700	45,437	45,437
Node 20	119	96	96	14,754,200	1,597,310	1,597,310
Average	107	73	71	20,779,582	513,649	403,328
Total	535	364	353	103,897,911	2,568,243	2,016,638

Figures 4, 5 and 6 show the results of having 1, 2 and 3 or more units of capacity. The sequence of links restored when capacity is equal to 1 is: 5-7-20-11-15. It is important to note that in this solution both demand nodes 11 and 15 are reached from non-demand nodes 4 and 19, respectively. This experiment clearly shows the importance of capacity considerations, since the ARP created when capacity is equal to 2 is substantially different from the one produced in the previous scenario with only one unit of capacity.

For capacity equal to 2 and 3 the sequence is the same: 11-15-5-7-20. However, there is a fundamental difference between these two solutions: access to demand node 7 is open from nodes 2-6-8. This essentially means

that the model is allocating resources to work in parallel and decrease the SC of the ARP. This result is counterintuitive, and reinforces the need for methodologies to aid disaster responders in making better decisions.

**Figure 42: Sioux Falls Network**

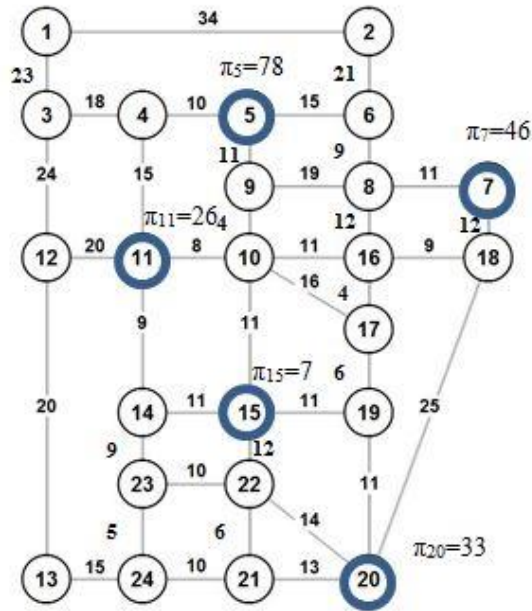


**Figure 43: Capacity equal to 1**

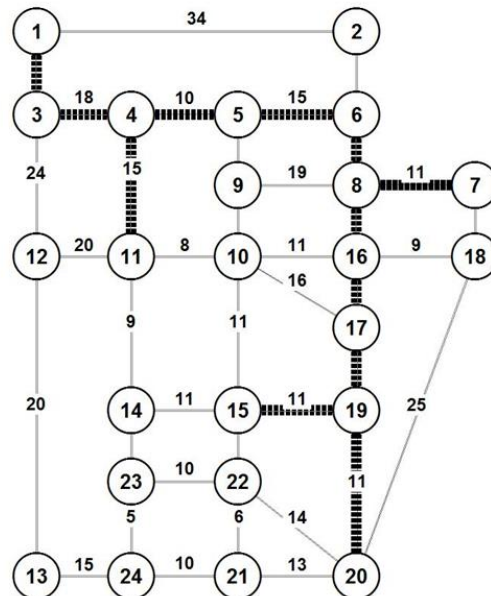


**Figure 44: Capacity equal to 2**

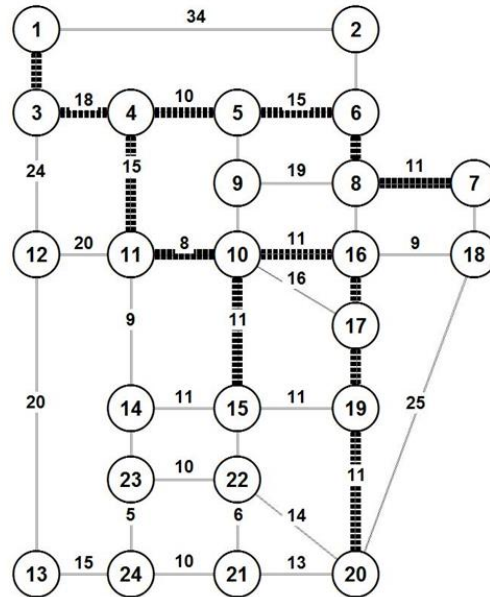
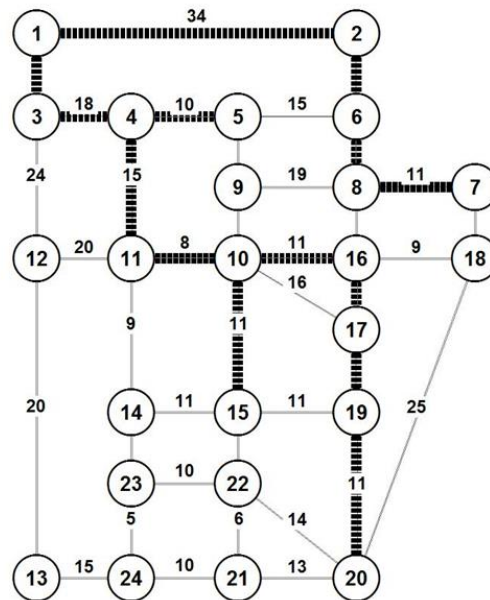


**Figure 45: Capacity equal or larger than to 3**



The numerical experiments in Sioux Falls provide important evidence that: (1) the available capacity determines the best strategy for AR; and (2) there is a maximum capacity for the response beyond which no additional benefits are found. These two conditions shed light on the need to constantly update the capacity available on the ground to achieve the best use of resources.

### **3.7.2 Manhattan, New York**

With a population of 1.6 million residents in 59 square kilometers, the island of Manhattan is the economic center of a large metropolitan area. Twenty-one bridges and tunnels connect the island with Brooklyn, Queens, Bronx, and New Jersey. During an emergency, the restoration of access and the arrival of external aid will commence from one of these entry points. Manhattan has 4,680 intersections and 8,204 streets connecting these intersections. From a computational perspective, a disaster responder would have to make approximately  $1.5 \times 10^{47}$  decisions to re-open Manhattan if there were only one entry point and a single truck opening access. This is a colossal challenge even for a computer, yet the problem of access restoration must be solvable both quickly and reliably. For all of these reasons, a disaster affecting Manhattan would impose immense challenges to disaster responders.

For the numerical experiments, twenty hospitals were selected in Manhattan to represent the locations of interest that must be reached after a disaster. As mentioned, solving this problem using commercial software is not possible.

### **3.7.3 Analysis of the Number of Entry Points Available**

The number of entry points available for the response is an important consideration, especially in the case of Manhattan. Bridges and tunnels are subject to structural failure. If the transit becomes unusable, the restoration of access has to find a way to connect the locations of interest with the outside using alternate routes.

Figure 46 shows the solution produced by the heuristic using a capacity equal to twenty (same as the number of locations of interest or terminal nodes). Diagram (a) shows the case in which all entry points are available to be used, while (b) shows only the Lincoln Tunnel available as an entry point. In the case of (a), the hospitals are reached using the closest entry point, and access is opened to the vicinity. This process is repeated unless a different entry expedites access to the next hospital. In other words, the marginal gain of using a new entry point has to be larger than reaching that hospital from the tree already in place by the process of access restoration. This idea will be used in the analysis of the different decision criteria needed to minimize the social impact of disaster response operations. Diagram (a) also shows the importance of the selection of the entry point. Once an entry point has been selected, the path to reach other locations of importance will be tied to this decision. For example, diagram (a) shows that Roosevelt Island would play an important role in the process of access restoration to Midtown Manhattan. This has important policy implications for disaster preparation. When only the Lincoln Tunnel is available, the restriction of the number of entry points forces the response to produce a unique tree. In this situation, the solution splits resources to go north and south of the Lincoln Tunnel, producing two branches. Capacity constraints play a key role because, ideally, these two branches are created in parallel. Otherwise, a decision must be made regarding which locations of interest to reach first in order to minimize social costs.

**Figure 46: Access restoration results for Manhattan**

(a) From all entry points

(b) From the Lincoln Tunnel



### 3.7.4 Effect of Capacity Constraints

The same five decision criteria considered in the case of Sioux Falls are tested for the Manhattan case study: population (POP), social cost (SC), marginal social cost (MSC), social cost divided by population (SC/POP), and marginal social cost divided by population (MSC/POP). Table 7 shows the results for different levels of capacity. Based on these results, the best decision criterion is MSC/POP. This criterion achieves the best results for almost all instances. The only exception is when capacity equals 15. In this situation, SC/POP reaches the best results, but MSC/POP is only 0.7% worse than the best solution.

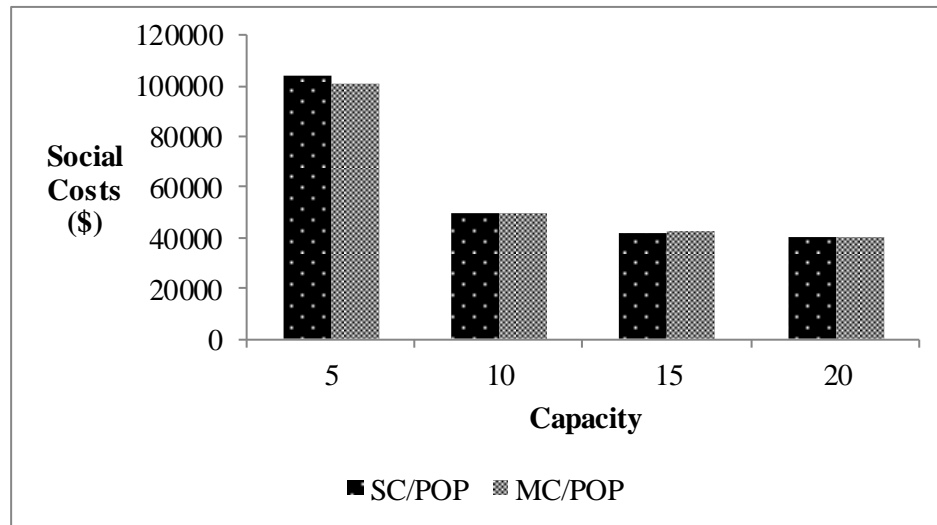
**Table 7: Summary results for different values of capacity**

Capacity	Maximum Population	Minimum Social Cost	Minimum Marginal Social Cost	Minimum Social Cost Divided by Population	Minimum Marginal Social Cost Divided by Population
1	1.28E+10	2.38E+10	5.44E+09	4.26E+09	4.26E+09
5	123,534	123,970	111,488	104,271	100,818
10	58,922	52,469	52,469	49,626	49,626
15	58,028	43,976	43,976	42,281	42,586
20	58,028	41,756	41,756	40,041	40,041

Figure 47 shows the best results obtained when capacity is greater or equal to five for the best two decision criteria. Capacity equal to one is not shown because the magnitude of the social costs does not allow illustration

of the results of the rest of the levels of capacity. The figure shows a significant improvement with an increase in capacity from five to ten units. The same magnitude of decrease in social costs does not occur for the same five units of increase between ten and fifteen units, or between fifteen and twenty units of capacity. These results are also found in the Sioux Falls case study, where there is no benefit gained when capacity is greater than three units (the number of locations of interest in the case of Sioux Falls is five). In the case of Manhattan, adding five units of capacity from five to ten decreases social costs by 50%. Increasing capacity from ten to fifteen units reduces social costs by an additional 16%, and twenty units of capacity decreases social cost by an additional 5%. This demonstrates the decreasing marginal benefit of capacity to the process of access restoration.

**Figure 47: Social costs results for different levels of capacity**



### 3.8 Conclusions

This project has developed a mathematical model that solves the problem of access restoration (AR). In addition, it designs a heuristic that delivers quick and reliable results even for large problems such as the transportation network of Manhattan. The mathematical model incorporates the impact of the allocation decisions using social costs (SC) as the objective function, although other priority metrics can be considered, such as population, time, cost and deprivation cost. While private costs account for the logistics costs, deprivation cost functions (DCF) measure the economic valuation of the lack of access to a good or service by an individual. The main issue of using traditional logistics is the minimization of only private costs instead of considering the impact that allocation decisions will have on the individuals affected.

The mathematical model integrates scheduling and capacity constraints into the process of AR. The model recognizes the temporal evolution of needs and availability of resources in the inclusion of varying parameters of capacity in different time periods along the planning horizon. This allows for integration of arriving resources throughout the response into disaster response operations. From the computational perspective, the complexity of the model makes it unfeasible to use commercial software to find optimal solutions to large instances. In response to this limitation, this report develops a heuristic procedure able to solve large instances in short execution times. Numerical experiments show that solving the problem of AR to twenty hospitals in the island of Manhattan, a network with more than four thousand nodes and eight thousand links, requires only three minutes of execution time. The model and the heuristic can serve as an operational decision-making tool to help disaster responders make better decisions quickly in the aftermath of a disaster.

The analysis of capacity constraints reveals the existence of diminishing marginal benefits of the capacity in AR. There is a level of capacity that reaches the optimal results and, at this point, adding capacity does not decrease SC. This is an important practical result that helps disaster responders recognize that excess of capacity is not beneficial to the response. In this situation, excess capacity can be directed to other disaster response activities.

## 4. TRANSITION TO PRACTICE

### 4.1 Introduction

Throughout the course of this project the team wanted to ensure that the research and associated DSS tools could be smoothly transitioned into practice, fully validated, and useful to responders. It was important to ensure that the DSS met the expectations of the end users, in terms of ease of use, quality of results, and usefulness. To accomplish this, the research team created a Technical Advisory Council, and conducted outreach, validation and training to assist with transitioning the research into practice. The following subsections discuss these efforts in more detail.

### 4.2 Technical Advisory Council (TAC)

To create a Decision Support System that transitions into practice and is useful to disaster respondents, the project created a Technical Advisory Council (TAC), comprised of eminent professionals from the various communities involved in the technical aspects of disaster response, including: (1) disaster response, (2) CRS monitoring of disasters, and (3) humanitarian logisticians. The TAC will advise the project team on technical matters, to ensure that the research is conducted according to the highest professional standards. Moreover, the TAC will be expected to collaborate in the design of a proactive outreach program to effectively disseminate results and products to relevant user communities.

The project team contacted the proposed members of the TAC to confirm their availability to participate, and the majority of the members confirmed their support. Moreover, two prominent practitioners in the field of humanitarian logistics were recruited to take part in the advisory council. The final roster of members, and their qualifications, is provided as follows:

- **Mrs. Kathy Fulton** is the Executive Director of American Logistics Aid Network, an organization founded by several professional and trade associations that came together after Hurricane Katrina to provide humanitarian relief. Today, ALAN is comprised of hundreds of supply-chain businesses that stand poised to respond in the event of disasters, including experts in transportation, warehousing, cold storage, and distribution. Their common objective is to help locate and move goods from suppliers to affected communities rapidly and efficiently. Mrs. Fulton graduated Summa Cum Laude from University of South Florida with dual Masters' degrees in Business Administration and Management Information Systems; she also holds a B.S. in Mathematics from Northwestern State University.
- **Mr. Jon Meyer** is an experienced transportation professional, with expertise in logistics, transportation and distribution, including a twenty-seven year career at CSX Transportation. A retired Colonel in the Air Force Reserve, he served as a logistics staff officer on the Air Staff, at the Pentagon. Meyer's awards include the Legion of Merit, Meritorious Service Medal, and an Air Force Commendation Medal. From 2012-2014 he chaired the TRB's task force on Logistics of Disaster Response and

Business Continuity, which later became a standing committee on which he serves as member. Mr. Meyer holds an MBA from Oregon State University, and a B.A. in Mathematics from the University of Oregon.

- **Mr. Phillip Palin** is the principal investigator for supply chain research at the Institute for Public Research. He is also a senior fellow in homeland security at Rutgers University Graduate School, and staff consultant for supply chain resilience at the National Academy of Sciences. Palin is the author of *Considering Catastrophe*, principal author of the *Catastrophe Preparation and Prevention* series from McGraw-Hill, principal author and editor of *Strategic Playbook: Regional Catastrophic Preparedness and Supply Chain Resilience*, and principal author of *Deterrence and the United States Coast Guard: Enhancing Current Practice with Performance Measures*. He is a regular contributor to Homeland Security Watch ([www.hlswatch.com](http://www.hlswatch.com)). Palin currently teaches and consults on strategy, leadership, and decision-making, with clients concentrated in the homeland security, higher education, and defense sectors. His specialties are: strategic choice, open source intelligence, strategic intelligence, prevention of catastrophe, and supply chain resilience.
- **Dr. Chris Renschler** is an Associate Professor of Geography and Co-Founder and of the Center for GeoHazards Studies at the University at Buffalo. Since 2010, he has been a faculty member of the Multidisciplinary Center for Earthquake Engineering Research. His research interests include Integrated Environmental Management, GIScience, Environmental Modeling and Extreme Events, on which he has over ninety publications. Dr. Renschler holds a Ph.D. in Natural Sciences from University of Bonn, Germany; B.Sc. and M.Sc. degrees in Geocology from Technical University of Braunschweig.
- **Dr. Jie Shan** is a Professor of Civil Engineering at Purdue University. His research interests are automated aerospace image mapping, spatial data modeling and analysis, remote sensing image processing and fusion, and 3-D Geographic information systems and visualization, in which he holds over fifty publications. Dr. Shan holds a Ph.D. in Photogrammetry and Remote Sensing from Wuhan Technical University of Surveying and Mapping, China, as well as a BS. and MS. from Zhengzhou Institute of Surveying and Mapping in China.
- **Professor Luk Van Wassenhove** is a leading management thinker and educator. He is a professor at INSEAD, where he holds the Henry Ford Chaired Professorship in Manufacturing. He is also the Director of the Humanitarian Research Group and a Fellow of CEDEP, The European Center for Executive Education, based in France. Professor Van Wassenhove is a Fellow of the Production and Operations Management Society, a Distinguished Fellow of the Manufacturing and Services Operations Management Society, and Honorary Fellow of the European Operations Management Association. He is also a member of the Royal Flemish Academy of Sciences. In 2006, he received the EURO Gold Medal for outstanding academic achievement, and in 2009 the Lifetime Achievement Faculty Pioneer Award from the European Academy of Business in Society (EABIS) and the Aspen Institute. His research and teaching are concerned with operational excellence, supply chain management, quality, continual improvement and learning. He currently leads INSEAD's Humanitarian Research Group.

- **Mr. Stephen White** is a career logistician with certifications in personal property and facilities management, and training in Six Sigma and process improvements. White is currently supply chain advisor to the assistant administrator of logistics at Federal Emergency Management Agency (FEMA). He holds an MBA in Industrial Management from Baker College Center for Graduate Studies, and a BS. from Limestone College

To kick-off the TAC, a webinar was conducted on January 27<sup>th</sup>, 2016. In this meeting, the advisors were advised on the status of the project, and a discussion about future steps took place. Appendix D contains the webinar presentation slides and a recording of the meeting can be found on the web link: <https://sufs.adobeconnect.com/p7wc3rf3ym3/>. The TAC worked closely with the project team to provide regular input to ensure that the DSS developed uses the highest technical standards and responds to the needs and expectations of practitioners.

### **4.3 Outreach and Validation**

Throughout the project, the team vigorously tested the DST and obtained validation from both public and private stakeholders. This was done through the TAC, and with the New York City Department of Transportation (NYCDOT) and the NYC Office of Emergency Management. The outreach and validation process assisted the team in identifying needs and developing requirements and guidelines. It also helped to create awareness of the upcoming DSS being developed. The NYCDOT was engaged in this process from the start, and provided insightful comments that helped craft the final deliverables, including the software.

Moreover, a CRS playbook was developed, and this document serves as a guide to provide NYCDOT emergency managers with insights into which remote sensing modalities would be appropriate for different response scenarios. Appendix E contains the CRS Playbook.

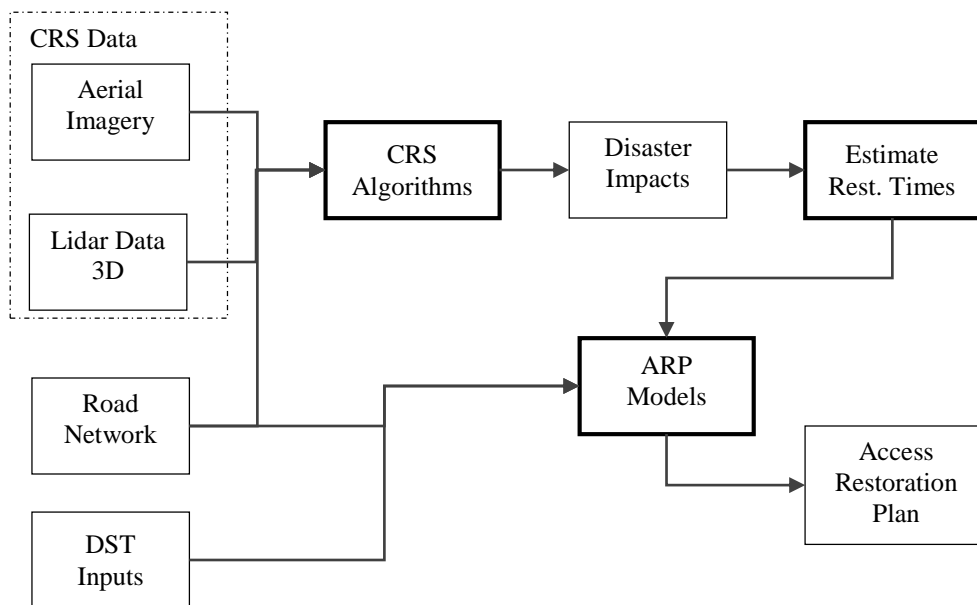
### **4.4 Transition to Implementation**

The team has worked closely with public and private-sector partners to ensure that the solution developed serves the needs of its final users. As part of this process, a case study scenario has been developed using NYCDOT data collected after Hurricane Sandy impacted the New York City in 2012. This case study served as the basis for the pilot test conducted. The details of the pilot test and the validation results are provided in this section.

#### 4.4.1 System Integration

The final solution produced by the project works as an integrated system that is able to process the CRS data, along with other inputs--such as road networks specification, capacity at entry points, and identification of terminal nodes--to produce the optimal restoration plan. To integrate all of the components developed as part of this project, an information flow was established, defining which inputs/outputs were produced by each subcomponent, and enabling them to function together as a system. The process was streamlined, as noted in Figure 48, which details the integrated information flow of all components.

**Figure 48: System integration**



The key inputs of the system are the CRS Data, and the road network information. These data inputs are complemented by the decision support inputs that characterize the situational assessment, including: entry points available, resources that will be used to clear the roads, and the terminal nodes for which access will be restored. As part of the system integration, a new module was developed to estimate restoration times based on the disaster impacts assessment produced by the CRS algorithms. These algorithms produce shapes files that describe the location of flood waters and debris on each link of the road network. The system then estimates the time it would take to clear the debris or flooding that is restricting access, as the details of the algorithm outlined. These restoration times serve as input for the mathematical models that produce the optimal access restoration plan. All of these components are integrated into a web-based software application. The team has created a project website<sup>1</sup>, where the project is described. Access to the web application is provided to stakeholders that have been trained in the use of the software. A user manual has also been developed, detailing all functionalities of the final solution, the complete manual can be found in Appendix F: Access Restoration Planning User Manual.

<sup>1</sup> <http://cite.rpi.edu/en/project-categories-2/humanitarian-logistics/item/arp>

---

**Algorithm 1** Debris Clearance

---

Step 0: *Parameters:* $\omega$ : desired lane width to be cleared; ▷ User Input $\zeta$ : plow free flow traveling speed in *kmph*; $v$ : plow cleaning speed *kmph*; $\eta$ : plow cleaning height; $L$ : Set of road links, indexed on  $l = 1 \dots a$ ; ▷ Read from Shape File / Road Network $D$ : Set of debris piles, indexed on  $d = 1 \dots b$ ; $S$ : Set of slices of debris, indexed on  $s = 1 \dots c$ ; $Z$ : Set of lanes in road link, indexed on  $y = 1 \dots z$ ; $J_l$ : Length of road link  $l$ ; $R_l$ : Width of road link  $l$ ; $G_l$ : Minimum height of obstructing debris piles in road link  $l$ ; $W_d$ : Distance to side for debris pile  $d$ ; $P_d$ : Passable width for debris pile  $d$ ; $I_s$ : Maximum height of obstructing debris on slice  $s$ ; $H_y$ : Maximum height of obstructing debris piles in lane  $y$ ; $Q_y$ : Maximum length of obstructing debris piles in lane  $y$ ; $U_s$ : Maximum length of obstructing debris on slice  $s$ ;Step 1: *Output:* $T_l$ : Restoration time for road link  $l$ ,  $l \in L$ ;Step 2: *Compute Clearance Times:* $l, d, s \leftarrow 1$ ;**while**  $l \leq a$  **do** ▷ Iterate over road links

{

 $z \leftarrow \left\lceil \frac{R_l}{\omega} \right\rceil$ ; ▷ Number of lanes on current road link $h_{1 \dots z} \leftarrow 0$ ; $d \leftarrow 1$ ;**while**  $d \leq b$  **do** ▷ Iterate over debris piles on current road link

{

**if**  $W_d < \omega$  and  $P_d < \omega$  { ▷ When there is not enough space to pass $s \leftarrow 1$ ;**while**  $s \leq c$  **do** ▷ Iterate over slices on current debris pile

{

 $y \leftarrow \left\lceil \frac{W_d + (0.1 \cdot s)}{\omega} \right\rceil$  ▷ Identify on which lane the slice is located**if**  $H_y < I_s$  ▷ Slice has maximum obstructing height $\{H_y \leftarrow I_s;$  $Q_y \leftarrow U_s;\}$  $s \leftarrow s + 1$ ;

}

}

 $d \leftarrow d + 1$ ;

}

 $G_l \leftarrow \text{Min}(H_{1 \dots y})$  ▷ Select lane with least obstructing debris**if**  $G_l = 0$  ▷ There is no debris to clear on this link $\{T_l \leftarrow \zeta \cdot J_l;\}$ **else** { ▷ Estimate cleaning time $T_l \leftarrow \lceil \frac{G_l}{\eta} \rceil \cdot Q_y \cdot v$ ; ▷ Number of passes required to clear debris**if**  $\lceil \frac{G_l}{\eta} \rceil$  is odd ▷ If passes are odd, need another pass over debris at FF speed $\{T_l \leftarrow T_l + Q_y \cdot \zeta;\}$  $T_l \leftarrow T_l + (J_l - Q_y) \cdot \zeta$ ; ▷ Add travel time for clear length of link

}

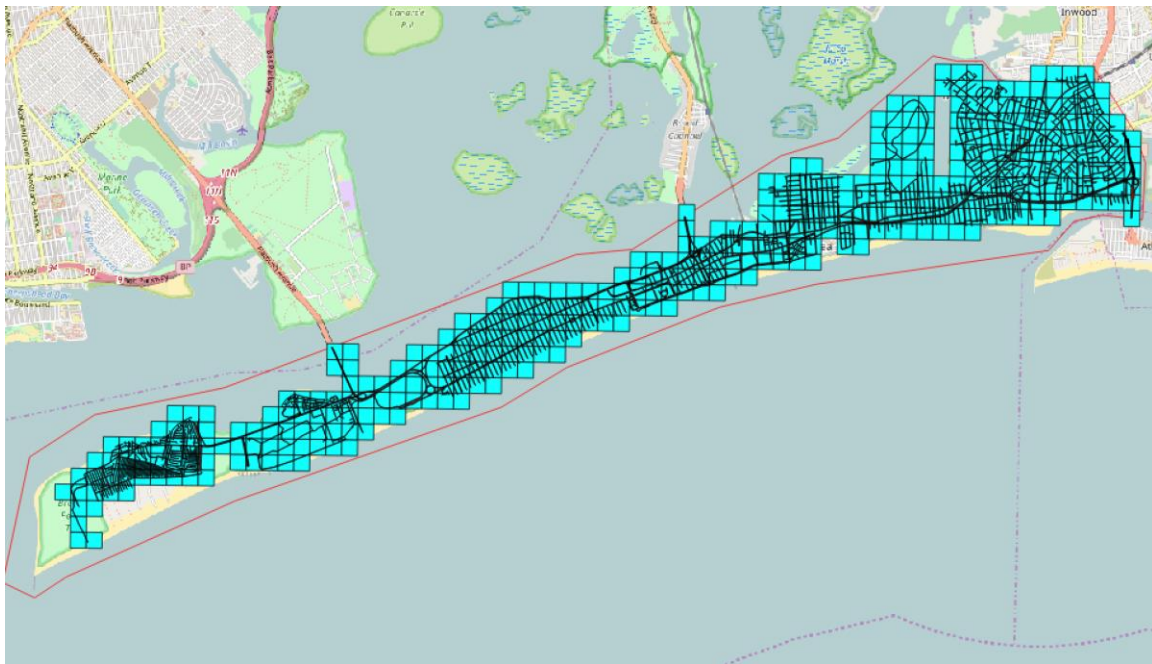
▷ Estimate cleaning time $l \leftarrow l + 1$ 

}

#### 4.4.2 Pilot Testing and Improvement

A pilot test was conducted to verify that the DST solution meets the project objectives, and that all integrated components work as specified to produce an optimal restoration plan. Since pilot testing consists of a deployment of the solution within a small scale, a subset of the NYC network was selected to test the product. The criterion for selecting the pilot test area was that the area exhibited a wide range of conditions so that all features of the solution could be tested. In this case, the selected area was Rockaway Beach, in Queens, which was heavily impacted by Hurricane Sandy in 2012. Using post disaster LIDAR data provided by NYC DOT, the team was able to assess the impacts of the storm on the roadway network. Figure 49 shows the selected area, and the Lidar Tiles that were processed as part of the pilot test.

**Figure 49: Lidar tiles and road network in Rockaway Beach**



Once the test area was selected, the CRS algorithms developed as part of the project were used to identify roadway debris. The results are presented in Figure 50. The results were used as input for the DST as per the established integration process. Other inputs required were also identified as part of the test, including entry points to the area and demand nodes, which correspond to the locations of the hospitals in the area, as well as schools that could have been used as shelters. In total, 3 entry points and 13 terminal nodes were identified. The DST tool produced an optimal restoration plan, which could reach these terminal nodes in 88 hours, given the volume of debris present, and the resources available for clearance. The test showed that the algorithm performed efficiently in the study area. The results of the test are shown in Figure 51.

**Figure 50: Debris piles in Rockaway Beach**



**Figure 51: Optimal restoration**



The pilot testing process helped identify areas where the information flow could be improved, as well as technical issues in the CRS algorithms developed. In terms of information flow, there was a need to estimate more features in the CRS phase that could improve the debris clearance time estimation. In this sense, algorithms were refined for debris pile slicing, and for calculating the distance to the road edge and neighboring debris piles. The slicing allows incremental volume calculations, which are used by the access restoration module, along with the distance to the edge of the road, to estimate restoration times. As a result of the test, the CRS algorithms were shown to produce false negatives caused by vegetation, shadows, and other obscurations. The algorithms were improved to account for these scenarios. Validation of the algorithms was extended to include five additional scenes, for a total of ten. The improved algorithm obtained an overall quality of 96.9%, which is an improvement of 4.9% over the results of the previous validation. The results are presented in Table 8.

**Table 8: Roadway pixel classification results**

Site	# Flood PX	TP	FP	FN	Completeness	Correctness	Quality
1	118,750	117,052	577	1,698	98.57	99.51	98.09
2	132,921	131,047	490	1,874	98.59	99.63	98.23
3	34,559	34,559	671	-	100.00	98.10	98.10
4	39,121	37,858	1,154	1,263	96.77	97.04	94.00
5	22,595	22,595	-	-	100.00	100.00	100.00
6	65,042	64,351	338	691	98.94	99.48	98.43
7	69,400	68,283	-	1,117	98.39	100.00	98.39
8	45,498	45,470	178	28	99.94	99.61	99.55
9	84,337	79,519	761	4,818	94.29	99.05	93.44
10	116,567	111,377	1,936	5,190	95.55	98.29	93.99
<b>All</b>	<b>728,790</b>	<b>712,111</b>	<b>6,105</b>	<b>16,679</b>	<b>97.71</b>	<b>99.15</b>	<b>96.90</b>

## 5. PROCEDURES FOR INTEGRATION OF OUTSIDE HELP

### 5.1 Introduction

Post-disaster logistics encompass a series of actions that are intended to address the different needs of both the impacted population, and the response itself (Holguín-Veras and Jaller, 2012; Holguín-Veras et al., 2012). Multi-focused, these efforts are also multi-staged. In simplified terms, several key stages can be identified: (1) preliminary needs assessment, (2) access restoration, (3) deployment of the assets required to conduct the various emergency response functions, (4) local distribution of supplies, (5) debris removal, and (6) infrastructure restoration. Results from fieldwork studies in post-disaster environments have shown that the convergence of volunteers, materials, and equipment brings to the impacted area large amounts of resources that are critical to the response. While these convergent resources should be fully exploited, coordinating amorphous groups of people as well as the material resources they bring is no trivial endeavor. The logistics processes necessary to coordinate relief efforts after catastrophic events are challenging for organizations working by themselves, but when one adds a plurality of organizations converging in response to catastrophic events, integration becomes critical. Despite increasing contributions or research, and emerging technology available in the field, coordination among agencies remains challenging. Results from fieldwork research has shown that lack of integration and coordination can lead to an increase in the resources needed to carry out the relief efforts, and can also hinder the response due to interference, conflict, or competition (Holguin-Veras et al., 2016).

Coordination and integration of multiple agents is vitally important for effective and efficient access restoration, and for any other post disaster activity. A thorough understanding of current practices key to gaining insight into aspects or practices that could enhance coordination. This report presents a review of current integration practices used by disaster response organizations (e.g., non-profit organizations, contractors, governments, official response agencies) and those suggested by the research community. The following sections provide an overview of Emergency Management and Emergency Support Functions and details regarding current integration practices.

## **5.2 Emergency Management**

Emergency management refers to how society responds to severe events. Throughout history, humans have taken precautions in anticipation of unexpected events to reduce the risk to their lives and property. Emergency management has the mission of developing and implementing policies to prepare for, respond to, and recover from, all hazards. How emergency management operates during a disaster depends on the preparations made, the competence and experience of the actors involved, and the legal preconditions. As such, emergency management should become a central activity of public administration, at all levels of government (Fredholm and Goransson, 2010).

In the United States, the Federal Emergency Management Agency (FEMA) is tasked with handling emergency management at the Federal level. The agency was created with the goal of integrating a fragmented system comprised of federal agencies, as well as state and local governments. FEMA has the authority to provide response and recovery assistance to areas impacted by major disasters. However, not all disasters are handled by FEMA; in many cases States do not request Federal assistance, and many disasters are handled at the State and local levels. Although the exact number of disasters successfully handled without requests for Federal assistance is not known, it is estimated at 3,500 to 3,700 annually (Federal Emergency Management Agency, 2015).

Response operations at every level, and for all sizes of disaster, involve the participation of voluntary and private agencies. All of these agents work in partnership, based on a framework of emergency management that relates the components of the response effort in time and sequence of actions. The Integrated Emergency Management System, based on the concept of a common set of functions for all emergencies, is the framework recommended by FEMA. These functions, called Emergency Functions, are detailed in Table 8 (Federal Emergency Management Agency (FEMA), 2008a).

**Table 9: Emergency Functions (EF)**

<p><b>EF #1: Transportation</b>          Aviation/airspace management and control          Transportation safety          Restoration/recovery..., * debris removal          Movement restrictions          Damage and impact assessment          *Evacuation planning/operations</p>	<p><b>EF #7B: Logistics, Management, Resource Support</b>          National incident logistics planning/management...          Resource support</p>
<p><b>EF #2: Communications</b>          Coordination with telecom. and IT industries          Restoration and repair of telecom. Infrastructure          Protection, restoration, and sustainment of IT</p>	<p><b>EF #8: Public Health and Medical Services</b>          Public Health          Medical          Mental health services          Mass fatality management</p>
<p><b>EF #3: Public Works and Engineering</b>          Protection and emergency repair          Restoration/recovery,* debris removal not in response          Engineering services and construction management          Contracting support for life-saving services</p>	<p><b>EF #9: Search and Rescue</b>          Life-saving assistance          Search and rescue operations</p>
<p><b>EF #4: Firefighting</b>          Coordination of Federal firefighting activities          Support to wildland, rural, and urban firefighting</p>	<p><b>EF #10: Oil and Hazardous Materials Response</b>          Oil and hazardous materials response          Environmental short- and long-term cleanup</p>
<p><b>EF #5: Emergency Management</b>          Coordination of incident management response          Issuance of mission assignments          Resource and human capital          Incident action planning          Financial management</p>	<p><b>EF #11: Agriculture and Natural Resources</b>          Nutrition assistance          Animal and plant disease and pest response          Food safety and security          Natural/cultural/historic resources protection/restoration          Safety and well-being of household pets</p>
<p><b>EF #6: Mass Care, Emergency Assistance...</b>          Mass care, * relief distribution planning/operations          Emergency assistance          Disaster housing          Human services</p>	<p><b>EF #12: Energy</b>          Energy infrastructure assessment/repair/restoration          Energy industry utilities coordination          Energy forecast</p>
<p><b>*EF #7A: Management of Convergent Help</b>          Material (solicited, unsolicited) donations          Monetary (solicited, unsolicited) donations          Service (solicited, unsolicited) donations          Information          Personnel</p>	<p><b>EF #13: Public Safety and Security</b>          Facility and resource security          Security planning and technical resource assistance          Public safety and security support          Support to access, traffic, and crowd control</p>
	<p><b>EF #14: Long-Term Community Recovery</b>          Social and economic community impact assessment          Long-term community recovery assistance          Analysis/review of mitigation program implementation</p>
	<p><b>EF #15: External Affairs</b>          Emergency public info and protective action guidance          Media and community relations          Congressional and international affairs          Tribal and insular affairs</p>

Note: Adapted from Federal Emergency Management Agency (FEMA) (2008a)

### 5.3 ERM Coordination

Emergency Response Management (ERM) is used to facilitate and support emergency response operations. The available literature on coordination issues involving ERM is limited to practitioner articles and government reports among others; academic work is scarce. In (Chen et al., 2008) a framework is proposed to analyze coordination patterns during emergency response environments, based on semi-structured interviews with 32 emergency response personnel, local and nation-wide emergency managers, and Federal Emergency Management Agency (FEMA) coordinators.

In emergency situations such as disasters and catastrophes, responses come from different actors acting with varied objectives and information about the situation. The absence of organization among these multiple players often leads to disorder, including excess supplies in some locations and scarcity in others, which highly reduces the effectiveness of the response. Therefore, effective coordination among participant organizations is extremely important in emergency response operations. Such coordination is a demanding and specialized task, which involves elevated levels of uncertainty and requires experience and resources. Effective coordination is essential for handling critical situations, due to the plurality of actors and the fact that these events are highly unpredictable. An understanding of the organizational, technical and human issues involved in ERM is necessary for coordination, as well as an understanding of the different organizations involved which may include public and private agencies at a national and international level.

In emergency response management, preparation and coordination is required prior to, and during the disaster, as well as in the recovery process in the affected region. In terms of preparedness and emergency response plans prior to the disaster, research is scarce, as only recent studies have considered preparation plans for disasters. Most of the early research work in emergency response management is devoted to reactive response warning systems. First outlined by Williams (1964), a reactive warning system included: (i) hazard detection; (ii) hazard evaluation; (iii) communication of warning messages to affected population; and (iv) response from receivers to warning message. Lindell and Perry (1987) describe the logical framework of the response from local governments through warning mechanisms, and present one of the earliest warning mechanisms that uses informal social networks. Studies have been conducted regarding the development of preparation plans in response to specific types of emergencies (Wein et al., 2003) and radiation disasters (Schleipman et al., 2004). However, there is still a lack of generalized emergency response preparation plans and frameworks that could help governments and participating organizations with the appropriate level of preparation to respond to disasters.

Dawes et al. (2004) analyze the responses from organizations in the World Trade Center crisis, and acknowledge the most valuable lessons for improving emergency response in such disasters. They point out that interdependencies among stakeholders in these situations are key, and could be of great help for government response groups. Emergency management and planning is the most important factor for an effective response to disasters, which in turn requires good information management. In recent literature there has been a development in terms of scenario planning models and information management systems for emergency response operations. Li et al. (2008) design a prototype emergency evacuation planning system, showing how this type of approach can be used to enhance emergency response operations through a good information management system. Chang et al. (2007) also present a scenario planning approach for flood emergencies. They show how a decision support system can be used effectively by government agencies in planning response operations to flood emergencies. Based on these findings, the development of a good coordination and planning framework that can identify, quantify and coordinate the different players and resources in emergencies and disasters would be greatly beneficial to government and participants in emergency management operations.

Studies have been made in search of strategies that could improve coordination among stakeholders, and the entire network of organizations involved in emergency response. Comfort et al. (2004) study the fragility of disaster response systems, conducting simulations of increasing demand and decreasing response capacity, and point out that access to core information is the factor that most increases the level of coordination among the participant organizations. High levels of coordination also depend on clearly stated roles among the different actors. Thus, established emergency response plans and protocols, as well as the management of resources and efforts, are highly beneficial for an effective response during disasters. Petrescu-Prahova and Butts (2005) state that “where agents with formal coordinative roles are present, they are substantially more likely to become actual

coordinators,” which means that predefined coordinator agents are more likely to perform effective coordination operations during disasters. Hence, effective emergency response coordination frameworks are needed to increase the efficiency of responses during emergency situations.

An important development for improving the level of coordination in emergency response is presented by the Federal Emergency Management Agency (FEMA) (2008b) through the National Incident Management System (NIMS), which integrates existing best practices in emergency response management and is intended to be effective for all types of emergencies. The approach is applicable nationwide, and combines information and resource management with supporting technologies, and combines best practices for preparedness, command and management. However, Chen et al. (2008) call attention to the fact that this system, although it presents guidelines for emergency response, has some limitations in terms of consistency between the established goals in the situations considered, and those established and prioritized by NIMS.

## **5.4 Review of Current Practices**

This section presents a summary of existing response frameworks that offer guidelines for emergency response management and coordination developed by either federal or local governments as a mean to increase the efficiency of the response in the event of an emergency.

### **5.4.1 National Disaster Recovery Framework (FEMA)**

The National Disaster Recovery Framework (NDRF) is part of the U.S. National Preparedness System that describes the principles, processes and capabilities needed for communities to more effectively manage and recover after an incident occurs (Federal Emergency Management - FEMA, 2011). Particularly the NDRF emphasizes the preparation needed for recovery in advance of a disaster. As they acknowledge in their framework, the preparation begins with initial efforts in the pre-disaster stage that include: “coordinating with whole community partners, mitigating risks, incorporating continuity planning, identifying resources, and developing capacity to effectively manage the recovery process, and through collaborative and inclusive planning processes.”

Following a disaster, regardless of its size or scale, the affected communities will have some recovery needs and will require some basic resources. This Framework includes the types of recovery resources: information for decision-making, technical assistance, experts for specific subject matter, labor and equipment. Coordination and funding mechanisms are also specified. The whole community partners include insurance companies, NGOs (voluntary, faith-based, nonprofit and philanthropic), and government departments and agencies.

The tasks described in the NDRF include planning, public information and warning, operational coordination, economic recovery, health and social services, housing, infrastructure systems, and natural and cultural resources. The planning task mainly involves developing strategic approaches that engage the community to meet objectives. The communication task is mainly concerned with delivering information to the entire community through “clear, consistent, accessible, and culturally and linguistically appropriate methods.” As economic recovery activities, the Framework contemplates the reactivation of economic activities and develops new business opportunities. It also emphasizes restoring health and social service capabilities, and implementing housing solutions for the benefit of the community. In terms of infrastructure systems, the NDRF proposes stabilizing infrastructure functions, minimizing safety threats, restoring systems to support the community, and protecting natural and cultural resources.

As stakeholders, NDRF highlights the participation of the “whole community” to aim for a successful recovery effort. The “whole community” involves: individuals, families and households, non-governmental organizations, private-sector entities, local governments, and State, Tribal, Territorial and Insular Area

Governments and Federal Governments. As stated, directly engaging people with different needs and/or disabilities in the planning process will enhance the national preparedness efforts. To ensure this, the Framework offers recovery practitioners with guidance on critical recovery functions such as leadership, organizational and coordination structures, among others. In accordance with NDRF principles, specific roles and responsibilities are clearly defined for each stakeholder. Beyond a clear understanding of roles and responsibilities among stakeholders, the Framework offers ways in which various individuals and groups can collaborate and share resources to support the affected population after a disaster.

With respect to the magnitude of the efforts required in the Framework, it should be noted that FEMA's expertise and reliability are important, as FEMA is the country's Federal organization for emergency response. The level of detail in the Framework reflects this responsibility, and the importance of FEMA's efforts. Even so, to ensure successful implementation, there must be resources assigned, and all stakeholders involved should be actively involved in the event of an emergency.

The NDRF highlights that the level of coordination needed is extensive, as many different entities and levels of expertise are required to develop most of the objectives mentioned. This coordination probably does not require a cooperation agreement, but some sort of formality should be involved when coordinating tasks. Agreements should ensure that staffing and expertise from all stakeholders are available post-disaster. As the Framework mentions, the stakeholders should include the "local, regional/metropolitan, state, tribal, territorial, insular area and Federal government."

To integrate outside help and take advantage of improvised and unanticipated participation, the NDRF has designed a coordinating structure that is scalable and adaptable to meet all levels and types of needs. This is the Recovery Support Function (RSF), which is also able to respond to the specific recovery requirements of large to catastrophic incidents. These RSFs are pre-designed to work together with the Federal Disaster Recovery Coordinator (FDRC) to "promote the communication and collaboration among its members," and to accommodate to the fast incoming Federal resources needed to assist these emergencies. RSFs organize in teams to cover multiple localities, and if there are further requirements or locations, the RSFs needed are also deployed to these areas. In all actions, the RSFs and FDRCs aim to: reach and cover the needs of affected residents; have an equitable distribution of resources; and have recovery programs that lead to full restitution of the socioeconomic and cultural status of the community.

#### **5.4.2 National Voluntary Organizations Active in Disaster (National VOAD)**

National Voluntary Organizations Active in Disaster (National VOAD) is a nonprofit, nonpartisan membership-based organization that serves as a forum for organizations to share knowledge and resources throughout the disaster cycle – preparation, response, recovery and mitigation – that will help communities prepare for and recover from disasters. The National VOAD coalition of over 100 member organizations includes over 50 of the country's most reputable national faith-based, community-based and other nongovernmental organizations that represent the diverse population of the United States. National VOAD is dedicated to whole community engagement, and recognizes that all sectors of the country's diverse cultural, linguistic and faith-based society must work together to foster more resilient communities nationwide.

Leveraging a strong set of values and principles, this organization has developed convening mechanisms for member organizations to build relationships. Members and partners gather or convene around topical issues and programmatic activities to improve the delivery of services throughout the disaster cycle, and to further create a climate for cooperation. Since the founding of National VOAD in 1970, many lessons have been learned, skills

developed and best practices shared. This has resulted in the establishment of Points of Consensus, documents that entail agreed upon protocols for guiding individual and collective work.

The organization is comprised of committees and task forces. Both committees and task forces are made up of subject matter experts in their respective fields to develop best practices and lessons learned. Key committees are centered on functional areas of: advocacy, communications, community preparedness, disaster case management, disaster health, donations management, emotional and spiritual care, housing, long term recovery, mass care and volunteer management. The task forces are developed on an as-needed basis to support agreed upon initiatives throughout the membership. Task forces usually address relevant issues such as droughts and other climatological phenomena, as well as organizational topics such as continuous training. Members of the organization collaborate and learn from each other by sharing best practices and holding conferences.

### **5.4.3 Hyogo Framework**

The Hyogo Framework for Action (HFA) was released by the United Nations as a 10-year plan (2005-2015) to reduce disaster risk among all countries of the world, and to establish a common system of coordination (International Strategy for Disaster Reduction, 2005). It came out of the World Conference held in Kobe, Hyogo, Japan, from January 18-22, 2005, with the theme “Building the Resilience of Nations and Communities to Disasters.” Five priorities in action, and guiding principles and practical means for achieving disaster resilience were identified. Since its release, it has been adopted by numerous countries, particularly in Asia and Africa, and has helped build more resilient communities. Such resiliency includes more accurate detection of climate change, communication to the population about emergency response practices, and country-specific policies for better infrastructure to respond to disasters.

The HFA incorporated all activities that extend to the capacity of a country to respond to disasters, including: research into disaster risk management; investment in new technologies that will improve response; and developing databases of disaster response records. The Framework contained the designation of responsibilities from the local level to the national level, and created a structure that facilitated coordination across different sectors. It also integrated risk reduction into legislation and policy, ensuring that laws do not conflict with the priorities of disaster risk management. In addition, it recognized local disaster patterns and encouraged recordkeeping to give to relevant authorities. The Framework ensures that all communities have access to the proper resources needed to properly respond to a disaster. It also promotes community participation by holding forums, and publicizing information, and ensuring that feedback and opinions are gathered from both genders, instead of just men. The Framework developed “systems of indicators of disaster risk and vulnerability at national and sub-national scales that will enable decision-makers to assess the impact of disasters on social, economic and environmental conditions and disseminate the results to decision makers, the public and populations at risk.” Risk maps were developed and distributed, as was statistical data on disaster response effectiveness. Where possible, early warning systems were created to effectively inform people of courses of action to preserve life and property, which take into account demographics when deciding how to distribute instructions. Information on disaster impacts is also compiled and standardized, with guidance on how these records can be exchanged with other areas.

Since a well-informed public is key to disaster preparedness, the HFA also serves to educate people on disaster risk management. With educational activities and other forms of training, it includes guidance on the propagation of information to the general public. Also, a better use of land-use planning and development of activities is encouraged to reduce risk, and promote a sustainable and efficient use of ecosystems. The HVA emphasizes that the response must be strengthened at all levels (local, regional, and national).

HVA also identifies the technological difficulties in some countries in developing databases of information and producing statistical modeling when there is a lack the expertise and knowledge required. The framework stresses that if the country needs to invest in research, it should access the disaster response research community already established. The key is not to build new efforts, but to incorporate stakeholders to participate in recovery plans. Further, the development of risk maps offers the aggregation of information and design in a form that it is not complicated for the audience. The distribution of information to the public becomes easier with technical familiarity, and much faster when technology is used.

As the Framework is extended to every sector, it is comprehensive, but requires a lot of effort to implement. The framework is composed of multiple goals to help a country respond to disasters better. It also requires significant investment, and staffing to participate in the different tasks. As their first priority action, the Hyogo Framework strove to establish disaster risk as a national and local priority. For this to happen, cooperation agreements must be established at the institutional levels. Since all sectors of society must be engaged, the Framework encourages cooperation. The Framework is able to integrate external stakeholders, including the various segments of the civil society, and to take advantage of their improvised and unanticipated participation. At a strategic level, the Framework does a good job of explaining and presenting the different strategies. Should a country detect disaster risk, with the HVA, authorities will be able to prepare accordingly, and be able to inform communities for adequate planning.

#### **5.4.4 Montana Emergency Response Framework**

The State of Montana, through the Montana Disaster & Emergency Services Planning Bureau, developed the Montana Emergency Response Framework for local, state and federal government as well as private sectors, participating agencies and non-governmental organizations cooperating in emergency relief activities. The document is a compendium of guidelines, policies and procedures designed to increase the efficiency of emergency response in the state, facilitating the coordination of stakeholders' participation and clarifying their roles. The State Emergency Coordination Centers (SECC) are the institutions responsible for the coordination of the organizational structures and chains of command, defined at a local, tribal, state and federal level. The participation of the different government levels depends on the magnitude of the disaster. The framework also details guidelines for operations, and the organization of resources, along with recommended response and recovery measures. A set of function and support annexes is presented, as a guide to organize resources and capabilities, and to support processes and administrative tasks. This framework is intended to serve as a guideline in all types of incidents, regardless of their nature (Montana Disaster & Emergency Services Planning Bureau, 2012).

The document does not make clear how a damage, tasks and resources assessment should be undertaken during an emergency response at any level, to help organize resources and activities. The framework does consider a capability assessment intended for preparedness activities, which is annually performed at the state level. Towns, Counties and tribes are also encouraged to perform their own capability assessments. The coordination and administration of activities and resources is considered by clearly defining a hierarchical structural organization and chain of command, with defined roles and responsibilities, which takes advantage of the help provided by voluntary organizations active in disasters: private organizations, nongovernmental organizations and Red Cross groups, all coordinated by local and state governments. The framework proposes guidelines through different agencies for such broad functions as: Transportation, which considers access restoration, transportation services, and support activities as well as damage in infrastructure assessment; Communication, which covers information transfer coordination; Firefighting and Public Works for pre- and post-incident technical assessment and

assistance of public works; Emergency and Logistics Management, which provides support for requirements and Public Health and Medical Services, among other functions.

#### **5.4.5 Nepal National Disaster Response Framework**

Another example of coordination practices in emergency response frameworks is presented in Nepal. The Government of Nepal through the Ministry of Home Affairs developed a National Disaster Response Framework, which contains guidelines and actions to be taken before, during and after a disaster (Government of Nepal, 2016). The aim of this framework is to have more coordination and effectiveness in the response to a large-scale disaster. The Disaster Relief Act of 1982, which contains a set of well-structured policies for disaster management, constitutes the main basis for the National Disaster Response Framework. The National Disaster Response Framework also describes a National and International Assistance and coordination Framework, which depicts the flow of actions to be taken to coordinate national and international assistance and resources. The framework considers continuous updates of needs, incoming support and progress. The course of actions starts with a situation analysis and a declaration of state of emergency, followed by an appeal for international assistance. After this initial process, relief operations are coordinated by United Nations and Red Cross, which in turn are coordinated by a humanitarian coordinator designated by the Government. The Government has also established a so-called National Emergency Operations Center, (NEOC), and a Cluster Coordination Structure with a set of clusters in areas such as health, shelter, logistics, education, and food security, led by the different Ministries. The NOEC is the institution empowered by the national government to prepare and prioritize action plans for all incoming resources, equipment and humanitarian team members, as well as the management of communications from coordination management centers and the military's coordination center.

A strength of Nepal's emergency response coordination framework is its clear identification of the responsible agency, the different stakeholders, and their roles in operations. The chain of command is also clearly identified, so that each and every participant knows to whom they respond. Since the designated coordinating institution is empowered by the government, access to resources would not be a problem or the development of agreements with participating agencies.

The framework also contains a set of predefined tasks and responsibilities to assess the situation, and the capacity and amount of resources and work forces among the stakeholders, along with procedures to take advantage of aid coming from outside. The government also controls the amount of resources that may be received from outside, and can reject some types of resources based on current necessities. All of these aspects are desirable in an emergency response coordination framework, however, a more structured program with clear procedures instead of a list of tasks, activities, institutions and responsibilities would be more effective and easier to implement and manage in the event of a disaster, where a rapid response is needed. The Nepal Framework does not consider too much in terms of access restoration activities, but it does include a table with required response activities and responsible leading agencies per time frame from the occurrence of the disaster.

#### **5.4.6 Sudan Emergency Response Framework**

Another proposed framework for emergency response operations coordination is presented in Sudan, with special attention to tackling situations where populations are displaced after disasters occur. In 2015, the government of Sudan through its Inter-Sector Coordination Groups and Inter-Agency Standing Committees proposed an Emergency Response Framework, as a guidance document for emergency response, and to ensure coordination and coherent contribution of these Inter-Agency Standing Committees with government efforts in disaster relief operations (Inter-Sector Coordination Group - ISCG, 2015). The framework clearly identifies the different roles and responsibilities of the Inter-Agency Standing Committees, along with specific modes of

coordination to generate a common methodology for emergency relief operations. The framework also describes commitments, performance standards, and procedures for an effective response to emergencies by the Government of Sudan. It considers assessment, alert, coordination, access, and response operations, stating the actions required, responsible agencies and desired outputs, divided by stages consisting of time intervals lapsed from the occurrence of the event. A set of sector-specific activities, such as Logistics and Emergency Telecommunications, Coordination and Common Services, Food Security, Shelter, Nutrition, Education are presented as well. Even though this Framework constitutes a powerful tool for the coordination of emergency response efforts for the Government of Sudan, the methodology is not replicable, or implementable in scenarios other than Sudan. As such, it is limited to an internal Inter-Agency Standing Committee guidance document.

## **6. CONCLUDING REMARKS**

The research reported in this document represents one of the first, if not the first, effort to integrate optimization techniques and Commercial Remote Sensing (CRS) outputs into a Decision Support System (DSS) to foster decision-making in post-disaster environments. In a way, the optimization procedures add value to the outputs directly produced by CRS, which in most cases provide accurate measurements of a specific aspect of the physical world. The team believes that such integration of optimization and CRS is the way of the future. There are challenges to overcome that should be tackled by future research. The team would like to share key observations based on the experience gained during this project to help researchers attempting to integrate optimization procedures and CRS to produce useful DSS.

To start, the use of optimization procedures requires that decision-makers agree on the specific metric to be optimized. The challenge is that, quite frequently: (1) multiple metrics could be used to drive the optimization; and (2) the use of different metrics could lead to different results. For instance, in this project the team considered 5 different metrics (i.e., population, private cost, time, deprivation time and cost, and social costs) and let the users of the DSS select the most appropriate one. Although providing the option to select the metric is a pragmatic way to deal with ambiguity in the objective function, the team believes in post-disaster conditions it is important to constrain the choice of metrics to those that meet humanitarian principles and ethics. In the ideal setting, potential users of DSS like the one developed here ought to reach an agreement among themselves on the metric to be used. This should be done before the DSS is used, to ensure no bias in the selection of the metric.

A second aspect worthy of discussion is the use of CRS. Currently, CRS technologies are extremely useful in providing quantitative snapshots, and continuous measurements, of the physical world. With improving CRS technologies, larger computing power, faster networks, easier-to-access cloud computing, faster mobile computing, and the like, disaster responders will have better tools at their disposal. However, in the case of disaster-related DSS, the physical impacts are not all that is at stake. The human impacts of disasters are a primary consideration. The challenge in the case of disaster-related DSS is that estimating human impacts, even in an approximate way, is still an elusive objective. CRS can definitely identify, for instance, what percent of the buildings in a given neighborhood have been destroyed by an earthquake. Producing an estimate of the likely number of fatalities and injuries is significantly more difficult, as such an estimate would depend on the time of day of the earthquake, its duration, the population density, among other factors. The CRS community ought to tackle this important challenge.

Taken together, the combined use of appropriate objective functions and the development of CRS methodologies increasingly able to estimate the human impacts of large disasters is bound to open new frontiers for effective DSS. The team's hope is that these concluding remarks help the research community accept these research challenges, and bring to reality such critically important DSS.

## 7. REFERENCES

- Ahuja, R. K., T. L. Magnanti and J. B. Orlin (1993). Network Flows: Theory, Algorithms, and Applications, Prentice Hall.
- Dijkstra, E. W. (1959). "A Note on Two Problems in Connexion with Graphs." Numerische Mathematik **1**(1): 269-271.
- Fritz, C. E. and J. H. Mathewson (1957). Convergent Behavior: A Disaster Control Problem. Special Report for the Committee on Disaster Studies. Disaster Study. Washington D.C., National Academy of Sciences. **9**: 1-102.
- Holguín-Veras, J. and M. Jaller (2012). "Immediate Resource Requirements after Hurricane Katrina." Natural Hazards Review **13**(2): 117-131.
- Holguín-Veras, J., M. Jaller, L. Van Wassenhove, N. Pérez and T. Wachtendorf (2013). "Material Convergence: An Important and Understudied Disaster Phenomenon." Natural Hazards Review.
- Holguín-Veras, J., M. Jaller, L. N. Van Wassenhove, N. Pérez and T. Wachtendorf (2012). "On the Unique Features of Post-Disaster Humanitarian Logistics." Journal of Operations Management **30**: 494-506.
- Holguín-Veras, J., M. Jaller and T. Wachtendorf (2012). "Comparative Performance of Alternative Humanitarian Logistic Structures after the Port-au-Prince Earthquake: ACEs, PIEs, and CANs." Transportation Research Part A: Policy and Practice **46**(10): 1623-1640.
- Holguín-Veras, J., N. Pérez, M. Jaller, L. N. Van Wassenhove and F. Aros-Vera (2013). "On the appropriate objective function for post-disaster humanitarian logistics models." Journal of Operations Management **31**(5): 262-280.
- Holguín-Veras, J., E. Taniguchi, F. Ferreira, M. Jaller and R. Thompson (2012). The Tohoku Disasters: Preliminary Findings Concerning The Post Disaster Humanitarian Logistics Response. Annual Meeting of the Transportation Research Board, Washington DC, Department of Transportation.
- Messinger, D. W., J. van Aardt, D. McKeown, M. Casterline, J. Faulring, N. Raqueño, B. Basener and M. Velez-Reyes (2010). High-resolution and LIDAR Imaging Support to the Haiti Earthquake Relief Effort. SPIE Optical Engineering+ Applications, International Society for Optics and Photonics.
- Nurre, S. G., B. Cavdaroglu, J. E. Mitchell, T. C. Sharkey and W. A. Wallace (2012). "Restoring infrastructure systems: An integrated network design and scheduling (INDS) problem." European Journal of Operational Research **223**(3): 794-806.
- Prim, R. C. (1957). "Shortest Connection Networks and Some Generalizations." Bell System Technical Journal **36**(6): 1389-1401.
- Takahashi, H. and A. Matsuyama (1980). "An Approximate Solution for the Steiner Problem in Graphs." Math. Japonica **24**(6): 573-577.
- van Aardt, J. A. N., M. Arthur, G. Sovkoplak and T. L. Swetnam (2011). LiDAR-based Estimation of Forest Floor Fuel Loads using a Novel Distributional Approach. Proceedings of SilviLaser 2011, 11th International Conference on LiDAR Applications for Assessing Forest Ecosystems, University of Tasmania, Australia, 16-20 October 2011., Conference Secretariat.
- Fritz, C. E. and J. H. Mathewson (1957). Convergent Behavior: A Disaster Control Problem. Special Report for the Committee on Disaster Studies. Disaster Study. Washington D.C., National Academy of Sciences. **9**: 1-102.
- Holguín-Veras, J. and M. Jaller (2012). "Immediate Resource Requirements after Hurricane Katrina." Natural Hazards Review **13**(2): 117-131.
- Holguín-Veras, J., M. Jaller, L. Van Wassenhove, N. Pérez and T. Wachtendorf (2013). "Material Convergence: An Important and Understudied Disaster Phenomenon." Natural Hazards Review.
- Holguín-Veras, J., M. Jaller, L. N. Van Wassenhove, N. Pérez and T. Wachtendorf (2012). "On the Unique Features of Post-Disaster Humanitarian Logistics." Journal of Operations Management **30**: 494-506.

Holguín-Veras, J., M. Jaller and T. Wachtendorf (2012). "Comparative Performance of Alternative Humanitarian Logistic Structures after the Port-au-Prince Earthquake: ACEs, PIEs, and CANs." Transportation Research Part A: Policy and Practice **46**(10): 1623-1640.

Holguín-Veras, J., E. Taniguchi, F. Ferreira, M. Jaller and R. Thompson (2012). The Tohoku Disasters: Preliminary Findings Concerning The Post Disaster Humanitarian Logistics Response. Annual Meeting of the Transportation Research Board, Washington DC, Department of Transportation.

Messinger, D. W., J. van Aardt, D. McKeown, M. Casterline, J. Faulring, N. Raqueño, B. Basener and M. Velez-Reyes (2010). High-resolution and LIDAR Imaging Support to the Haiti Earthquake Relief Effort. SPIE Optical Engineering+ Applications, International Society for Optics and Photonics.

van Aardt, J. A. N., M. Arthur, G. Sovkoplak and T. L. Swetnam (2011). LiDAR-based Estimation of Forest Floor Fuel Loads using a Novel Distributional Approach. Proceedings of SilviLaser 2011, 11th International Conference on LiDAR Applications for Assessing Forest Ecosystems, University of Tasmania, Australia, 16-20 October 2011., Conference Secretariat.



## **APPENDICIES**

**Appendix A:** Algorithms for Debris Volume and Water Depth Computation

**Appendix B:** Algorithms for Detection of Roadway Debris and Flooding

**Appendix C:** Generating GIS Products from Detection and Characterization Algorithm Outputs

**Appendix D:** Technical Advisory Committee Meeting Slides

**Appendix E:** CRS Playbook

**Appendix F:** Access Restoration Planning User Manual

**Appendix G:** Debris Utility User Manual

**Appendix H:** Flood Utility User Manual